Chapter 8
Orbital Maneuvering

The most important maneuver in space is the one to change the orbit of a space vehicle. Because the initial and final orbits are subject to a central gravitational potential such a S/C will transit between two Keplerian orbits. This is true not only for planetary orbits but also for interplanetary flights with the Sun as the central body. In general, for all these transfers there are two cases to be distinguished:

- *Orbital transfer*
  A S/C is on an initial orbit and just needs to be transferred to another orbit.
- *Orbital rendezvous*
  A S/C on a specific point on the initial orbit needs to be transferred to a specific point on the final orbit (e.g., target object).

For instance, a lunar space probe does an orbital transfer when it is in a circular Earth orbit and heads into a translunar orbit, or, to give another example, when the International Space Station due to drag needs to be transferred to a higher circular orbit. We will treat orbital transfers in Sects. 8.1–8.4. Orbital rendezvous, on the other hand, for instance, is the situation where a Shuttle orbiter performs a maneuver to approach the International Space Station for docking. For methodical reasons we split the orbital rendezvous case into "orbital rendezvous in planetary orbits" (Sect. 8.6) and "interplanetary orbital rendezvous" (Sect. 9.3). The reason that interplanetary rendezvous is treated in a different chapter is because interplanetary flight is a complex three-body problem (Sun, target planet, and S/C), in which orbital rendezvous needs to be embedded.

Orbital Transfer

Let us first consider the orbital transfer case. The two orbits, between which the S/C is to be transferred, may either intercept in one ore two points, or they may not intercept at all.

U. Walter, *Astronautics*, https://doi.org/10.1007/978-3-319-74373-8_8

Intercepting orbits
If the two orbits intercept, an impulsive thrust maneuver (see Sects. 2.3 and 2.4.1) at any interception point will do to directly attain the target orbit. Such orbital transfers are called **one-impulse maneuvers**, and they are discussed in detail in Sect. 8.1.

Non-intercepting orbits
If the two orbits do not intercept

- a first impulsive maneuver may bring the S/C into a transfer orbit until it hits the target orbit where a second impulsive maneuver transits it into the final orbit. In total, this would be a classical **two-impulse transfer**. The most general case, where the transfer orbit intersects both orbits—the so-called *Lambert transfer*—is discussed in Sect. 8.2. The optimal case when the transfer orbit just touches both orbits—the so-called *Hohmann transfer*—is discussed in Sect. 8.3.
- There are rare cases where it might be useful to transfer first into an outer intermediate orbit and from there into the target orbit. In these cases, three (or more) impulsive firings are required and the subsequent **three-impulse transfers**. This is examined in Sects. 8.4.2 and 8.4.3.
- Alternatively, the S/C might be powered by a continuously fired thruster. In that case the transfer orbit will not be a conic section but usually a spiraling orbit, a **continuous thrust transfer orbit** as explored in Sect. 8.4.5.

Orbital Rendezvous
Orbital rendezvous maneuvers are of high practical relevance and are treated in Sect. 8.6. The specific equation of motions for relative rendezvous are developed in Sect. 8.5.

8.1 One-Impulse Maneuvers

The one-impulse maneuver is the foundation of any maneuvering in space. It ideally is a finite thrust firing with vanishingly short duration, a so-called *boost*, *kick-burn* or just *burn* for short, causing a certain $\Delta \boldsymbol{v}$. We have examined impulsive maneuvers already in Sects. 2.3 and 2.4.1 to derive its extent of validity and the corresponding rocket equation to determine the fuel demand for a given $\Delta \boldsymbol{v}$. This section now will investigate how a $\Delta \boldsymbol{v}$ changes a given orbit and what is the $\Delta \boldsymbol{v}$ for a given change of state vector.

8.1.1 Elementary Maneuvers

We first consider the question of how a maneuver $\Delta \boldsymbol{v}$ at a given orbit position θ changes the orbital elements a, e, i, ω, Ω. Because the evaluation of orbit changes due to arbitrarily large kick-burns becomes quite complex, we consider in the following only small impulse maneuvers $\delta \boldsymbol{v} \ll \boldsymbol{v}$ and their effect, δa, δe, δi, $\delta \omega$, $\delta \Omega$, on the orbital elements. To facilitate the calculation and without loss of generality, we decompose $\delta \boldsymbol{v}$ into the following elementary components (see Fig. 8.1):

$\delta v_{\parallel}$ **tangent maneuver**
kick-burn in the direction, i.e. tangent to the orbital motion (along-track)

$\delta v_{\perp \mathrm{O}}$ kick-burn perpendicular to the direction of motion, but within the orbital plane, outbound

$\delta v_{\perp\perp}$ **plane change maneuver**
kick-burn perpendicular to the orbital direction and perpendicular to the orbital plane, in the direction of the angular momentum vector.

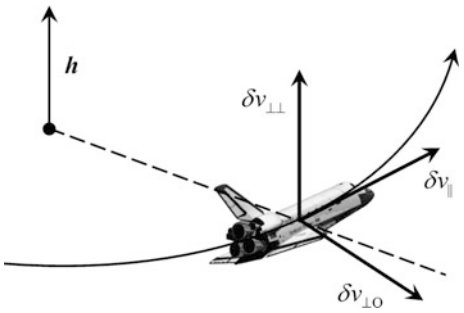

Fig. 8.1 Decomposition of a kick-burn into the along track and two cross-track directions within and outside the orbital plane

Generally, the following applies to these kick-burns:

- Kick-burns perpendicular to the direction of orbital motion can change only the direction of motion and not its speed, and hence not the orbital energy ε. So because $\varepsilon = -\mu/2a$, $\delta v_{\perp \mathrm{O}}$ and $\delta v_{\perp\perp}$ cannot influence the semi-major axis.
- Because $\delta v_{\parallel}$ and $\delta v_{\perp \mathrm{O}}$ are in the orbital plane, they cannot change those orbital elements that determine the orientation of the orbital plane, that is i and Ω. On the other hand, $\delta v_{\perp\perp}$ changes only the orientation of the orbital plane and therefore cannot change a and e. This is why above we called it plane change maneuver.

So, from these general considerations alone we are able to exclude the impact of the kick-burns on some of the orbital elements, which are indicated by empty white boxes in Table 8.1.

Given this decomposition we are now able to analyze the sensitivity of the orbital elements to these elementary kick-burns. The corresponding relations can be derived (exercise, Problem 8.6a) from the Gaussian variational Eq. (12.1.2) with transformations (see Fig. 8.2).

Table 8.1 The effects (matrix elements) of the three different kinds of kick-burns on the orbital elements at the special orbit positions (rightmost column)

	$\delta v_{\parallel}/v_h$	$\delta v_{\perp O}/v_h$	$\delta v_{\perp\perp}/v_h$	
$\delta a/a$	$2/(1\mp e)$			Peri/ Apoapsis $\theta = 0°$ $\theta = 180°$
δe	± 2	–		
$\delta \omega$	–	$\mp 1/e$	○	
δi			$\pm c_{\pm}$	Nodes $\omega + \theta = 0°$ $\omega + \theta = 180°$
$\delta \Omega$			–	
$\delta \omega$	○	○	–	
δi			–	Orthogonal to nodes $\omega + \theta = +90°$ $\omega + \theta = -90°$
$\delta \Omega$			$\pm s_{\pm}/\sin i$	
$\delta \omega$	○	○	$\mp s_{\pm} \cot i$	

White boxes and relations not shown in this table indicate that there are no effects at any orbit position. Dark gray boxes give the dependencies: a dash indicates that for this orbit position the effect vanishes, open circles denote complex dependencies without practical use, and the terms displayed are the factors, that multiplied with the kick-burn of that column gives the change of orbital element of that row. The upper/lower signs correspond to the upper/lower orbit positions in the orbit position column

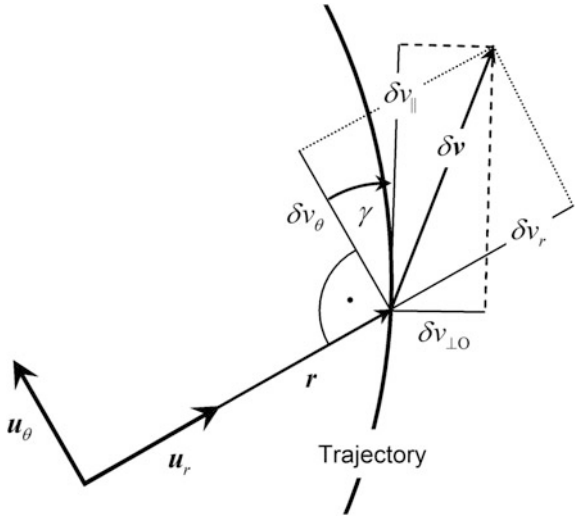

Fig. 8.2 Decomposition of the kick-burn vector in the two different reference systems

$$a_r = \delta v_r = \cos\,\gamma \cdot \delta v_{\perp \mathrm{O}} + \sin\,\gamma \cdot \delta v_{||}$$
$$a_\theta = \delta v_\theta = -\sin\gamma \cdot \delta v_{\perp \mathrm{O}} + \cos\,\gamma \cdot \delta v_{||}$$

and with $\sin\gamma, \cos\gamma$ from Eq. (7.3.16) to get

$$\begin{aligned}
\frac{\delta a}{a} &= \frac{2v}{(1-e^2)v_h}\frac{\delta v_{||}}{v_h} + 0 \cdot \delta v_{\perp \mathrm{O}} + 0 \cdot \delta v_{\perp\perp} \\
\delta e &= 2(e + \cos\theta) \cdot \frac{\delta v_{||}}{v} + \frac{(1-e^2)\sin\theta}{1 + e\cos\theta} \cdot \frac{\delta v_{\perp \mathrm{O}}}{v} + 0 \cdot \delta v_{\perp\perp} \\
\delta i &= 0 \cdot \delta v_{||} + 0 \cdot \delta v_{\perp \mathrm{O}} + \frac{\cos(\theta+\omega)}{1 + e\cos\theta}\frac{\delta v_{\perp\perp}}{v_h} \\
\delta\Omega &= 0 \cdot \delta v_{||} + 0 \cdot \delta v_{\perp \mathrm{O}} + \frac{\sin(\theta+\omega)}{(1 + e\cos\theta)\sin i}\frac{\delta v_{\perp\perp}}{v_h} \\
\delta\omega &= \frac{2\sin\theta}{e} \cdot \frac{\delta v_{||}}{v} - \left(1 + \frac{1}{e}\frac{e + \cos\theta}{1 + e\cos\theta}\right) \cdot \frac{\delta v_{\perp \mathrm{O}}}{v} - \frac{\sin(\theta+\omega)\cot i}{1 + e\cos\theta}\frac{\delta v_{\perp\perp}}{v_h}
\end{aligned} \tag{8.1.1}$$

where

$$v = v_h\sqrt{1 + 2e\,\cos\,\theta + e^2}$$

and

$$v_h := \frac{\mu}{h} = \sqrt{\frac{\mu}{a(1-e^2)}}$$

which corresponds to the orbital velocity at the orbit angle $\cos\theta = -e/2$.

Note *In a circular orbit θ and ω are undefined and therefore the impact of a kick-burn on most orbital elements cannot be determined from* Eq. (8.1.1). *We will treat maneuvers in circular orbits separately in* Sect. 8.1.2.

For practical purposes there are six special orbit positions for optimal firing, which are given in Table 8.1 in the rightmost column. The matrix of the table shows how the three different normalized kick-burns (entries of the three middle columns) at the given special positions affect the different orbital elements (row headings). A dash denotes that the effect just vanishes at this position; a circle denotes that the term describing the effect is more complex and of no practical use; the given terms are the factors, that multiplied by the normalized kick-burn from the column entry deliver the change of orbital element given in the row entry. The important point is, that at the six positions the orbital elements are both selectively and optimally affected, where "optimally" means that for a given change of orbital elements the utilized propulsion mass is minimal. The coefficients shown in the terms are

$$c_{\pm}(\omega) = \frac{1}{1 \pm e \cos \omega} \tag{8.1.2}$$

$$s_{\pm}(\omega) = \frac{1}{1 \pm e \sin \omega} \tag{8.1.3}$$

Note that possible changes of the orbital period are derived via Eq. (7.4.12) to be

$$\frac{\delta T}{T} = \frac{3}{2}\frac{\delta a}{a} \tag{8.1.4}$$

So, only tangential kick-burns effect the orbital period. But tangential burns at the periapsis or apoapsis always change the semi-major axis jointly with the eccentricity according to Table 8.1. The reason is as follows. As for a kick-burn in the peri-/apoapsis, this orbital point is also the peri-/apoapsis for the initial ellipse and the target ellipse, the following is valid:

$$const = r_{apo/per} = a(1 \pm e)$$

Differentiating this equation delivers $0 = \delta a(1 \pm e) \pm a \cdot \delta e$ and hence

$$\frac{\delta a}{a} = -\frac{\delta e}{e \pm 1} \quad @\ \delta v_{||} \quad \text{kick-burn at apo-/periapsis} \tag{8.1.5}$$

Change of Eccentricity

There exists an orbit position not given in Table 8.1, at which with a $\delta v_{\perp O}$ kick-burn the eccentricity can be changed selectively, that is without effecting other orbital elements, namely a or ω. This is from Eq. (8.1.1) position $(e + \cos \theta)/(1 + e \cos \theta) = -e$ or

$$\cos \theta = -\frac{2e}{1 + e^2} \tag{8.1.6}$$

The change at this position amounts to

$$\delta e = \pm\sqrt{1 + e^2}\,\frac{\delta v_{\perp O}}{v_h} \quad \text{where} \quad \begin{matrix} + : & 90^\circ \le \theta < 180^\circ \\ - : & 180^\circ < \theta \le 270^\circ \end{matrix} \tag{8.1.7}$$

However, the following two-impulse maneuver is more efficient to just change the eccentricity and therefore is widely used, in particular in GEO. If one kick-burn $\delta v_{||,\theta}$ is performed at θ in the orbit and another one with $\delta v_{||,180} = -\delta v_{||.\theta}$ at $\theta + 180^\circ$, i.e. at the opposite side of the orbit and in the opposite direction, we get in total

$$\delta e = 4 \cos \theta \left[1 + e \cos \theta + O\left(e^2\right)\right] \cdot \frac{\delta v_{||,\theta}}{v(\theta)}$$

From this we see that eccentricity corrections are most efficient at the peri/apoapsis (or anywhere in a circular orbit, see Sect. 8.1.2) where we have

$$\delta e = 4 \cdot \frac{\delta v_{||,per}}{\sqrt{\mu/a}} \cdot \left[1 + O\left(e^2\right)\right] \tag{8.1.8}$$

Thus the eccentricity can be increased by one kick-burn $\delta v_{||,per} > 0$ at the periapsis and a second with $-\delta v_{||,per} < 0$ at the apoapsis, and can be decreased by the same procedure with reversed kick-burn directions.

If we assume the same total delta-v as in the one-impulse maneuver above, i.e., $\left|\delta v_{||,per}\right| = \delta v_{\perp \mathrm{O}}/2$, then

$$\delta e \approx \pm 2 \cdot \frac{\delta v_{\perp \mathrm{O}}}{\sqrt{\mu/a}} \left[1 + O\left(e^2\right)\right]$$

which for $e \to 0$ is twice as efficient as the one-impulse maneuver given in Eq. (8.1.7).

Change of Semi-major Axis

We have seen above that it is not possible to separate changes in semi-major axis from changes in eccentricity at one kick-burn. But this is different for a two-impulse maneuver. If one kick-burn $\delta v_{||,\theta}$ is performed at θ in the orbit and the other

$$\frac{\delta v_{||,180}}{v_{180}} = \frac{\cos\,\theta + e}{\cos\,\theta - e} \frac{\delta v_{||,\theta}}{v_\theta} \tag{8.1.9}$$

at $\theta + 180°$, i.e., at the opposite side of the orbit and in the same direction, then $\delta e = 0$ and we get for changes in the semi-major axis

$$\frac{\delta a}{a} = \frac{2}{1 - e^2} \left(\frac{v_\theta^2}{v_h^2} + \frac{\cos\,\theta + e}{\cos\,\theta - e} \frac{v_{180}^2}{v_h^2} \right) \frac{\delta v_{||,\theta}}{v_\theta}$$

and after some expansions

$$\begin{aligned} \frac{\delta a}{a} &= \frac{4\,\cos\,\theta}{\cos\,\theta - e} \frac{\delta v_{||,\theta}}{v_\theta} \\ \delta e &= 0 \end{aligned} \tag{8.1.10a}$$

This reduces for a circular orbit to $\delta v_{||,180} = \delta v_{||,\theta}$ and $\cos\theta = 1$ (see Sect. 8.1.2) and hence

$$\begin{aligned} \delta v_{||,180} &= \delta v_{||,\theta} =: \delta v_{||} \\ \frac{\delta a}{a} &= 4 \frac{\delta v_{||}}{\sqrt{\mu/a}} \\ \delta e &= 0 \end{aligned} \quad @\ e = 0 \tag{8.1.10b}$$

This two-impulsive maneuver is quite common to raise a satellite at its end of life into a higher graveyard orbit.

Change of Periapsis and Apoapsis Radius

We finally note that the periapsis and apoapsis radius r_{per} and r_{apo} can be changed selectively by kick-burns $\delta v_{||,\,apo}$ and $\delta v_{||,\,per}$, respectively, which is highly relevant for orbit maintenance. To show how this comes about we start out again with the above equation

$$r_{apo} = a(1+e)$$

Differentiating this equation yields

$$dr_{apo} = (1+e)\cdot da + a\cdot de$$

hence

$$\frac{dr_{apo}}{r_{apo}} = \frac{da}{a} + \frac{de}{1+e}$$

From Table 8.1 we get

$$\frac{\delta r_{apo}}{r_{apo}} = \left(\frac{2}{1-e} + \frac{2}{1+e}\right)\frac{\delta v_{||,\,per}}{v_h}$$

and finally with $v_h = \sqrt{\mu/[a(1-e^2)]}$

$$\begin{aligned}\frac{\delta r_{apo}}{r_{apo}} &= \frac{4}{\sqrt{1-e^2}}\frac{\delta v_{||,\,per}}{\sqrt{\mu/a}}\\ \frac{\delta r_{per}}{r_{per}} &= \frac{4}{\sqrt{1-e^2}}\frac{\delta v_{||,\,apo}}{\sqrt{\mu/a}}\end{aligned} \tag{8.1.11}$$

where the second equation follows by the same procedure with $r_{per} = a(1-e)$. We hence see that an apse can be lowered or raised by a corresponding kick burn at the apse *opposite* to the one to be changed.

Change of Angular Elements

As seen from Eq. (8.1.1), the angular elements Ω, i can be changed solely by plane change maneuvers $\delta v_{\perp\perp}$

$$\begin{aligned}\delta i &= \frac{\cos(\theta+\omega)}{1+e\,\cos\,\theta}\frac{\delta v_{\perp\perp}}{v_h}\\ \delta\Omega &= \frac{\sin(\theta+\omega)}{(1+e\,\cos\,\theta)\sin\,i}\frac{\delta v_{\perp\perp}}{v_h}\end{aligned}$$

Although the argument of periapsis ω changes for any kick-burn, we neglect it here, because Earth orbits are mostly circular, in case of which ω is irrelevant, or orbits are near-circular and hence the role of ω negligible.

From the above it follows that inclination can be changed selectively and optimally at the two orbital nodes $\omega+\theta=0,\ 180^\circ$

$$\delta i=\pm\frac{1}{1\pm e\,\cos\,\omega}\frac{\delta v_{\perp\perp}}{v_h}\quad @\quad \begin{matrix}+:&\omega+\theta=0^\circ\\-:&\omega+\theta=180^\circ\end{matrix}\tag{8.1.12}$$

Observe that for a given kickburn $\delta v_{\perp\perp}$, the angular elements $\delta\Omega,\delta\omega$ change in the same way except with opposite sign. Therefore a RAAN change by $\delta v_{\perp\perp}$ comes always hand in hand with a change of argument of periapsis, even if two kick-burns in any direction are performed at opposite abeam positions.

RAAN is changed selectively at orbital positions abeam from the nodal points according to

$$\delta\Omega=\pm\frac{1}{(1\pm e\,\cos\,\omega)\sin\,i}\frac{\delta v_{\perp\perp}}{v_h}\quad @\quad \begin{matrix}+:&\omega+\theta=90^\circ\\-:&\omega+\theta=-90^\circ\end{matrix}\tag{8.1.13}$$

Note that is a matter of kick-burn direction $\delta v_{\perp\perp}>0$, $\delta v_{\perp\perp}<0$ to determine whether at a given abeam position RAAN change is positive or negative. Also note that if the orbit has a small eccentricity or acquires it due to gravitational perturbations (see Sect. 12.3.4) with an often unknown argument of periapsis, then two smaller kick-burns with opposite directions and half the magnitude, $\pm\frac{1}{2}\delta v_{\perp\perp}$ at the two different positions yield the simple results

$$\delta i=\frac{\delta v_{\perp\perp}}{v_h}$$
$$\delta\Omega=\frac{1}{\sin\,i}\frac{\delta v_{\perp\perp}}{v_h}\left(1+O\left(e^2\right)\right)$$

8.1.2 *Elementary Maneuvers in Circular Orbits*

The most common orbits around planets are circular orbits, $e=0$, because at a given orbital energy they minimize atmospheric drag and provide steady orbit conditions. But circular orbits do not exhibit a periapsis line, implying an undefined true anomaly θ and argument of periapsis ω. Therefore, the change of orbital elements cannot be determined from Eq. (8.1.1) and Table 8.1. We have to fall back on more basic considerations to treat this problem.

Change of the Semi-major Axis

An exception is δa for which we immediately derive from Eq. (8.1.1), for $e=0$ and hence $v=v_h=\sqrt{a/\mu}$,

$$\frac{\delta a}{a}=2\sqrt{\frac{a}{\mu}}\,\delta v_{\parallel}+0\cdot\delta v_{\perp\mathrm{O}}+0\cdot\delta v_{\perp\perp}$$

To determine $\delta e,\ \delta i$, and $\delta\Omega$ ($\delta\omega$ is irrelevant for circular orbits), we have to take a different approach.

Change of Eccentricity

For δe we go back to the key Eq. (7.3.3) for the eccentricity that reads with $\mu/r = v^2$

$$\mu \boldsymbol{e} = \left(v^2 - \frac{\mu}{a}\right)\boldsymbol{r} - (\boldsymbol{r}\boldsymbol{v})\boldsymbol{v}$$

A $\delta v_{||}$ kick-burn implies $\boldsymbol{\delta v}_{||} \perp \boldsymbol{r}$ in a circular orbit. The velocity after the kick-burn is, therefore, $v = v_0 + \delta v_{||}$, with $v_0^2 = \mu/a = v_h^2$. For the eccentricity after the kick-burn we thus obtain

$$\mu \boldsymbol{e} = \left(v_0^2 + 2\delta v_{||} v_0 - v_0^2\right)\boldsymbol{r} - 0 = 2\delta v_{||} v_0 \boldsymbol{r}$$

Because at kick-burn $\boldsymbol{e} || \boldsymbol{r}$ applies, we have $\theta = 0°$ at that moment. As we had $e = 0$ before the kick-burn we get

$$\delta e = 2\delta v_{||} v_0 \frac{r}{\mu} = 2\delta v_{||} \frac{v_0}{v_0^2} = 2\frac{\delta v_{||}}{v_h}$$

If we perform a $\delta v_{\perp \mathrm{O}}$ kick-burn in a circular orbit, then $\boldsymbol{\delta v}_{\perp \mathrm{O}} || \boldsymbol{r}$ and $\boldsymbol{\delta v}_{\perp \mathrm{O}} \perp \boldsymbol{v}_0$ and therefore $v = v_0$. This renders

$$\mu \boldsymbol{e} = 0 - (\boldsymbol{r}\boldsymbol{v}_0)\boldsymbol{v} - (\boldsymbol{r} \cdot \delta \boldsymbol{v}_{\perp \mathrm{O}})\boldsymbol{v} = -r \cdot \delta v_{\perp \mathrm{O}} \boldsymbol{v}$$

Therefore the S/C right after the kick-burn is at $\theta = 90°$, and because $r = a$, we find

$$\delta e = \frac{a}{\mu} v \cdot \delta v_{\perp \mathrm{O}} = \frac{\delta v_{\perp \mathrm{O}}}{v_h}$$

Change of Inclination

For the inclination change Eq. (8.1.1) yields for a circular orbit

$$di = \cos(\omega + \theta) \cdot \frac{dv_{\perp\perp}}{v_h}$$

On the other hand, according to Fig. 8.4, the change of inclination should be just

$$\delta i = \frac{\delta v_{\perp\perp}}{v} = \frac{\delta v_{\perp\perp}}{v_h}$$

This implies $\omega + \theta = 0$.

Change of RAAN

Finally, we obtain with the condition $\omega + \theta = 0$ for the change of RAAN

$$\delta\Omega = \frac{\sin(\omega+\theta)}{(1+e\,\cos\,\theta)\sin\,i}\frac{dv_{\perp\perp}}{v_h} = 0\cdot\frac{dv_{\perp\perp}}{v_h}$$

Summary
Summing up we find the following expressions of the change of orbital elements of a circular orbit due to kick-burns

$$\begin{pmatrix}\delta a/a\\ \delta e\\ \delta i\\ \delta\Omega\end{pmatrix} = \sqrt{\frac{a}{\mu}}\begin{pmatrix}2 & 0 & 0\\ 2 & 1 & 0\\ 0 & 0 & 1\\ 0 & 0 & 0\end{pmatrix}\begin{pmatrix}\delta v_{||}\\ \delta v_{\perp \mathrm{O}}\\ \delta v_{\perp\perp}\end{pmatrix} \tag{8.1.14}$$

After $\delta v_{||}$, $\delta v_{\perp \mathrm{O}}$ kick-burns the orbit is elliptic with a true anomaly

$$\theta = \begin{cases} 0^\circ & @\ \delta v_{||}\\ 90^\circ & @\ \delta v_{\perp \mathrm{O}}\end{cases} \tag{8.1.15}$$

Note that this true anomaly plus the position on the circular orbit (argument of latitude u, see Sect. 7.3.5) where the kick-burn was performed determine the induced argument of periapsis ω of the final ellipse: $\omega = u - \theta$.

After a $\delta v_{\perp\perp}$ kick-burn in a circular orbit with initial inclination $i = 0$ the final inclination of the circular orbit is $i = \delta i$ and the position on the orbit is

$$u = \omega + \theta = \begin{cases} 0^\circ & @\ \delta v_{\perp\perp} > 0\\ 180^\circ & @\ \delta v_{\perp\perp} < 0\end{cases} \tag{8.1.16}$$

8.1.3 General Maneuvers

We now want to study arbitrary finite one-impulse maneuvers, which at a given point $\boldsymbol{r}$ in space transfers the state vector $(\boldsymbol{r}, \boldsymbol{v}_1)$ of the initial orbit into the state vector $(\boldsymbol{r}, \boldsymbol{v}_2)$ of the final orbit as depicted in Fig. 8.3. From the vector triangle we hence get very generally

$$\Delta\boldsymbol{v} = \boldsymbol{v}_2 - \boldsymbol{v}_1$$

To determine the corresponding propulsion demand, one has to square this equation and take the root on both sides, resulting in

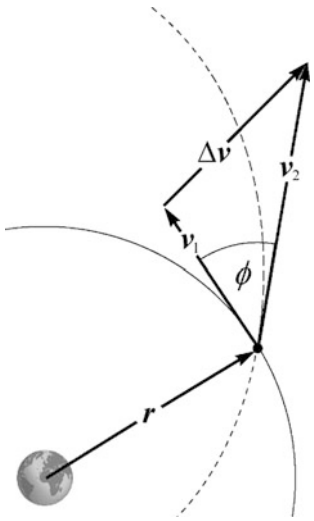

Fig. 8.3 The general one-impulse maneuver

$$\begin{aligned}\Delta v &= \sqrt{v_1^2 + v_2^2 - 2v_1 v_2 \cos\,\phi} \\ &= \sqrt{(v_1 - v_2)^2 + 4v_1 v_2 \sin^2(\phi/2)}\end{aligned} \tag{8.1.17}$$

where ϕ is the **transition angle** enclosed between $\boldsymbol{v}_1$ and $\boldsymbol{v}_2$. This is the most general equation to calculate a single-burn delta-v.

Oberth Effect

There exists a general effect, the Oberth effect, governing some types of orbit transfers. Suppose we move on a Keplerian orbit from any position with state elements r, v to another position with state elements r', v'. Then the vis-viva equation states that the total energy at both positions must be the same

$$v^2 - \frac{2\mu}{r} = v'^2 - \frac{2\mu}{r'}$$

Now let's suppose we do a boost Δv at r. We then want to know: How much is the velocity increase $\Delta v'$ at any other r'? Or in general: How does the increase in velocity impart different radial distances? The according energy equation with boost reads

$$(v + \Delta v)^2 - v^2 = \Delta v(2v + \Delta v) = \Delta v'(2v' + \Delta v') = (v' + \Delta v')^2 - v'^2$$

or

$$\Delta v = \Delta v' \frac{v' + \Delta v'/2}{v + \Delta v/2}$$

This is a telling result. It claims that for a given $\Delta v'$ the required boost Δv to achieve it at radial distances $0 < r \leq r'$, equalling $\infty > v \geq v'$, changes monotonically in the interval

$$0 < \Delta v \leq \Delta v'$$

So, the boost Δv to achieve $\Delta v'$ is minimal at the lowest orbital radius and hence highest velocity v of the orbit. This unexpected effect is called the *Oberth effect*, after Hermann Oberth, an Austro-Hungarian-born rocket scientist who discovered this effect in 1929. It is due to the fact that although momentum changes Δv are key for fuel considerations and thus mission design, energy conservation calling for $(v + \Delta v)^2 - v^2$ governs the motion.

This effect sounds powerful, yet its application is quite limited in space flight, because any boost at a given position in orbit also changes the orbital elements and hence the further trajectory. This is usually not what the mission designer asked for. So, a key phrase describing the Oberth effect above is "How does the increase in velocity impart another radial distance?", rather than "… achieves a given target point". There are three cases where "solely an increase in radial distance" is sufficient. One is for the transfer from an ellipse to a (near)-circular target orbit, which we examine in Sect. 8.3.3. The second is an initial elliptic orbit, usually in LEO, the line of apsides of which is adjustable by the injection conditions or orbit maintenance (keep this important case always in mind); and finally the powered flyby (see Sect. 9.5.3) where the change in flight direction can be counteracted by an adjusted impact parameter, i.e., flyby distance.

Two-Burn Escape Maneuvers

As already suggested by Hermann Oberth in 1928, the consequent application of the Oberth effect gives rise to making escape transfers more efficient. Rather than performing an Oberth maneuver (see Eq. (7.4.26)) at the lowest orbital radius to escape the gravity well, the spacecraft first performs a breaking maneuver (first maneuver) to dive down into the central body's gravity well for a flyby (nicknamed *solar fryby* for a solar flyby). Then at its periapsis an Oberth maneuver (second maneuver) is performed to accelerate the spacecraft to escape speed. According to the Oberth effect, such a two-burn maneuver is more efficient than the direct single-burn Oberth maneuver.

8.1.4 Tangent Plane Maneuvers

A general maneuver changes the shape of an orbit, a, e, its orientation ω within the orbital plane, and the orientation of the plane, i, Ω. Practically, the orientation ω of the orbital plane is largely irrelevant, because most of the spacecraft are in a circular orbit having no ω. In addition, for orbit transitions a Hohmann transfer altering a, e jointly with a plane change i, Ω is essential. We read from Eq. (8.1.1) that to solely change a, e and i, Ω only $\delta v_{||}$ and $\delta v_{\perp\perp}$ kick-burns are relevant. This implies that $\boldsymbol{v}_1$ and $\boldsymbol{v}_2$ span a plane, tangent to the orbit at the kick-burn location. This important class of orbit maneuvers is therefore called *tangent plane maneuvers*. Figure 8.4 shows a tangent change maneuver with $v_1 = v_2 =: v$, that is, without a, e changes. Such a particular tangent plane maneuver is hence called *genuine plane change maneuver* (see next section).

Transition Angle in Terms of Orbital Elements

The important property of a tangent plane maneuver is that because the plane spaned by $\boldsymbol{v}_1$ and $\boldsymbol{v}_2$ is vertical to the initial and final plane, the maneuver causes a tilt of the initial (index 1) to the final (index 2) orbit about a mutual nodal line, for which $\phi = \angle(\boldsymbol{v}_1, \boldsymbol{v}_2) = \angle(\boldsymbol{I}_1, \boldsymbol{I}_2)$ holds. Here $\boldsymbol{I}$ is the three-dimensional inclination vector (see Eq. (7.3.25)) given as

$$\boldsymbol{I} = \begin{pmatrix} \sin\Omega \sin i \\ -\cos\Omega \sin i \\ \cos i \end{pmatrix}_{IJK}$$

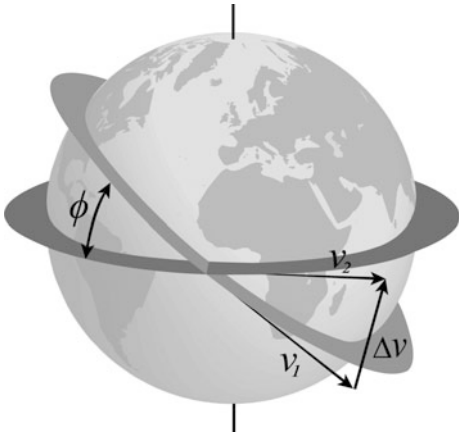

Fig. 8.4 A tangent plane maneuver with $v_1 = v_2$ (a.k.a. genuine plane change maneuver) in a circular orbit. The point where the maneuver takes place is the node of the mutual nodal line between the initial and final orbit plane

With this the transition angle is determined by

$$\cos\phi = \hat{\boldsymbol{v}}_1\hat{\boldsymbol{v}}_2 = \boldsymbol{I}_1\boldsymbol{I}_2 = \sin i_1 \sin i_2 \cos\Delta\Omega + \cos i_1 \cos i_2$$

or after some trigonometric modifications alternatively

$$\sin^2\frac{\phi}{2} = \sin^2\frac{\Delta i}{2} + \sin i_1 \sin i_2 \sin^2\frac{\Delta\Omega}{2} \tag{8.1.18}$$

where $\Delta i := i_2 - i_1$ and $\Delta\Omega := \Omega_2 - \Omega_1$. Obviously, the vector $\boldsymbol{N}$ of the nodal line between the initial and final orbit is given by

$$\boldsymbol{N} = \boldsymbol{I}_1 \times \boldsymbol{I}_2 \tag{8.1.19}$$

Maneuvers with either Inclination Change or RAAN Change
There are two special plane change maneuvers, which are of practical interest. One, in which the RAAN is kept constant, $\Delta\Omega = 0$. We thus obtain from Eq. (8.1.18)

$$\begin{aligned}\phi &= \Delta i\\ \Delta v &= \sqrt{v_1^2 + v_2^2 - 2v_1v_2\cos\Delta i}\end{aligned} \quad @\ \Delta\Omega = 0 \quad \textbf{nodal transfer} \tag{8.1.20}$$

According to Table 8.1 this plane tilt is achieved for a $\Delta\boldsymbol{v}$ that lies in either plane tangent to the two nodes of the initial orbit with the reference plane. Such transfers are therefore called *nodal transfers* and are the most frequently used plane change maneuvers.

The other special case is achieved if the inclination is kept constant, $\Delta i = 0$. We thus have from Eq. (8.1.18)

$$\begin{aligned}\sin(\phi/2) &= \sin i \cdot |\sin(\Delta\Omega/2)|\\ \Delta v &= \sqrt{(v_1 - v_2)^2 + 4v_1v_2\sin^2 i \sin^2(\Delta\Omega/2)}\end{aligned} \quad @\ \Delta i = 0 \tag{8.1.21}$$

According to Table 8.1 $\Delta i = 0$ is achieved for a $\Delta\boldsymbol{v}$ that lies in either plane tangent to the two points at 90° abeam from the nodes of the initial orbit with the reference plane.

8.1.5 *Genuine Plane Change Maneuvers*

We finally study just plane change maneuvers without a change in orbital velocity, $v_1 = v_2 =: v$ as depicted in Fig. 8.4. Because we now apply only a $\delta v_{\perp\perp}$ kick-burn, genuine plane change maneuvers are a subset of tangent plane maneuvers, which

according to Eq. (8.1.1) only change i, Ω, ω. From Eq. (8.1.17) we derive for $v = v_1 = v_2$ quite generally

$$\Delta v = 2v \cdot \left| \sin \frac{\phi}{2} \right| \quad @ \quad v := v_1 = v_2 \tag{8.1.22}$$

Because $\Delta v \propto v$ we find the general rule of thumb

Plane Change Rule
An orbit plane change should be performed at the smallest possible orbital velocity, i.e. at best at the apoapsis.

For this reason it might be even preferable to bring the vehicle first into a higher orbit, change the plane there at apoapsis at low speed and low budget, and finally take it back to its original orbit. It is this principle, that the bi-elliptic transfer (Sect. 8.4.2) and the super-synchronous transfer (Sect. 8.4.3) make use of.

Genuine Inclination Change Maneuver
For $\Omega_1 = \Omega_2$ we have from Eq. (8.1.20) $\phi = \Delta i$. We hence obtain from Eq. (8.1.22)

$$\Delta v = 2v \cdot \left| \sin \frac{\Delta i}{2} \right| \quad @ \; v := v_1 = v_2, \; \Delta\Omega = 0 \tag{8.1.23}$$

According to Table 8.1 this tilt is achieved for a $\Delta \boldsymbol{v}$ that lies in either plane tangent to the two nodes of the initial orbit with the reference plane and is orthogonal to the plane bisecting the old and new orbit plane.

Genuine RAAN Change Maneuver
For $\Delta i = 0$ we have from Eq. (8.1.21)

$$\Delta v = 2v \cdot \sin i \cdot \left| \sin \frac{\Delta\Omega}{2} \right| \quad @ \; v := v_1 = v_2, \Delta i = 0 \tag{8.1.24}$$

This is the effort to rotate the inclination vector by $\Delta\Omega$ about the K-axis in the geocentric equatorial reference frame. According to Table 8.1 this rotation is achieved for a $\Delta \boldsymbol{v}$ that lies in either plane tangent to the two points at 90° abeam from the nodes of the initial orbit with the reference plane. Obviously, a RAAN change by $\Delta\Omega = 180°$ is identical to an inclination change by $\Delta i = 2i$.

Because $\Delta v \propto v \sin i$ we find the general rule of thumb.

RAAN Change Rule
Adjust RAAN at the lowest inclination and/or orbital velocity possible.

8.1.6 Tangent Maneuver

Another quite special case of a tangent plane maneuver is $\phi = 0°$, i.e., the burn is along the direction of motion. We call this a *tangent maneuver* for which from Eq. (8.1.17) follows

$$\Delta v_{||} = |v_2 - v_1| \quad @ \quad \phi = 0° \tag{8.1.25}$$

From Eq. (8.1.1) we see that such a maneuver changes a, e, ω. As we will see in Sect. 8.3.1 this is the most efficient maneuver to increase the size of an orbit and hence to transfer to an outer orbit.

Let us assume we are in an initial orbit with a_1, e_1, ω_1 and perform at $r := r_1 = r_2$ a tangent maneuver $r, v_1, \theta_1 \rightarrow r, v_2, \theta_2$ with

$$v_2 = v_1 \pm \Delta v_{||} \tag{8.1.26}$$

We want to know what is a_2, e_2, ω_2? From the vis-viva Eq. (7.2.15) we immediately find

$$\frac{1}{a_2} = \frac{2}{r} - \frac{v_2^2}{\mu} \tag{8.1.27}$$

To determine the other modified orbital elements we make use of the fact that a tangent maneuver obviously does not change the flight path angle $\gamma := \gamma_1 = \gamma_2$ (see Sect. 7.3.3). From Eq. (7.3.16) we derive the relationships

$$v \cos\gamma = \frac{h}{r}$$
$$\frac{1}{2} v^2 \sin 2\gamma = \frac{\mu}{r} e \sin\theta$$

Applying these equations to the orbits before and after the tangent maneuver we find

$$\frac{v_2}{v_1} = \frac{h_2}{h_1} = \frac{a_2\left(1 - e_2^2\right)}{a_1\left(1 - e_1^2\right)}$$

$$\frac{v_2^2}{v_1^2} = \frac{e_2 \sin\theta_2}{e_1 \sin\theta_1}$$

from which we derive

$$e_2 = \sqrt{1 - \frac{a_1 v_2}{a_2 v_1}\left(1 - e_1^2\right)} \tag{8.1.28}$$

$$\sin\,\theta_2 = \frac{v_2^2}{v_1^2}\frac{e_1}{e_2}\sin\,\theta_1 \tag{8.1.29}$$

To finally determine ω_2 we make use of the fact that a tangent maneuver also does not change the argument of latitude $u = \omega + \theta$ (see Sect. 7.3.5). We hence obtain

$$\omega_2 = \omega_1 + \theta_1 - \theta_2 \tag{8.1.30}$$

Example (GEO Positioning)

Let us assume that a communication satellite is launched with an ATLAS rocket from Cape Canaveral with orbital inclination $i_L = 28°$ after launch and needs to be positioned in GEO (see Berlin (2005)). As we will see in Sect. 12.6.1, due to lunisolar perturbations an optimum initial state in GEO would be $i_{GEO} = 3°$, $\Omega_{GEO} = 280°$. After launch and at the descending node the rocket will make an injection burn at $r_{LEO} = 6578.14$ km into the GTO with apoapsis at $r_{GEO} = 42{,}166$ km. Because the descending node happens to coincide with the Greenwich meridian we have $\Omega_{GTO} = 180°$.

To place the satellite in its final orbit position we have the choice of many different maneuver sequences for all of which are based on the following velocities before (−) and after (+) the kick-burns in LEO and GEO (see Eqs. (7.4.3) and (7.4.10)):

$$\begin{aligned} v_{LEO-} &= 7.784\,\mathrm{km\,s^{-1}} \\ v_{LEO+} &= 10.239\,\mathrm{km\,s^{-1}} \end{aligned} \quad \text{and} \quad \begin{aligned} v_{GEO-} &= 1.597\,\mathrm{km\ s^{-1}} \\ v_{GEO+} &= 3.075\,\mathrm{km\ s^{-1}} \end{aligned}$$

We now study exemplarily four different maneuvering sequences with the following total delta-v:

Sequence 1

- At the descending node after launch an inclination change maneuver ((Eq. (8.1.20) into Eq. (8.1.17)) is made that brings the satellite into a GTO with $i_{GEO} = 3°$, $\Omega_{GTO} = 180°$.
- At apogee a genuine RAAN change maneuver (see Eq. (8.1.24)) changes the orbit plane to $\Omega_{GEO} = 280°$.
- Finally, a tangent maneuver (see Eq. (8.1.25)) brings the satellite into a circular GEO.

$$\begin{aligned}\Delta v &= \sqrt{v_{LEO-}^2 + v_{LEO+}^2 - 2v_{LEO-}v_{LEO+}\cos(28^\circ - 3^\circ)} \\ &\quad + 2v_{GEO-}\sin 3^\circ \cdot \sin[(280^\circ - 180^\circ)/2] + (v_{GEO+} - v_{GEO-}) \\ &= 4.578 + 0.128 + 1.478 = 6.184\,\text{km s}^{-1}\end{aligned}$$

Sequence 2

- At the descending node after launch a tangent maneuver transfers the satellite into a GTO, i.e., $i_{GTO} = 28^\circ,\ \Omega_{GTO} = 180^\circ$.
- At apogee a genuine RAAN change maneuver (see Eq. (8.1.24)) changes the orbit plane to $\Omega_{GEO} = 280^\circ$.
- Finally, a inclination change maneuver (Eq. (8.1.20) into Eq. (8.1.17)) is performed that circularizes the satellite into GEO at $i_{GEO} = 3^\circ$.

$$\begin{aligned}\Delta v &= (v_{LEO+} - v_{LEO-}) + 2v_{GEO-}\sin 28^\circ \cdot \sin[(280^\circ - 180^\circ)/2] \\ &\quad + \sqrt{v_{GEO-}^2 + v_{GEO+}^2 - 2v_{GEO-}v_{GEO+}\cos(28^\circ - 3^\circ)} \\ &= 2.455 + 1.149 + 1.762 = 5.366\,\text{km s}^{-1}\end{aligned}$$

Sequence 3

1. At the descending node after launch a tangent maneuver transfers the satellite into a GTO, i.e., $i_{GTO} = 28^\circ,\ \Omega_{GTO} = 180^\circ$.
2. At apogee a genuine inclination change maneuver (see Eq. (8.1.23)) changes the inclination to $i_{GEO} = 3^\circ$.
3. Still at apogee it is immediately followed by a genuine RAAN change maneuver (see Eq. (8.1.24)) that changes the orbit plane to $\Omega_{GEO} = 280^\circ$.
4. Finally, the orbit is circularized with an apogee kick-burn.

$$\begin{aligned}\Delta v &= (v_{LEO+} - v_{LEO-}) + 2v_{GEO-}\cdot\sin 12.5^\circ \\ &\quad + 2v_{GEO-}\sin 3^\circ \cdot \sin[(280^\circ - 180^\circ)/2] + (v_{GEO+} - v_{GEO-}) \\ &= 2.455 + 0.691 + 0.128 + 1.478 = 4.752\,\text{km s}^{-1}\end{aligned}$$

Sequence 4

- At the descending node the satellite is transferred into a GTO, i.e., $i_{GTO} = 28^\circ, \Omega_{GTO} = 180^\circ$.
- At apogee, an inclination-change maneuver (Eq. (8.1.20) into Eq. (8.1.17)) is performed such that the orbit is circularized at $i_{GEO} = 3^\circ$.
- Finally, a genuine RAAN change maneuver (see Eq. (8.1.24)) positions the satellite at $\Omega_{GEO} = 280^\circ$.

$$\begin{aligned}\Delta v &= (v_{LEO+} - v_{LEO-}) + \sqrt{v_{GEO-}^2 + v_{GEO+}^2 - 2v_{GEO-}v_{GEO+}\cos(28^\circ - 3^\circ)} \\ &\quad + 2v_{GEO+}\sin 3^\circ \cdot \sin[(280^\circ - 180^\circ)/2] \\ &= 2.455 + 1.762 + 0.247 = 4.464\,\text{km s}^{-1}\end{aligned}$$

The essence of comparing the four sequences is that for GEO positioning an inclination change should be combined with the orbit circularization at apoapsis and RAAN should be adjusted at the lowest possible inclination. This is how GEO positioning is actually performed.

This example corroborates the following rule of thumb, which is based on the fact (see Problem 8.1) that a tangent plane maneuver is always more efficient than a tangent maneuver and plane change maneuver performed sequentially at the same point in space:

All-in-One Rule
If possible combine all orbital changes that need to be done into one kick-burn at one orbital position rather than making single burns at successive positions.

8.2 Lambert Transfer

Having explored the characteristics of one-impulse maneuvers between intersecting orbits we are now set to perform orbital transfers between two conic orbits that do not intersect and therefore require a transfer orbit with two orbital transition maneuvers at each end. The most general case is the so-called Lambert transfer, which we will investigate first. It played an important role in the 1960s for Gemini and Apollo orbital rendezvous. Today, Hohmann transfers are more common, which will be studied in Sect. 8.3.

8.2.1 Orbital Boundary Value Problem

Lambert Transfer
Let us assume that we have a S/C at point P_1 on an conic Earth orbit that needs to transfer to point P_2 on a coplanar conic target orbit, both of which do not intersect. (If they intersect we can perform an one-impulse maneuver at the intersection point, as described in Sect. 8.1, and move from there on the target orbit to point P_2.) Because the orbits and hence also the transfer orbit are coplanar they are fully characterized by their form and orientation to each other, i.e., by three orbital elements, namely $a_i, \boldsymbol{e}_i$ for the initial Earth orbit, $a, \boldsymbol{e}$ for the transfer orbit, and $a_f, \boldsymbol{e}_f$

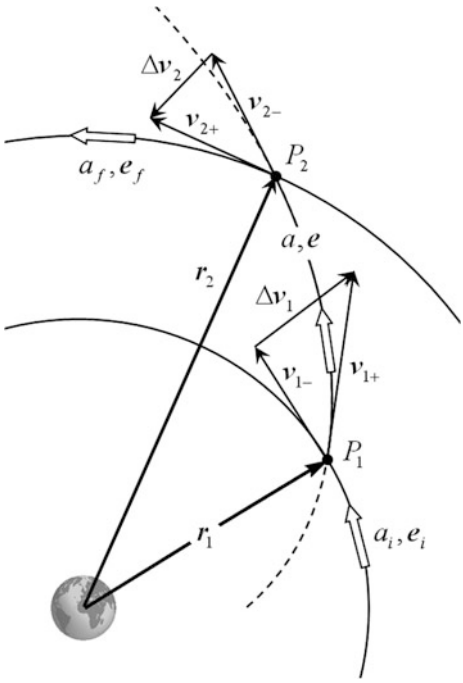

Fig. 8.5 A Lambert transfer (see text for details)

for the final target orbit. The most general description of this problem is that under the influence of a common central gravitational potential a S/C in the initial orbit at P_1 possesses the state vector $(\boldsymbol{r}_1, \boldsymbol{v}_{1-})$ and wants to transfer to P_2 with state vector $(\boldsymbol{r}_2, \boldsymbol{v}_{2+})$. This is a general two-impulse transfer, which we call a *Lambert transfer*, embracing a first impulse maneuver $\Delta\boldsymbol{v}_1$ at P_1 resulting in an unpowered conic coplanar Lambert transfer orbit with orbital elements $a, \boldsymbol{e}$ that ends at P_2 where the second impulse maneuver $\Delta\boldsymbol{v}_2$ takes place.

This can be shown as follows (see Fig. 8.5):

$$(a_i, \boldsymbol{e}_i) \underbrace{[\Delta\boldsymbol{v}_1]}_{P_1} \xrightarrow{a,\boldsymbol{e}} \underbrace{[\Delta\boldsymbol{v}_2]}_{P_2} (a_f, \boldsymbol{e}_f)$$

Lambert transfer

$$(\boldsymbol{r}_1, \boldsymbol{v}_{1-}) \underbrace{-[\Delta\boldsymbol{v}_1]_+}_{P_1} \xrightarrow{a,\boldsymbol{e}} \underbrace{-[\Delta\boldsymbol{v}_2]_+}_{P_2} (\boldsymbol{r}_2, \boldsymbol{v}_{2+})$$

where the $+$ and $-$ signs indicate the situation just before or after an impulse maneuver. Since only the initial and final orbits and P_1 and P_2 are specified, while $\Delta\boldsymbol{v}_1$ and $\Delta\boldsymbol{v}_2$ remain unspecified, there in general exist many different Lambert transfer orbits connecting the two points P_1 and P_2.

Orbital Boundary Value Problem

The problem of finding a transfer orbit connecting two given points P_1 and P_2 is called the *orbital boundary value problem*, which is a special case of the general mathematical *two-point boundary value problem*.

Let us study the orbital boundary value problem by first assuming that just P_1 and P_2 are given through the position vectors $\boldsymbol{r}_1, \boldsymbol{r}_2$. With these we get from the orbit Eqs. (7.3.4) and (7.3.6) the two conditional equations for the three orbital elements $a, \boldsymbol{e}$

$$r_1 + \boldsymbol{e}\boldsymbol{r}_1 = a\left(1 - e^2\right)$$
$$r_2 + \boldsymbol{e}\boldsymbol{r}_2 = a\left(1 - e^2\right)$$

Therefore, two orbital points are not sufficient to unequivocally define a Keplerian transfer orbit, but leave one orbital element undefined. We need a third position vector or an additional scalar specification to concretize the transfer orbit. Solving the orbital boundary value problem by three position vectors is accomplished by Gibbs' method, which will not be investigated here, but see e.g., Vallado (2001) or Curtis (2005). An additional scalar specification might be for instance the transfer time. This famous orbital boundary value problem is called *Lambert's problem* and will be discussed in Sect. 8.2.3.

As we will see in Sect. 8.2.2, even an additional scalar specification generally still leaves the alternative between two so-called *conjugate orbits*: a long path and a short path transfer orbit. Therefore the general orbital boundary value problem for a Lambert transfer to find the orbital elements $a, \boldsymbol{e}$ of the transfer orbit is uniquely defined only by providing the following boundary conditions:

$$\boxed{\begin{array}{l}\boldsymbol{r}_1,\ \boldsymbol{r}_2 \\ +\ \text{an additional scalar specification} \\ +\ \text{a specification for a long or short path transfer orbit}\end{array}} \quad \textbf{boundary conditions} \tag{8.2.1}$$

Given these boundary conditions we are able derive a unique solution $a, \boldsymbol{e}$ to the orbital boundary value problem in the following way. *Suppose we have found the unique transfer orbit by providing p*. According to Battin (1987), the terminal velocities at P_1 and P_2 are then determined as

$$\begin{aligned}\boldsymbol{v}_{1+} &= \frac{\sqrt{\mu p}}{r_1 r_2 \sin(\Delta\theta)}\left[(\boldsymbol{r}_2 - \boldsymbol{r}_1) + \frac{r_2}{p}(1 - \cos\,\Delta\theta)\boldsymbol{r}_1\right] \\ \boldsymbol{v}_{2-} &= \frac{\sqrt{\mu p}}{r_1 r_2 \sin(\Delta\theta)}\left[(\boldsymbol{r}_2 - \boldsymbol{r}_1) - \frac{r_1}{p}(1 - \cos\,\Delta\theta)\boldsymbol{r}_2\right]\end{aligned} \tag{8.2.2}$$

where $\Delta\theta = \angle(\boldsymbol{r}_1, \boldsymbol{r}_2)$ is the so-called *transfer angle*. Having thus found the state vectors $(\boldsymbol{r}_1, \boldsymbol{v}_{1+})$ at point P_1 and $(\boldsymbol{r}_2, \boldsymbol{v}_{2-})$ at point P_2 of the transfer orbit we derive from Eq. (7.3.3) the orientation of the conic transfer orbit as

$$\boldsymbol{e} = \left(\frac{1}{r_1} - \frac{1}{a}\right)\boldsymbol{r}_1 - \frac{1}{\mu}(\boldsymbol{r}_1\boldsymbol{v}_{1+})\boldsymbol{v}_{1+} = \left(\frac{1}{r_2} - \frac{1}{a}\right)\boldsymbol{r}_2 - \frac{1}{\mu}(\boldsymbol{r}_2\boldsymbol{v}_{2-})\boldsymbol{v}_{2-} \tag{8.2.3}$$

Having thus determined the relevant orbital elements $a, \boldsymbol{e}$ of the Lambert transfer orbit, we have found the solution to the orbital boundary value problem. Note that with such methods the orbital boundary value problem is also used to preliminarily determine an unknown orbit. Preliminary orbit determination will be discussed in Chap. 14.

With the state vectors $(\boldsymbol{r}_1, \boldsymbol{v}_{1+})$ and $(\boldsymbol{r}_2, \boldsymbol{v}_{2-})$ we also know the required orbital maneuvers and the total delta-v

$$\begin{aligned} \Delta\boldsymbol{v}_1 &= \boldsymbol{v}_{1+} - \boldsymbol{v}_{1-} \\ \Delta\boldsymbol{v}_2 &= \boldsymbol{v}_{2+} - \boldsymbol{v}_{2-} \\ \Delta\boldsymbol{v} &= |\Delta\boldsymbol{v}_1| + |\Delta\boldsymbol{v}_2| \end{aligned} \tag{8.2.4}$$

Having thus fully determined the Lambert transfer we recognize that everything hinges on the problem of finding the semi-latus rectum p of the Lambert transfer orbit under the given boundary conditions Eq. (8.2.1) to which we turn now.

8.2.2 *Lambert Transfer Orbits*

We will first study the characteristics of the solutions of the orbital boundary value problem if only the position vectors $\boldsymbol{r}_1$, $\boldsymbol{r}_2$ are given. In this case there exists an infinite number of orbits with different a and e connecting P_1 and P_2. Let us first assume that with an additional specification we have picked a particular but otherwise arbitrary a.

Conjugate Orbits: One a, But Two Transfer Orbits

It is a basic property of the orbital boundary value problem that for any particular semi-major axis a in general there exist two different transfer orbits, so-called *conjugate orbits*, with different eccentricity and hence semi-latus rectum, which we will label p and $\tilde{p}$.

From geometrical reasoning, it is enlightening to see why. Suppose there is a transfer orbit with a given a. We define the distances from its empty focus F' to the points P_1 and P_2 as r_1' and r_2', respectively. Then from the definition of an ellipse we have

$$\begin{aligned} r_1 + r_1' &= 2a \\ r_2 + r_2' &= 2a \end{aligned}$$

Since the location of the focal point F is given by the central mass, we can establish the transfer ellipses by determining their empty focal points $F_{1,2}'$. We do so by drawing a circle with radius $r_1' = 2a - r_1$ around P_1 and a circle with radius

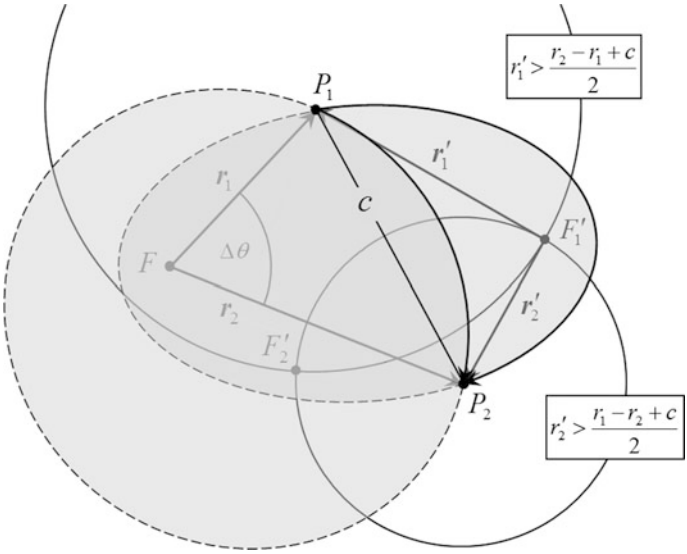

Fig. 8.6 Circles, with radii larger than some critical value, drawn around the points P_1 and P_2 intersect at two points defining the empty focal points F' of the two different transfer ellipses

$r_2' = 2a - r_2$ around P_2. If a is large enough ("large enough" will be shown in a moment to be $a \geq (r_1 + r_2)/2$), the two circles will intersect at two empty focal points on opposite sides of the chord connecting P_1 and P_2 as shown in Fig. 8.6, which define the two transfer ellipses.

A transfer orbit is called a *short path ellipse* if it has the shorter path between P_1 and P_2, and hence a smaller eccentricity, and a shorter transfer time; while the other is called a *long path ellipse*.

Note that their major-axes are indeed of identical length, only their eccentricities and their orientations are different.

When a is known, it can be shown (see Battin (1964, 1987), or Kemble (2006)) that the semi-latus rectum p of the two paths are given as

$$\begin{aligned} p &= a\,\frac{r_1 r_2}{c^2}(1-\cos\Delta\theta)[1-\cos(\alpha+\beta)] \\ &= 2a\,\frac{r_1 r_2}{c^2}(1-\cos\Delta\theta)\sin^2\frac{\alpha+\beta}{2} \end{aligned} \quad @\ \text{short path} \tag{8.2.5a}$$

$$\begin{aligned} \tilde{p} &= \frac{r_1 r_2}{a}\frac{1-\cos\Delta\theta}{1-\cos(\alpha+\beta)} \\ &= 2a\,\frac{r_1 r_2}{c^2}(1-\cos\Delta\theta)\sin^2\frac{\alpha-\beta}{2} \end{aligned} \quad @\text{long path} \tag{8.2.5b}$$

where the chord length c, which is the separation distance between P_1 and P_2, is given from trigonometry by

$$c = \sqrt{r_1^2 + r_2^2 - 2r_1 r_2 \cos \Delta\theta} \tag{8.2.6}$$

and

$$\sin\frac{\alpha}{2} := \sqrt{\frac{r_1 + r_2 + c}{4a}}, \quad \sin\frac{\beta}{2} := \sqrt{\frac{r_1 + r_2 - c}{4a}}$$

From Eqs. (8.2.5a) and (8.2.5b) we see immediately that

$$p \cdot \tilde{p} = \left[\frac{r_1 r_2}{c}(1 - \cos \Delta\theta)\right]^2 = p_{\min}^2$$

where $p_{\min}$ is the semi-latus rectum of the minimum energy transfer orbit discussed in the following (see Eq. (8.2.9)). We also see that owing to $0 \le \beta \le \alpha \le \pi$

$$c\tilde{p} < r_1 r_2(1 - \cos \Delta\theta) < cp \quad \textbf{long/short path condition} \tag{8.2.7}$$

Minimum Energy Transfer Orbit, But Maximum Transfer Time

Because Eq. (7.3.18) directly relates the magnitude of the semi-major axis to the orbital energy by $\varepsilon = -\mu/2a$, this condition states that among all transfer orbits that

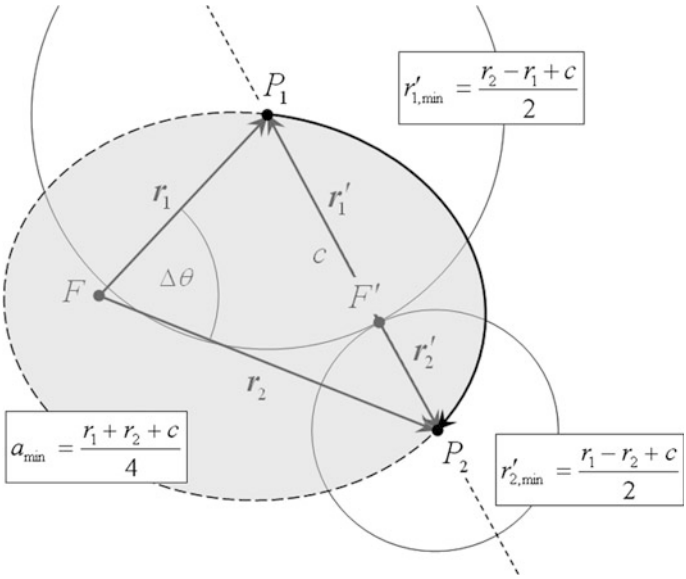

Fig. 8.7 The minimum energy transfer orbit occurs when the empty focal point lies on the chord c connecting point P_1 and P_2

go through P_1 and P_2 there is an orbit with minimum orbital energy. To figure out what its a is, we consider again $r_1 + r_1' = 2a$ and, $r_2 + r_2' = 2a$ from which follows

$$4a = r_1 + r_2 + r_1' + r_2'$$

With $r_1 + r_2$ as a given quantity, a is minimum if $r_1' + r_2'$ becomes minimal, which from Fig. 8.7 is the case if $F_{1,2}'$ lies on the chord c joining P_1 and P_2. Therefore the minimum energy transfer orbit has

$$a_{\min} = \frac{r_1 + r_2 + c}{4} \tag{8.2.8}$$

We recognize that in this limiting situation the two circles around P_1 and P_2 do not intersect, but just touch each other leading to just one empty focal point and therefore to one, and only one, transfer ellipse. If a is smaller than the minimum value the circles will not intersect and no transfer solution exists—the minimum energy orbit is its own conjugate. On the other hand, because $c \leq r_1 + r_2$ always holds, a transfer orbit with $a \geq (r_1 + r_2)/2$ will always be large enough to ensure intersecting circles and hence link the points P_1 and P_2. It can be shown (see, e.g., Battin (1987) or Vallado (2001)) that $p_{\min}$ for the minimum energy orbit, is given by

$$p_{\min} = \frac{r_1 r_2}{c}(1 - \cos\Delta\theta) = \frac{c}{2}\left[1 - \left(\frac{r_1 - r_2}{c}\right)^2\right] \tag{8.2.9}$$

We summarize by stating that

> The **minimum energy ellipse** has a minimum semi-latus rectum given by Eq. (8.2.9) and its empty focal point lies on the chord connecting P_1 and P_2.

Notice that with the additional specification "minimum energy transfer" we have rounded out all boundary conditions and hence settled on a specific solution with an unique $a = a_{\min}$ and $e = \sqrt{1 - p_{\min}/a_{\min}}$.

Note that the occurrence of the minimum energy transfer orbit does not necessarily mean that the total delta-v for the Lambert transfer also becomes a minimum. As seen from Eqs. (8.2.2) and (8.2.4) the total delta-v rather depends in a complex way on the transition from the initial velocity to the transfer velocity at P_1 and back to the final orbital velocity at P_2. But, in general it can be said that any transfer close to a minimum energy transfer is a "good" transfer. Observe that for a minimum energy transfer Δt no longer is a variable that can be freely chosen. The free variable then is the proper configuration of the objects at P_1 and P_2 in their orbits around F that complies with a minimum energy transfer. The search for such an optimal configuration, the so-called orbit phasing, is the objective of Sect. 9.3 for interplanetary transfers.

It can be shown (Problem 8.8) that the minimum energy transfer orbit goes hand in hand with a maximum transfer time. The semi-latus rectum for a minimum energy transfer is given above as $4a_{\min} = r_1 + r_2 + c$. With the transformations introduced for Lambert's problem in Sect. 8.2.3, we have

$$\sin\frac{\alpha_{\min}}{2} = \sqrt{\frac{r_1 + r_2 + c}{4a_{\min}}} = 1,$$
$$\sin\frac{\beta_{\min}}{2} = \sqrt{\frac{r_1 + r_2 - c}{r_1 + r_2 + c}}$$

and hence $\alpha_{\min} = \pi$. With Lambert's equation (see Eq. (8.2.13)) the maximum transfer time of the minimum energy transfer orbit then reads

$$\begin{aligned}\Delta t_{\max} &= \sqrt{\frac{a_{\min}^3}{\mu}}[\pi - \beta_{\min} + \sin\beta_{\min}] \\ &= \sqrt{\frac{a_{\min}^3}{\mu}}\left[\pi - \arccos\left(\frac{c}{a_{\min}} - 1\right) + \sqrt{\frac{c}{a_{\min}}\left(2 - \frac{c}{a_{\min}}\right)}\right]\end{aligned} \tag{8.2.10}$$

The Fundamental Ellipse

There are many transfer orbits with metric orbital elements a, e that connect P_1 and P_2. However, as there is just one transfer orbit with a characteristic a—the minimum energy orbit—there exists just one transfer orbit with a specified characteristic eccentricity: the *fundamental ellipse* with a minimum eccentricity.

To find the orbit with minimum e we first investigate the eccentricity vector as given by the orbit equation Eq. (7.3.4) in vectorial form and apply it to the points P_1 and P_2, obtaining

$$\boldsymbol{e}\boldsymbol{r}_1 = p - r_1$$
$$\boldsymbol{e}\boldsymbol{r}_2 = p - r_2$$

Subtracting these from each other yields

$$\boldsymbol{e}(\boldsymbol{r}_1 - \boldsymbol{r}_2) = r_1 - r_2$$

Since $\boldsymbol{r}_1 - \boldsymbol{r}_2 = c\boldsymbol{u}_c$ is the cord with unit vector $\boldsymbol{u}_c$ and length c, we get

$$\boldsymbol{e}\boldsymbol{u}_c = \frac{r_1 - r_2}{c}$$

This equation states that the eccentricity vector of any transfer orbit between P_1 and P_2 has the same projection on the chord. The fundamental ellipse now is that one of those with the minimum eccentricity. Because the minimum eccentricity is achieved if $\boldsymbol{e}||\boldsymbol{u}_c$, we have for the fundamental ellipse

$$e_F = \frac{r_1 - r_2}{c} = \min \tag{8.2.11}$$

and because $\boldsymbol{e}||\boldsymbol{u}_c$ implicates $2a = r_1' + r_2' = r_1 + r_2$ we have

$$p_F = a\left(1 - e_F^2\right) = \frac{r_1 r_2}{c^2}(r_1 + r_2)(1 - \cos\,\Delta\theta) \tag{8.2.12}$$

Because the fundamental ellipse has a particular p_F it has a particular flight time, which is identical with that of its conjugate orbit having the same semi-latus rectum but different eccentricity.

Note that though the minimum energy transfer ellipse and the fundamental ellipse share the same semi-latus rectum $a_{\min} = a_F = (r_1 + r_2)/2$, they do not share the same position of the empty focal point F'. While F' for the minimum energy orbit lies on the chord, the one for the fundamental ellipse lies on a line through F that runs parallel to the chord (see the "low-e" ellipse in Fig. 8.6 that is close to the fundamental ellipse). Therefore,

> The **fundamental ellipse** has the lowest eccentricity and shares the minimum semi-latus rectum given by Eq. (8.2.12) of all elliptic orbits that lie on P_1 and P_2. Its line of apsides runs parallel to the chord line.

8.2.3 *Lambert's Problem*

Apart from the minimum energy or minimum eccentricity specifications there might be other specifications that settle on a transfer orbit between P_1 and P_2 with a particular a. From a practical and historical point of view the most important, however, is the specification of a transfer time. The problem to find the according transfer orbit is called *Lambert's problem* (Lambert 1761). It can be stated as follows: "the determination of an orbit, having a specified transfer time and connecting two position vectors", or in other words "to solve for the trajectory connecting two position vectors with a given time of flight".

Because in Lambert's problem both transfer time and orbital anomalies are involved, for a solution we start out with Kepler's Eq. (7.4.15) for an elliptic transition and Eq. (7.4.30) for a hyperbolic orbit

$$n \cdot (t_1 - t_2) = n \cdot \Delta t = E_1 - E_2 - e(\sin E_1 - \sin E_2) \qquad @\ \text{elliptic orbit}$$
$$n \cdot (t_1 - t_2) = n \cdot \Delta t = e(\sinh F_1 - \sin F_2) - (F_1 - F_2) \qquad @\ \text{hyperbolic orbit}$$

It can be shown (for a proof see, e.g., Battin (1964, 1987), or Kemble (2006)) that with the substitutions

$$\sin\frac{\alpha - \beta}{2} := \frac{E_2 - E_1}{2}, \cos\frac{\alpha + \beta}{2} := e\,\cos\frac{E_2 + E_1}{2} \qquad @\ \text{elliptic}$$

$$\sinh\frac{\gamma - \delta}{2} := \frac{F_2 - F_1}{2}, \cosh\frac{\gamma + \delta}{2} := e\,\cosh\frac{F_2 + F_1}{2} \qquad @\ \text{hyperbolic}$$

and with the quantities

$$c = \sqrt{r_1^2 + r_2^2 - 2r_1 r_2 \cos\,\Delta\theta} \qquad @\ 0 \le \Delta\theta \le \pi$$
$$s_\pm := \frac{1}{2}\sqrt{\frac{r_1 + r_2}{c} \pm 1}$$

Kepler's equations can be rewritten to yield *for the short path and hence short transition times and for small transfer angles* $0 \le \Delta\theta \le \pi$ the Lambert's equations

Elliptic Orbit (short path, $0 \le \Delta\theta \le \pi$)

$$\boxed{\Delta t = \sqrt{\frac{a^3}{\mu}}[\alpha - \beta - (\sin\,\alpha - \sin\,\beta)]} \quad \textbf{Lambert's equation} \qquad (8.2.13)$$

with

$$\sin\frac{\alpha}{2} = \sqrt{\frac{r_1 + r_2 + c}{4a}} = \sqrt{\frac{c}{a}}s_+ > 0$$
$$\sin\frac{\beta}{2} = \sqrt{\frac{r_1 + r_2 - c}{4a}} = \sqrt{\frac{c}{a}}s_- > 0 \qquad @ \quad 0 \le \beta \le \alpha \le \pi$$
$$p = a\frac{r_1 r_2}{c^2}(1 - \cos\Delta\theta)[1 - \cos(\alpha + \beta)]$$

Hyperbolic Orbit (short path, $0 \le \Delta\theta \le \pi$)

$$\boxed{\Delta t = \sqrt{\frac{-a^3}{\mu}}[\sinh\gamma - \sinh\delta - (\gamma - \delta)]} \quad \textbf{Lambert's equation} \qquad (8.2.14)$$

with

$$\sinh\frac{\gamma}{2} = \sqrt{-\frac{r_1 + r_2 + c}{4a}} = \sqrt{\frac{c}{-a}}s_+ > 0$$
$$\sinh\frac{\delta}{2} = \sqrt{-\frac{r_1 + r_2 - c}{4a}} = \sqrt{\frac{c}{-a}}s_- > 0 \qquad @\ 0 \le \delta \le \gamma$$
$$p = a\frac{r_1 r_2}{c^2}(1 - \cos\Delta\theta)[1 - \cosh(\gamma + \delta)]$$

where c again is the chord length, i.e., the straight distance between the points P_1 and P_2, and $\Delta\theta = \angle(\boldsymbol{r}_1, \boldsymbol{r}_2)$ is again the so-called *transfer angle*. Obviously, $r_1 + r_2 + c \ge r_1 + r_2 - c$ implies that $0 \le \beta \le \alpha \le \pi$ must hold.

Parabolic and Near-Parabolic Trajectories

If $|a| \to \infty$, i.e., if we have a near-parabolic transfer path, it can be shown (see Problem 8.9) that a can be provided analytically as

$$\frac{c}{a} = \frac{5}{2}\frac{\Delta t\sqrt{\mu/c^3} - \frac{4}{3}\left(s_+^3 - s_-^3\right)}{s_+^5 - s_-^5} \quad @\ \text{near-parabolic path} \tag{8.2.15}$$

Equation (8.2.15) provides also the condition at which $|a| \to \infty$, namely $\frac{3}{4}\Delta t\sqrt{\mu/c^3} \approx s_+^3 - s_-^3$. To determine the semi-latus rectum p for $c/a > 0$ Eq. (8.2.13), and for $c/a < 0$ Eq. (8.2.14) need to be applied.

If

$$\Delta t = \frac{4}{3}\sqrt{\frac{c^3}{\mu}}\left(s_+^3 - s_-^3\right) \quad @\ \text{parabolic path}$$

then $a = \infty$ and we have a parabolic transfer path with a single p given by

$$\begin{aligned} p &= 2\frac{r_1 r_2}{c}(1 - \cos\Delta\theta)(s_+ + s_-)^2 \\ &= 2\frac{r_1 r_2}{c^2}\sin^2\frac{\Delta\theta}{2}\left(r_1 + r_2 + 2\sqrt{r_1 r_2}\cos\frac{\Delta\theta}{2}\right) \end{aligned} \quad @\ \text{parabolic path} \tag{8.2.16}$$

With this the orbit orientation $\boldsymbol{e}$ can be deduced via Eqs. (8.2.2) and (8.2.3).

Lambert's Theorem

From these results Lambert's theorem can be derived.

Lambert's theorem

The transfer time of a body moving between two points on a conic trajectory is a function only of the sum of the distances of the two points from the origin of force, the length c of the chord joining these two positions, and the semi-major axis of the conic: $\Delta t = f(r_1 + r_2, c, a)$

Alternatively, Lambert's theorem can be stated as

$$\Delta t = f(r_1, r_2, a, \Delta\theta)$$

This more explicitly shows that the transfer time does not depend on the individual locations of the starting or arrival point or their true anomalies, but just on their separation angle $\Delta\theta$. This is for instance useful in finding a solution to the orbital rendezvous problem (see Sect. 8.6). It is remarkable that transfer time does not depend on the eccentricity of the transfer orbit. Remarkably, this is the third orbital

quantity, besides the specific orbital energy (Eq. (7.3.19)) and the orbital period of an ellipse (Eq. (7.4.2)), that does not depend on the eccentricity. It is just this independency of e that makes the fundamental ellipse dispensable for practical purposes.

Universal Formulation of Lambert's Equation

Given Lambert's equation we are set to provide a universal formulation of Lambert's equation. With P_1 and P_2 given, we know $\boldsymbol{r}_1, \boldsymbol{r}_2$, $\Delta\theta$, and hence chord length c. For a given Δt we then can derive from Lambert's equation (8.2.13) the semi-major axis a of the corresponding short transfer path numerically, for instance with Newton's method (see Sect. 7.4.2).

In the following we want to provide a numerically robust algorithm for any Keplerian orbit. For that we first define the dimensionless numbers

$$
\begin{aligned}
x &:= c/a \\
\Delta\tau &:= \Delta t \sqrt{\frac{\mu}{c^3}} \\
\boldsymbol{\rho}_1 &= \boldsymbol{r}_1/c,\ \boldsymbol{\rho}_2 = \boldsymbol{r}_2/c \\
s_\pm &= \frac{1}{2}\sqrt{\rho_1 + \rho_2 \pm 1} \\
c_\pm(x) &:= \sqrt{1 - x s_\pm^2}
\end{aligned}
$$

With this and the condition $0 \le \beta \le \alpha \le \pi$ we find for an elliptic orbit

$$
\begin{aligned}
\sin\alpha - \sin\beta &= 2\left(\sin\frac{\alpha}{2}\cos\frac{\alpha}{2} - \sin\frac{\beta}{2}\cos\frac{\beta}{2}\right) \\
&= 2(s_+ c_+ - s_- c_-)\sqrt{x} > 0 \\
\alpha - \beta &= 2\left(\arcsin s_+\sqrt{x} - \arcsin s_-\sqrt{x}\right) \\
&= 2\arcsin\left[(s_+ c_- - s_- c_+)\sqrt{x}\right] > 0
\end{aligned}
$$

and for a hyperbolic orbit with $0 \le \beta \le \alpha$

$$
\begin{aligned}
\sinh\gamma - \sinh\delta &= 2\left(\sinh\frac{\gamma}{2}\cosh\frac{\gamma}{2} - \sinh\frac{\delta}{2}\cosh\frac{\delta}{2}\right) \\
&= 2(s_+ c_+ - s_- c_-)\sqrt{-x} > 0 \\
\gamma - \delta &= 2\left(\operatorname{arsinh} s_+\sqrt{-x} - \arcsin s_-\sqrt{-x}\right) \\
&= 2\operatorname{arsinh}\left[(s_+ c_- - s_- c_+)\sqrt{-x}\right] > 0
\end{aligned}
$$

so that we can rewrite and merge Lambert's equations for both elliptical and hyperbolic orbits into one equation

$$
\frac{\Delta\tau}{2}x = \frac{g\left[(s_+ c_- - s_- c_+)\sqrt{|x|}\right]}{\sqrt{|x|}} - (s_+ c_+ - s_- c_-) \quad @\ \text{Keplerian orbits}
$$

where

$$g\left(\sqrt{|u|}\right) := \begin{cases} \arcsin(\sqrt{u}) & @\ 0 < u \le 1 \\ \operatorname{arsinh}(\sqrt{-u}) & @\ u < 0 \end{cases}$$

The similarity of the power series expansion in both cases gives rise to an universal **L-function**

$$\begin{aligned} L(u) &= 1 + \frac{1}{2 \cdot 3}u + \frac{1 \cdot 3}{2 \cdot 4 \cdot 5}u^2 + \frac{1 \cdot 3 \cdot 5}{2 \cdot 4 \cdot 6 \cdot 7}u^3 \ldots \\ &\quad + \frac{(2n-1)!!}{2^n n!(2n+1)}u^n + \ldots \qquad @ -\infty < u \le 1 \\ &= \begin{cases} \dfrac{\arcsin\sqrt{u}}{\sqrt{u}} & @\ 0 \le u \le 1 \\ \dfrac{\operatorname{arsinh}\sqrt{-u}}{\sqrt{-u}} = \dfrac{\ln\left(\sqrt{-u} + \sqrt{1-u}\right)}{\sqrt{-u}} & @\ u < 0 \end{cases} \end{aligned}$$

(For the mathematically inclined reader: Note the relationship between the L-function and Stumpff function $c_2(u)$, see Sect. 7.4.8). We therefore finally obtain

$$\boxed{\frac{\Delta\tau}{2}x = (s_+ c_- - s_- c_+) \cdot L(u) - (s_+ c_+ - s_- c_-)} \quad @\ \text{Keplerian orbits} \quad (8.2.17)$$

with $u = (s_+ c_- - s_- c_+)^2 x$. Note that for $x = 0$ due to $L(0) = 1$ and $c_\pm(0) = 1$ the right hand side vanishes and so does the left hand side.

Owing to the above dimensionless formulation of Lambert's equation, Lambert's theorem can be reduced to $\Delta\tau = f\left(\frac{c}{r_1+r_2}, \frac{c}{a}\right)$ or $\frac{c}{a} = g\left(\Delta\tau; \frac{c}{r_1+r_2}\right)$, respectively, as displayed in Fig. 8.8. Because $0 \le |r_2 - r_1| \le c \le r_2 + r_1$ the parameter $c/(r_1 + r_2)$ is restricted to

$$0 \le \frac{c}{r_1 + r_2} \le 1$$

and according to Eq. (8.2.8)

$$4a \ge r_1 + r_2 + c$$

Universal Semi-Latus Rectum

To determine the semi-latus rectum we further define the dimensionless numbers

$$\rho := (r_1 r_2 - \boldsymbol{r}_1 \boldsymbol{r}_2)/c^2 = \frac{1}{2}\left[1 - \left(\frac{r_1 - r_2}{c}\right)^2\right]$$

$$\lambda := 2(s_+ c_- + s_- c_+)^2$$

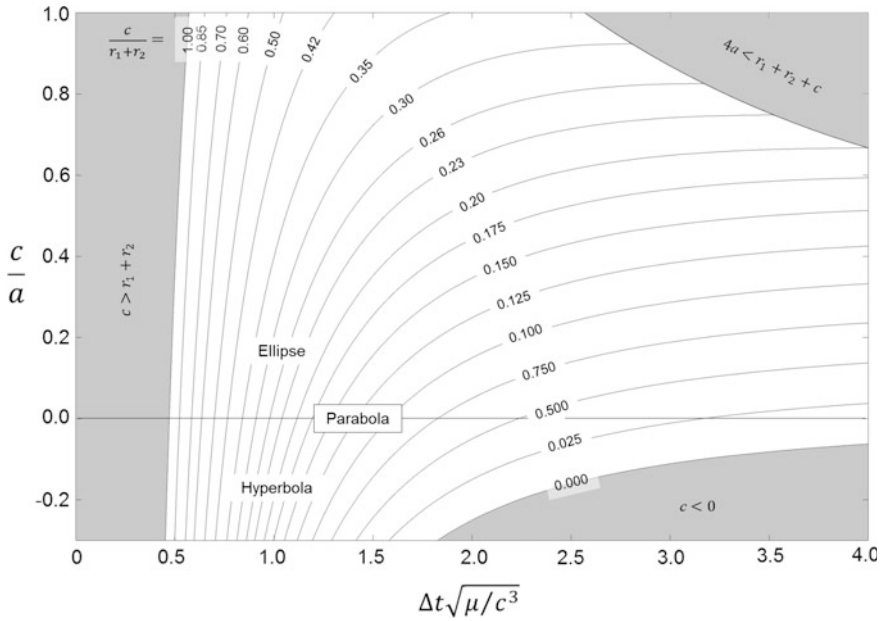

Fig. 8.8 Solution of Lambert's Problem in graphical form

which yields

$$r_1 r_2(1-\cos\Delta\theta) = r_1 r_2 - r_1 r_2\cos\Delta\theta = r_1 r_2 - \boldsymbol{r}_1\boldsymbol{r}_2 = c^2\rho$$

$$\begin{aligned} a[1-\cos(\alpha+\beta)] &= 2a\sin^2\frac{\alpha+\beta}{2} = 2a\left(\sin\frac{\alpha}{2}\cos\frac{\beta}{2} + \cos\frac{\alpha}{2}\sin\frac{\beta}{2}\right)^2 \\ &= 2c(s_+c_- + s_-c_+)^2 = c\lambda \qquad @ \quad x \geq 0 \end{aligned}$$

$$\begin{aligned} a[1-\cosh(\gamma+\delta)] &= -2a\sinh^2\frac{\lambda+\delta}{2} = -2a\left(\sinh\frac{\gamma}{2}\cosh\frac{\delta}{2} + \cosh\frac{\gamma}{2}\sinh\frac{\delta}{2}\right)^2 \\ &= 2c(s_+c_- + s_-c_+)^2 = c\lambda \qquad @ \quad x \leq 0 \end{aligned}$$

We therefore have from Eqs. (8.2.13), (8.2.14), and (8.2.16) for the short path of any Keplerian orbit

$$p = c\rho\lambda \quad @ \text{ Keplerian orbit} \quad \textbf{semi-latus rectum} \tag{8.2.18}$$

With this and some trigonometric expansions we find the following calculation scheme:

Calculation Scheme for an Universal Solution to Lambert's Problem

0. Given $\boldsymbol{r}_1, \boldsymbol{r}_2$, Δt, and μ

1. With $c := \sqrt{r_1^2 + r_2^2 - 2\boldsymbol{r}_1\boldsymbol{r}_2}$ calculate the dimensionless numbers

$$\Delta\tau = \Delta t\sqrt{\frac{\mu}{c^3}}$$

$$s_\pm = \frac{1}{2}\sqrt{\frac{r_1 + r_2}{c} \pm 1}$$

2. With $c_\pm := \sqrt{1 - xs_\pm^2}$ and $u = (s_+c_- - s_-c_+)^2 x$ solve the equation

$$\frac{\Delta\tau}{2} \cdot x + s_+c_+ - s_-c_- = (s_+c_- - s_-c_+)L(u)$$

for x with Newton's method or for difficult hyperbolic orbits $x<0$ with the bisection method. (If $x = c/a<0$ hyperbola, if $x = 0$ parabola, if $x > 0$ ellipse)

3. Calculate the dimensionless number and vectors

$$\lambda = 2(s_+c_- + s_-c_+)^2$$

$$\boldsymbol{\rho}_1 = \boldsymbol{r}_1/c,\ \boldsymbol{\rho}_2 = \boldsymbol{r}_2/c$$

$$\rho = \rho_1\rho_2 - \boldsymbol{\rho}_1\boldsymbol{\rho}_2 = \frac{1}{2}\left[1 - \left(\frac{r_1 - r_2}{c}\right)^2\right]$$

With this the eccentricity vector (see Eq. (8.2.3)) and the dimensionless terminal velocities (see Eq. (8.2.2)) and transfer path eccentricity (see Eq. (8.2.3)) are determined as

$$\boldsymbol{v}_{1+}\sqrt{\frac{c}{\mu}} = \frac{\sqrt{\rho\lambda}}{|\boldsymbol{\rho}_1 \times \boldsymbol{\rho}_2|}\left[\boldsymbol{\rho}_2 - \boldsymbol{\rho}_1 + \frac{1}{\lambda}\hat{\boldsymbol{\rho}}_1\right]$$

$$\boldsymbol{v}_{2-}\sqrt{\frac{c}{\mu}} = \frac{\sqrt{\rho\lambda}}{|\boldsymbol{\rho}_1 \times \boldsymbol{\rho}_2|}\left[\boldsymbol{\rho}_2 - \boldsymbol{\rho}_1 - \frac{1}{\lambda}\hat{\boldsymbol{\rho}}_2\right]$$

$$\boldsymbol{e} = (1 - x\rho_1)\hat{\boldsymbol{\rho}}_1 - \frac{c}{\mu}(\boldsymbol{\rho}_1\boldsymbol{v}_{1+})\boldsymbol{v}_{1+}$$

8.2.4 Minimum Effort Lambert Transfer

Having analyzed the Lambert transfer orbit we will now finally turn to the most important problem from a practical point of view: Given two transfer points P_1 and P_2 with state vectors $(\boldsymbol{r}_1, \boldsymbol{v}_{1-})$ and $(\boldsymbol{r}_2, \boldsymbol{v}_{2+})$ what is the Lambert transfer orbit with the least propulsion effort? So the additional scalar specification here is the least effort equaling a minimum total $\Delta \boldsymbol{v}$ as given in Eq. (8.2.4). In order to determine that transfer orbit, we recall the two orbital equations at P_1 and P_2

$$r_1 + \boldsymbol{e}\boldsymbol{r}_1 = a\left(1 - e^2\right)$$
$$r_2 + \boldsymbol{e}\boldsymbol{r}_2 = a\left(1 - e^2\right)$$

These conditional equations leave one of the three orbital elements undetermined. It is this undetermined element that provides us with the freedom to optimize the transfer orbit. We choose as the free element the orientation of the conic orbit, position vector $\boldsymbol{r}_1$. We denote this angle as

$$\varphi = \angle(\boldsymbol{e}, \boldsymbol{r}_1)$$

We therefore have $\hat{\boldsymbol{e}}\hat{\boldsymbol{r}}_1 = \cos\,\varphi$ and for geometrical reasons $\hat{\boldsymbol{e}}\hat{\boldsymbol{r}}_2 = \cos(\Delta\theta - \varphi)$. From the first equation we then have

$$p = a\left(1 - e^2\right) = r_1(1 + e\,\cos\,\varphi) \tag{8.2.19}$$

Subtracting from this equation the second one from above yields

$$r_1 - r_2 + e r_1 \cos\,\varphi - e r_2 \cos(\Delta\theta - \varphi) = 0$$

from which we derive

$$e = \frac{r_2 - r_1}{r_1 \cos\,\varphi - r_2 \cos(\Delta\theta - \varphi)} \tag{8.2.20}$$

Hence, we have derived the orbital elements a, e and p as a function of the orientation of the transfer orbit $\varphi = \angle(\boldsymbol{e}, \boldsymbol{r}_1)$. We insert this result into Eq. (8.2.2) and find with Eq. (8.2.4) the total Δv as a function of φ. Employing an optimization algorithm that does "minimize $\Delta v(\varphi)$", one finds the optimal φ and from the above equations also the optimal orbital elements.

8.3 Hohmann Transfer

We have already seen that a minimum energy Lambert orbit does not necessarily imply a minimum energy Lambert transfer because for that we also have to take into account the delta-v of the two impulse maneuvers into and out of the transfer orbit. So we are now seeking for a minimum energy Lambert transfer. This is the Hohmann transfer.

The general problem statement is this: What is the transfer orbit between two Keplerian orbits with the least propulsion demand? Because this general problem is quite complex, we will restrict ourselves to the following conditions:

- The two orbits are elliptic and coplanar.
- The orbital bodies revolve around the same central body with the same orientation (co-revolving), so their angular momentum vectors are collinear, only their magnitudes are different.
- The orbital elements are such that the two orbits nowhere touch or cross each other.

Due to the last constraint we can define an inner and an outer orbit, which we will denote by the symbols • and O.

Throughout this section we assume in addition that the transfers are achieved with impulsive thrust maneuvers, so-called *boosts* or *kick-burns* with $F_* \gg F_{ext}$ (see Sect. 2.3) so that the created Δv is determined solely by the thrust characteristics. This assumption is in general valid for today's chemical propulsion engines for orbit control.

8.3.1 The Minimum Principle

As an example for an orbit transfer, let us consider the situation where we are in an elliptic LEO, and we want to get from any point on this orbit into an elliptic geosynchronous orbit, GSO (a GSO is in sync with Earth's rotation only on the average of an orbit) (see Fig. 8.9). A kick-burn in LEO will first take us into an elliptic transfer orbit, the so-called GSO transfer orbit (GTO). This transfer orbit has to cross or touch the GSO at some point. Once we are at the crossing point, a second kick-burn would bring us into GSO.

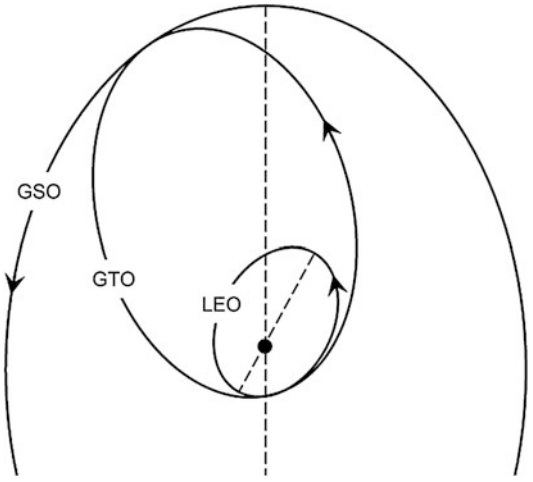

Fig. 8.9 The GTO as a Hohmann transfer orbit from an elliptic LEO to an elliptic GSO (not to scale)

Now, an optimal transfer will minimize the sum of the two Δv at the two transition points. Because a kick-burn $\Delta \boldsymbol{v}$ at a point in space increases the kinetic energy $\varepsilon_{kin}(\boldsymbol{v}+\Delta\boldsymbol{v}) = \frac{1}{2}m(\boldsymbol{v}+\Delta\boldsymbol{v})^2$ but leaves the potential energy unchanged, the orbital energy ε of the S/C increases by the same amount. Owing to $\varepsilon = -\mu/2a$, the upshot is that the semi-major axis expands. In fact, an essential part of the transfer is to enlarge the semi-major axis of the initial LEO to that of the final GSO.

In essence, an optimal transfer will in part maximize the increase of the vehicle's orbital energy at a given amount of Δv. The question is this: How is a kick-burn performed to maximize the increase? The change of the orbital energy due to a kick-burn $\Delta \boldsymbol{v}$ is given by

$$\Delta\varepsilon = \varepsilon_{kin}(\boldsymbol{v}+\Delta\boldsymbol{v}) - \varepsilon_{kin}(\boldsymbol{v}) = \frac{1}{2}(\boldsymbol{v}+\Delta\boldsymbol{v})^2 - \frac{1}{2}\boldsymbol{v}^2 = \boldsymbol{v}\cdot\Delta\boldsymbol{v} + \frac{1}{2}(\Delta v)^2 \qquad (8.3.1)$$

So, for a given amount of boost Δv the orbital energy is maximally increased if the boost $\Delta \boldsymbol{v}$ is parallel to the current velocity vector $\boldsymbol{v}$. In other words,

> A maximum increase in orbital energy is achieved if the transfer boost is in the direction of motion, i.e., tangentially to the initial trajectory.

Since this principle also applies to the second transition point to achieve the final orbit (another increase of a), we immediately obtain the rule for an energetically optimal transfer between to ellipses with only two boosts, the so-called Hohmann transfer:

> A **Hohmann transfer** orbit is an elliptic orbit that for any transfer with two impulses between any two coplanar, co-revolving, non-crossing elliptic orbits is energetically minimal and therefore has the least propulsion demand in the two-body system. It tangentially touches these orbits at two points where the S/C transits with a kick-burn.

Note *That the Hohmann transfer is the energetically minimal two-impulse transfer holds only in the two-body problem, i.e., for a transfer just between two orbits about a common center mass. If the transfer is to a celestial body on the target orbit (i.e., an orbital rendezvous) or a particular point in the vicinity of a celestial body (e.g., libration point) then we have a three-body problem* (see Chap. 11) *and there are more favorable* (*even more favorable than a three-impulse transfer* (see Sects. 8.4.2 and 8.4.3)*) but more complex transfers* (see Sect. 11.5.2) *possible.*

Such a Hohmann transfer orbit is shown in Fig. 8.9. A Hohmann transfer of course also works the other way round, i.e., for a transfer from an outer to an inner elliptic orbit. So we have arrived at an answer to our optimization problem for a given starting point on the initial orbit. This leaves open the answer to the following question: At which point on the initial orbit should we perform the kick-burn to optimize the overall transfer between two elliptic orbits. One could presume that due to $\Delta\varepsilon \propto \boldsymbol{v} \cdot \Delta\boldsymbol{v}$ a first kick-burn at the highest orbital velocity, i.e., at the periapsis, would always be a good choice. But this neglects the second kick-burn at low speeds at the apoapsis of the transfer ellipse. A survey of the transfer at different orbital elements shows that the ratio of the eccentricities of the inner and the outer orbit is important. In general one can say that if the inner orbit has a higher eccentricity than the outer orbit, the optimal transfer varies, but

> If the inner orbit has a lower eccentricity than the outer orbit, the transfer to or from the apoapsis of the outer orbit requires the least delta-v budget.

The Earth–Mars transfer is a nice example for this rule, because here $e_{earth} = 0.0167$ and $e_{mars} = 0.0934$. Figure 8.10 shows the delta-v budget of the transfer as a function of the orbit angle of the transition point on the Mars orbit.

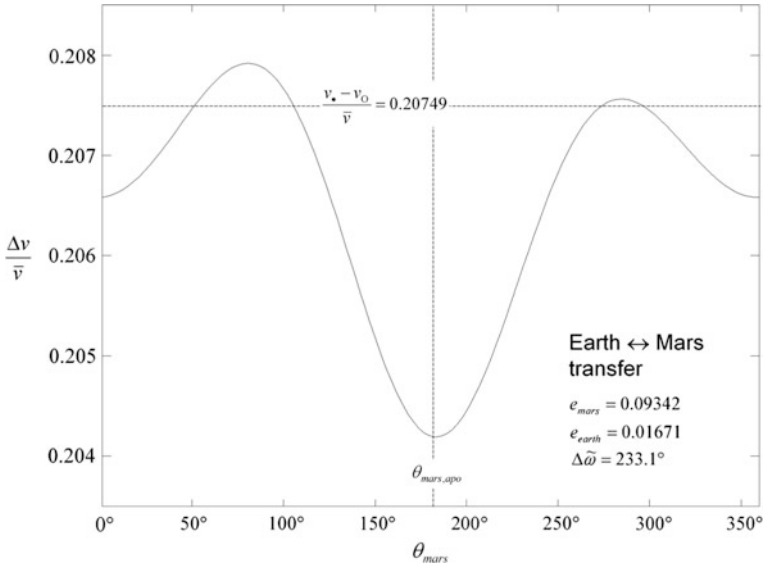

Fig. 8.10 Normalized delta-v budget for Earth ↔ Mars Hohmann transfers as a function of the orbit angle of the intersection with Mars orbit. The angle between their lines of apsis is 233.1°. The horizontal dashed line is the limiting value if both orbits were circular. Note the stretch of the *y*-scale

The transfer optimization problem gets even more intricate if arbitrary angles between the lines of apsides, or non-coplanar, or crossing orbits are considered. Because these cases become too complex to lay them out in a textbook, we skip them. In the following, we rather focus on the transfer between circular and near-circular orbits, which are of great practical value.

8.3.2 Transfer Between Circular Orbits

Hohmann transfers are specifically interesting between two circular orbits. Planetary orbits are mostly circular because at a given orbital energy they minimize atmospheric drag and provide steady orbit conditions, or because in the geostationary orbit the satellite has to rotate exactly in accord with the Earth. For circular orbits $r_\bullet = a_\bullet = const$ and $r_\mathrm{O} = a_\mathrm{O} = const$. It is easy to find out the metric orbital elements of a Hohmann transfer orbit between circular orbits. For the semi-major axis of this Hohmann transfer orbit, the following is obviously applicable:

$$a_H = \frac{1}{2}(a_\bullet + a_\mathrm{O}) \tag{8.3.2}$$

The transfer time is exactly half a period of the transfer ellipse, so according to Eq. (7.4.12)

$$t_H = \pi\sqrt{\frac{a_H^3}{\mu}} \tag{8.3.3}$$

The transfer ellipse with its two degrees of freedom a_H and e_H is completely and unambiguously determined by the boundary condition $r_{H,per} = a_H(1 - e_H)$ (see Eq. (7.4.6)) and by $r_{H,per} = a_\bullet$ and $r_{H,apo} = a_\mathrm{O}$. As for the semi-minor axis $b_H = a_H\sqrt{1 - e_H^2}$ applies, and the other metric orbital elements can be easily derived:

$$e_H = \frac{a_\mathrm{O} - a_\bullet}{a_\mathrm{O} + a_\bullet} \tag{8.3.4}$$

$$b_H = \sqrt{a_\bullet a_\mathrm{O}} \tag{8.3.5}$$

Let us determine the Δv demand for a Hohmann transfer between two circular orbits. According to Eq. (2.4.1), this is calculated for two Hohmann transfer kick-burns as the sum of the individual amounts (see Fig. 8.11):

$$\begin{aligned}\Delta v &= \left\{\begin{array}{ll} |\Delta v_{\bullet\to H}| + |\Delta v_{H\to\mathrm{O}}| & @\ \bullet\to\mathrm{O} \\ |\Delta v_{\mathrm{O}\to H}| + |\Delta v_{H\to\bullet}| & @\ \mathrm{O}\to\bullet \end{array}\right\} \\ &= (v_{H\bullet} - v_\bullet) + (v_\mathrm{O} - v_{H\mathrm{O}})\ @\ \bullet\leftrightarrow\mathrm{O}\end{aligned}$$

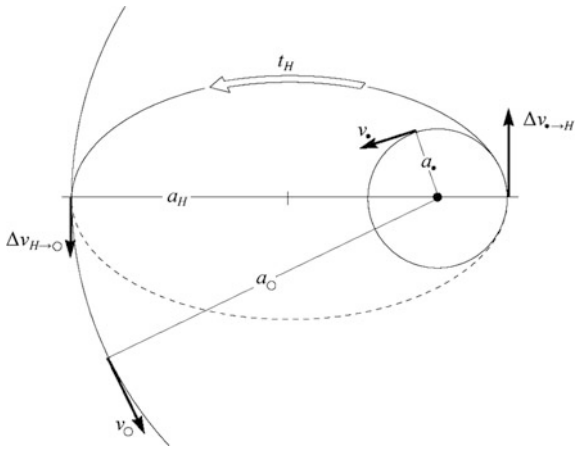

Fig. 8.11 Hohmann transfer between an inner and an outer circular orbit

The latter holds because $|\Delta v_{\bullet\to H}| = |\Delta v_{H\to\bullet}| = v_{H\bullet} - v_\bullet$ and $|\Delta v_{O\to H}| = |\Delta v_{H\to O}| = v_O - v_{HO}$. According to Eq. (8.3.4) $(1+e_H)/(1-e_H) = a_O/a_\bullet$ and therefore from Eq. (7.4.10) follows $v_{H\bullet} = v_{per} = v_\bullet\sqrt{a_O/a_H}$ and $v_{HO} = v_{apo} = v_O\sqrt{a_\bullet/a_H}$. Inserting this into the above equation yields the two contributions

$$\begin{aligned} |\Delta v_{\bullet\leftrightarrow H}| &= v_\bullet\left(\sqrt{\frac{a_O}{a_H}} - 1\right) \\ |\Delta v_{O\leftrightarrow H}| &= v_O\left(1 - \sqrt{\frac{a_\bullet}{a_H}}\right) \end{aligned} \tag{8.3.6}$$

which are shown in Fig. 8.12. So, in total we get

$$\Delta v = |\Delta v_{\bullet\leftrightarrow H}| + |\Delta v_{H\leftrightarrow O}| = v_\bullet\left(\sqrt{\frac{a_O}{a_H}} - 1\right) + v_O\left(1 - \sqrt{\frac{a_\bullet}{a_H}}\right) \tag{8.3.7}$$

If the terms in Eq. (8.3.7) are arranged skillfully and extended by $\sqrt{\mu} = v_\bullet\sqrt{a_\bullet} = v_O\sqrt{a_O}$, we get

$$\boxed{\Delta v = (v_\bullet - v_O)\left(\frac{\sqrt{a_\bullet} + \sqrt{a_O}}{\sqrt{a_H}} - 1\right) < v_\bullet - v_O} \quad @\ \bullet \leftrightarrow O \tag{8.3.8}$$

Equation (8.3.8) is valid for both transfer directions, i.e., $\bullet \to O$ and $O \to \bullet$.

Why is There a Bump?

The two contributions exhibit quite different shapes. Why? And why does $\Delta v_{O\leftrightarrow H}$ have a bump? The first (transfer injection) boost increases continuously with increasing distance between the orbits. This is quite easy to understand, as the semi-major axis a_H of the transfer orbit is determined by this distance, and the

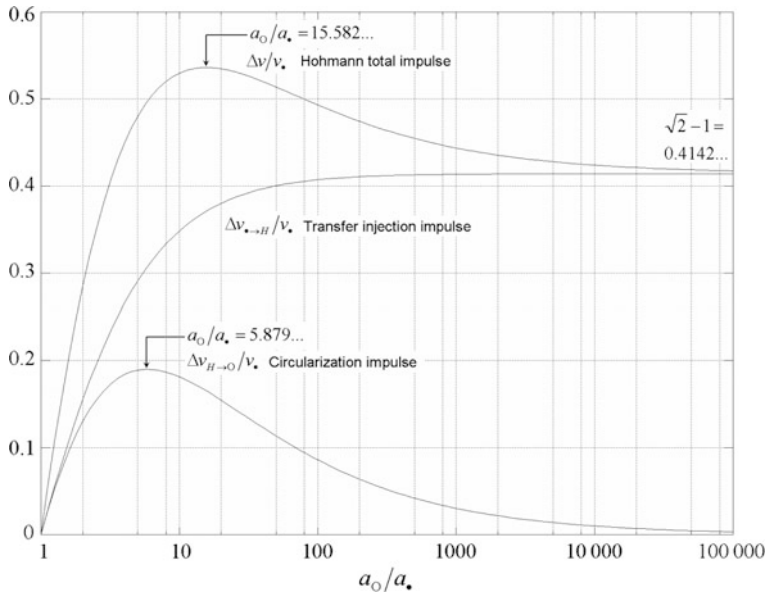

Fig. 8.12 Propulsion demand for Hohmann transfers from an inner to an outer orbit

transfer orbital energy also increases non-linearly with $\varepsilon = -\mu/2a$ according to Eq. (7.3.19). The second (circularization) boost, however, has a maximum at $a_O/a_\bullet = 5.879362\ldots$ (exercise, Problem 8.4a). The reason is as follows. At the one extreme, if both orbits are in close vicinity to each other, i.e., $\Delta a = a_O - a_\bullet \to 0$, we have with

$$a_H = \frac{1}{2}(a_\bullet + a_O) = a_\bullet\left(1 + \frac{1}{2}\frac{\Delta a}{a_\bullet}\right)$$

and according to Eq. (8.3.6)

$$|\Delta v_{H\leftrightarrow O}| \approx v_O\left(1 - 1\Big/\sqrt{1 + \frac{1}{2}\frac{\Delta a}{a_\bullet}}\right) \approx \frac{1}{4}\frac{\Delta a}{a_\bullet}v_0$$

So, for $\Delta a = 0$ the second boost of course is zero and increases roughly linearly with increasing distance Δa. At the other extreme, when $a_O \to \infty$, then $a_H, \Delta a \to \infty$ as well, and we have for the second boost at infinite distance

$$|\Delta v_{H\leftrightarrow O}| = v_O\left(1 - \sqrt{\frac{a_\bullet}{a_H}}\right) \approx v_0\left(1 - \sqrt{\frac{2a_\bullet}{\Delta a}}\right) \approx v_0 \approx 0$$

So, because at infinity the Hohmann and the target orbital velocity is zero the transfer boost between the two vanishes as well. Because the second boost is

positive between these limiting cases it must exhibit a maximum somewhere in between. Because of this maximum of the second boost, the total Hohmann transfer also has a maximum $\Delta v_{\max} \approx 0.536258 \cdot v_\bullet$ at $a_O/a_\bullet = 15.58172\ldots$ (exercise, Problem 8.4b).

Adjacent Circular Orbits

For a Hohmann transfer between adjacent circular orbits, $a_O \approx a_\bullet$, we can approximate (exercise, Problem 8.2)

$$\frac{\sqrt{a_\bullet}+\sqrt{a_O}}{\sqrt{a_H}} - 1 \approx 1 - \frac{1}{16}\left(\frac{a_O - a_\bullet}{a_\bullet}\right)^2 \to 1 \tag{8.3.9}$$

hence

$$\boxed{\Delta v \approx v_\bullet - v_O} \quad @\ a_O \approx a_\bullet \tag{8.3.10}$$

Example

For $a_O/a_\bullet \leq 2.5$, i.e., for orbits with altitudes up to 10,000 km above Earth's surface, the error due to Eq. (8.3.10) is smaller than 5.1%.

Distant Circular Orbits

For circular orbits that are distant from each other, we rewrite Eq. (8.3.8)

$$\frac{\Delta v}{v_\bullet} = \left(1 - \sqrt{\frac{a_\bullet}{a_O}}\right)\left(\sqrt{2}\frac{1+\sqrt{a_\bullet/a_O}}{\sqrt{1+a_\bullet/a_O}} - 1\right) = \sqrt{2}\frac{1-a_\bullet/a_O}{\sqrt{1+a_\bullet/a_O}} - 1 + \sqrt{\frac{a_\bullet}{a_O}}$$

For these distant orbits $a_\bullet/a_O \ll 1$ and we can approximate

$$\frac{\Delta v}{v_\bullet} = \sqrt{2} - 1 + \sqrt{\frac{a_\bullet}{a_O}} - \frac{3}{\sqrt{2}}\frac{a_\bullet}{a_O} + \cdots \tag{8.3.11}$$

Using $v = \sqrt{\mu/a}$ we therefore obtain in the limit of infinite distances

$$\Delta v = \left(\sqrt{2} - 1\right)v_\bullet + v_O \quad @\ a_O/a_\bullet \to \infty \tag{8.3.12}$$

Between these two limiting cases the expression $\left(\sqrt{a_\bullet} + \sqrt{a_O}\right)/\sqrt{a_H} - 1$ is strictly monotonously decreasing (see Fig. 8.13), and that is why in Eq. (8.3.8) the inequality strictly holds.

Hohmann Transfer as a Special Case of the Minimum Energy Lambert Transfer

Let us consider the case of a Lambert transfer orbit (see Sect. 8.2) between two circular orbits without specified transition points. We examine the minimum energy transfer orbit of Sect. 8.2.2, pick any P_1 on the initial circle, and, as shown in Fig. 8.14, move P_2, because it is arbitrary, until $\Delta\theta = \pi$. In this special case $c = r_1 + r_2$ and both the occupied and empty focal points lie on the chord. This is

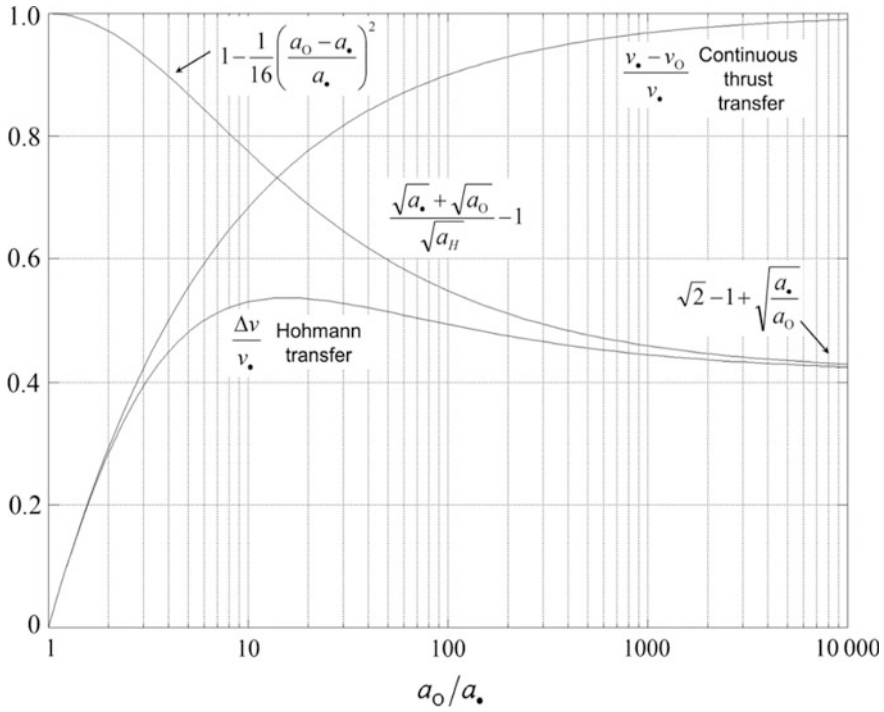

Fig. 8.13 The terms of the Eq. (8.3.8) and their limiting values. The factor $(v_\bullet - v_O)/v_\bullet$ is the propulsion demand of a continuous thrust transfer (see Sect. 8.4.5)

the condition of a minimum energy transfer orbit and it obviously is a Hohmann transfer orbit. By this procedure, we in a different way have verified that the Hohmann transfer is a minimum energy transfer with maximum transfer time.

Note that for this special Lambert transfer the eccentricity is no longer defined. In fact, whatever e might be, the transfer time is independent of e! For the Hohmann transfer, this additional degree of freedom is taken to adjust the tangents of the transfer ellipse to those of the circles at the touching points so that delta-v becomes minimal.

8.3.3 Transfer Between Near-Circular Orbits

We now consider Hohmann transfers between two coplanar, co-revolving, non-crossing ellipses, with small eccentricities $e_\bullet, e_O \ll 1$. The detailed analytical approximations are quite convoluted due to $e_\bullet e_O$ cross-terms, but the general upshot is that the dependency of delta-v as a function of $e_\bullet, e_O$ is very weak. This can be observed, for instance, in Fig. 8.15 where for Hohmann transfers between two apsides points on two orbits with $a_O/a_\bullet = 1.52365$ (Earth–Mars) the normalized delta-v is depicted as a function of $e_\bullet = e_O$ numerically.

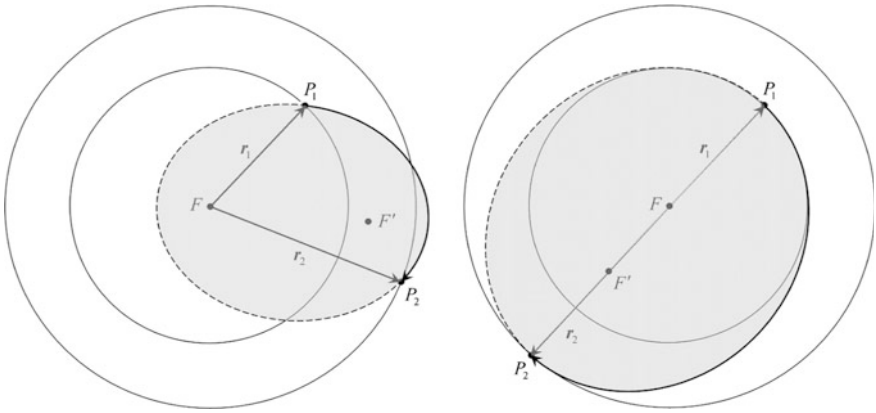

Fig. 8.14 A Lambert transfer between arbitrary points on two circular orbits (left) and the crossover to the Hohmann transfer for $\Delta\theta = \pi$ (right)

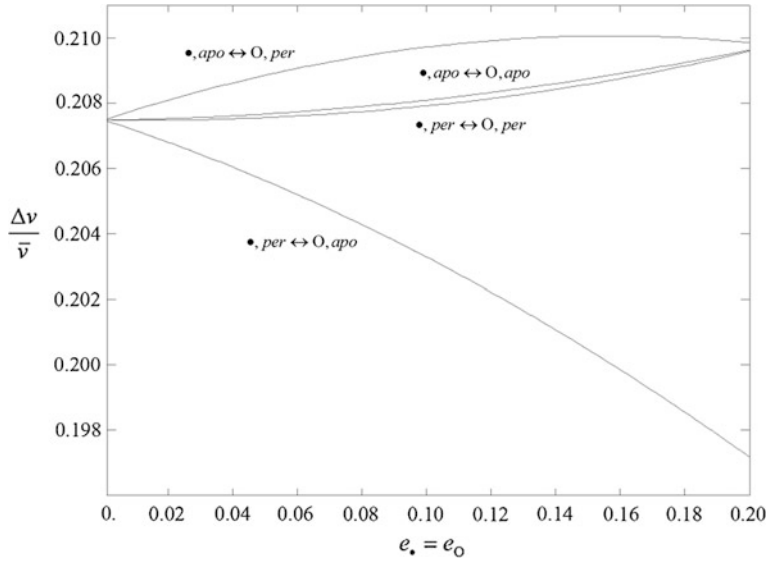

Fig. 8.15 The delta-v budget as a function of the common eccentricities. The dependencies are given for orbits with $a_O/a_\bullet = 1.52365$ (Earth–Mars). Note the stretched Δv-scale

For $e \leq 0.1$ the variations are smaller than 2% of their corresponding circular orbits value $(v_\bullet - v_O)/\bar{v} = 0.20749$. As we can see from Fig. 8.10 this is in accordance with the Earth ↔ Mars transfer, $e_{Mars} = 0.09342$ and $e_{earth} = 0.01671$, even if the transfers would be performed from any position of the orbit. So for all practical purposes, we get the same result as for a transition between two circular orbits.

$$\Delta v \approx (v_\bullet - v_O)\left(\frac{\sqrt{a_O}+\sqrt{a_\bullet}}{\sqrt{(a_O+a_\bullet)/2}} - 1\right) \qquad @\ e_\bullet, e_O \le 0.1 \tag{8.3.13}$$

Nevertheless, owing to the Oberth effect as discussed in Sect. 8.1.3, the general transfer rule is

> The most delta-v efficient Hohmann transfer between a near-circular or even elliptic inner orbit and any outer orbit is always from or to the periapsis of the inner orbit.

8.3.4 Sensitivity Analysis

From an energy point of view Hohmann transfers are the most favorable two-impulse transfer orbits. But they also have some disadvantages. They can be very sensitive to small inaccuracies of the transfer injection impulse. Let us have a closer look at this dependence for transfers between circular orbits.

Let r_{per} and r_{apo} be the periapsis and the apoapsis radius of the transfer orbit respectively (for convenience, we drop the index H to indicate the Hohmann transfer orbit). The periapsis is determined by the initial orbit radius. From the vis-viva Eq. (7.2.15) we get for the velocity on the Hohmann transfer orbit at the periapsis

$$v_{per}^2 = \frac{2\mu}{r_{per}} - \frac{\mu}{a} = \frac{\mu_\oplus}{a}\frac{1+e}{1-e}$$

If the transfer injection burn has a small error dv_{per} at the fixed periapsis $r_{per} = const$ we get

$$2v_{per}dv_{per} = \frac{\mu}{a^2}da$$

from which follows

$$\frac{da}{a} = 2\frac{av^2}{\mu}\frac{dv_{per}}{v_{per}} = 2\frac{1+e}{1-e}\frac{dv_{per}}{v_{per}} \tag{8.3.14}$$

So, a thrust error generates a certain variation of the semi-major axis. Now we want to know how this affects the position of the apoapsis. We start with Eq. (7.4.7)

$$r_{apo} = a(1+e)$$

Its change in position is determined by differentiation

$$\frac{dr_{apo}}{r_{apo}} = \frac{da}{a} + \frac{de}{1+e} \tag{8.3.15}$$

Both parameters a and e are not independent of each other, but linked by the constancy of the periapsis of the initial orbit:

$$const = r_{per} = a(1-e)$$

After differentiating this equation, we see how their changes depend on each other

$$de = (1-e)\frac{da}{a} \tag{8.3.16}$$

So together with Eq. (8.3.15), we get

$$\frac{dr_{apo}}{r_{apo}} = \frac{2}{1+e}\frac{da}{a}$$

and finally with Eq. (8.3.14), we get

$$\frac{dr_{apo}}{r_{apo}} = \frac{4}{1-e}\frac{dv}{v} = \frac{4a}{r_{per}}\frac{dv_{per}}{v_{per}} = 2\left(1+\frac{r_{apo}}{r_{per}}\right)\frac{dv_{per}}{v_{per}} \tag{8.3.17}$$

That is, for a given injection burn error dv_{per}, the relative target point accuracy decreases with increasing transfer distances.

Example 1

Let us examine the Hohmann transfer from an initial LEO orbit (h = 400 km) to GEO. Because of $r_{GEO}/r_{LEO} = 6.232$, we get

$$\frac{dr_{apo}}{r_{apo}} = 14.46\frac{dv_{per}}{v_{per}}$$

A relatively small burn error of just 0.5% would lead to an inaccuracy in the target distance of 7.2%. That is, 3000 km deviation from the GEO orbit!

Example 2

Let us have a look at the Hohmann transfer from an initial LEO orbit (h = 400 km) to the Moon. Because of $r_{moon}/r_{earth} = 56.654$, we get

$$\frac{dr_{apo}}{r_{apo}} = 115.3\frac{dv_{per}}{v_{per}}$$

This means that the same small burn error of just 0.5% would lead to an inaccuracy in the target distance of 58%. That would just bring us to nirvana!

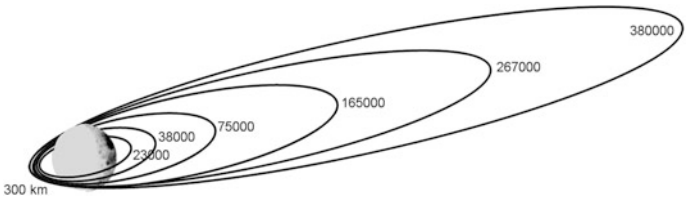

Fig. 8.16 The transfer trajectories of Chandrayaan-1 from Earth to Moon. The apogee (given in km) was increased step by step by successive kick-burns at 300 km perigee

Summary
Plain Hohmann transfers may be the most favorable transfer orbits from an energy point of view, but they implicate long transfer times and the large possible target errors.

However, already small deviations from an ideal Hohmann transfer and in-flight corrections strongly reduce these drawbacks as discussed in Sect. 9.3.2 for near-Hohmann transfers to Mars. In addition, if transfer time is not an issue, one can get a grip on the high sensitivity of highly elliptic transfer orbits by gradually raising the apogee of the transfer orbit to the final Hohmann transfer orbit. Thereby after each raising maneuver the next maneuver can be adjusted to the actual apogee. Figure 8.16 shows the transfer trajectory of the Indian Chandrayaan-1 Moon mission, which was launched on October 22, 2008 and arrived at the Moon 13 days, later where it was captured by Moon's gravitation into a highly elliptic Moon orbit.

8.4 Other Transfers

In this section we study some orbit transfers which are non-Hohmann, but nevertheless of practical value.

8.4.1 Parabolic Escape Transfer

In Sect. 7.4.4. we have studied parabolic orbits. They have the special property that the body reaches infinity at zero velocity. Therefore the simplest escape orbit is a parabolic orbit. We also saw that at a given orbital radius the escape velocity v_{esc} enables a spacecraft to go to infinity independent of the direction in which the final velocity vector points. Yet, the propulsion effect to achieve the escape velocity strongly depends on this direction (see Sect. 8.1.3). In Sect. 8.3.1 we saw that at a given orbital position with $\boldsymbol{r}_0, \boldsymbol{v}_0$ the least effort to achieve a predetermined $\boldsymbol{v}_{esc}$ is by the impulse maneuver $\Delta\boldsymbol{v}||\boldsymbol{v}_0$, i.e. a boost into the instantaneous flight direction in the initial orbit. From Eq. (7.3.16) this implies that the flight angle λ of an initial elliptic orbit with a, e and final parabolic orbit with p_p then is identical

$$\cos\gamma = \sqrt{\frac{a(1-e^2)}{r_0(2-r_0/a)}} = \sqrt{\frac{p_p}{2r_0}}$$

From this it follows that the semi-latus rectum of the parabolic escape orbit is

$$p_p = 2\frac{a(1-e^2)}{2-r_0/a} \quad @\ \Delta\boldsymbol{v}||\boldsymbol{v}_0 \tag{8.4.1}$$

The orientation of the escape orbit, i.e. its line of apsides is given from the parabolic orbit equation as

$$\angle(\boldsymbol{e}_p, \boldsymbol{r}_0) = \cos\,\theta_{p,0} = \frac{p_p}{r_0} - 1 \tag{8.4.2}$$

The initial elliptic orbit and the final parabolic orbit are coplanar.

Finally it would be interesting to know at which point on the ellipse an escape would be most efficient. We calculate Δv from the vis-viva equation to be

$$\Delta v = \sqrt{\mu}\left(\sqrt{\frac{2}{r_0}} - \sqrt{\frac{2}{r_0} - \frac{1}{a}}\right) \tag{8.4.3}$$

From this equation it is obvious that the required Δv lessens with smaller orbit radius. Therefore it is minimal at its periapsis and maximal at its apoapsis, although the differences are only slight for $e<0.1$. Nevertheless, this result is a good example of the Oberth effect decribed in Sect. 8.1.3.

But, most importantly, the boost position solely determines the asymptotic direction of motion. So, the escape procedure is to first figure out the direction of asymptotic motion and measure it as an orbit angle relative to the line of apsides of the initial elliptic orbit. Call this angle θ_∞. Then $\theta_0 = \theta_\infty + \theta_{p,0}$ or

$$\cos(\theta_0 - \theta_\infty) = \cos\,\theta_{p,0} = \frac{p_p}{r_0} - 1 = \frac{2(1+e\,\cos\,\theta_0)^2}{1+2e\,\cos\,\theta_0+e^2} - 1 \tag{8.4.4}$$

So, for a given θ_∞ the orbit angle θ_0 of the boost position is the root of this equation.

Example

We assume a circular orbit with $r = r_0 = a,\ e = 0$. At any point in orbit we want to transfer into an escape parabola with the least Δv effort. What then is the escape parabola?

From Eq. (8.4.1) follows $p = 2r_0$ and from Eq. (7.3.16) $\sin\gamma = \sin 0^\circ = 0 = \sin\theta \rightarrow \theta = 0^\circ$. This means that the boost location constitutes the periapsis of the escape parabola.

8.4.2 Bi-elliptic Transfer

The maximum of the total delta-v for Hohmann transfers (see Fig. 8.12) at $a_O/a_\bullet = 15.582$ occurs because $\Delta v_{H\to O}$ achieves its maximum at $a_O/a_\bullet \approx 5.88$ for turning into the target orbit. This second delta-v contribution however vanishes for $r \to \infty$. This gives rise to the assumption that it might be possible to save propulsion demand with a total of three impulses by first escaping from the initial orbit to far out or even to infinity, and then turning back again to the coplanar target orbit (see Fig. 8.17).

We want to determine the propulsion demand for such a three-impulse transfer (a.k.a. *bi-elliptic transfer*). According to Eq. (8.3.12) the delta-v budget to a remote circular orbit with orbit radius $a_\times \gg a_O > a_\bullet$ and orbital velocity $v_\times = \sqrt{\mu/a_\times}$ is

$$|\Delta v_{\bullet\to\times}| \approx \left(\sqrt{2}-1\right)v_\bullet + v_\times$$

The delta-v budget for a kick-burn that brings us back into the target orbit in turn amounts to

$$|\Delta v_{\times\to O}| \approx \left(\sqrt{2}-1\right)v_O + v_\times$$

So, in total we have

$$\Delta v = |\Delta v_{\bullet\to\times}| + |\Delta v_{\times\to O}| \approx \left(\sqrt{2}-1\right)(v_\bullet + v_O) + 2v_\times \quad @\ a_\times \gg a_O \qquad (8.4.5)$$

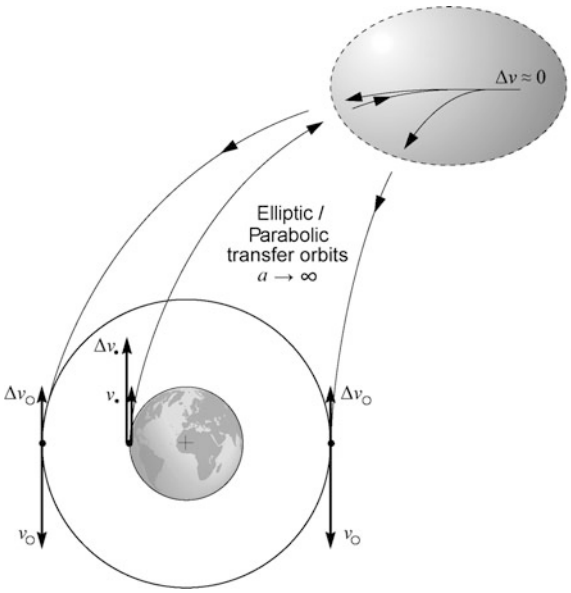

Fig. 8.17 Schematic of a bi-elliptic transfer with an infinite intermediate orbit

For a bi-parabolic transfer, when the intermediate orbit is infinitely far away, then $v_\times = 0$ and the total delta-v budget becomes minimal

$$\Delta v = \left(\sqrt{2} - 1\right)(v_\bullet + v_O) \quad @\, a_\times/a_O \to \infty \tag{8.4.6}$$

Equation (8.4.6) is illustrated in Fig. 8.18. For $a_O/a_\bullet > 11.938765\ldots$ the propulsion demand is indeed more favorable with bi-parabolic transfers than with Hohmann transfers (exercise, Problem 8.5). A practical and hence important benefit of a bi-parabolic transfer is that at the outermost position, where $v \approx 0$, a change of the orbital plane, flight direction, or even the direction of rotation of the orbital curve may be done virtually without any propulsion demand. The serious drawback is that it takes increasingly longer to get farther out.

Break-Even Point with Hohmann Transfer

To ease this problem, it would be interesting to know at which intermediate orbit distance the bi-elliptic transfer starts to be advantageous to the Hohmann transfer. From Eqs. (8.4.5) and (8.3.11) we get the conditional equation $\left(\text{note that } O(v_\times) = O(v_O^2/v_\bullet)\right)$

$$\Delta v_{bi} \approx \left(\sqrt{2} - 1\right)(v_\bullet + v_O) + 2v_\times < \left(\sqrt{2} - 1\right)v_\bullet + v_O - \frac{3}{\sqrt{2}}\frac{v_O^2}{v_\bullet} \approx \Delta v_H$$

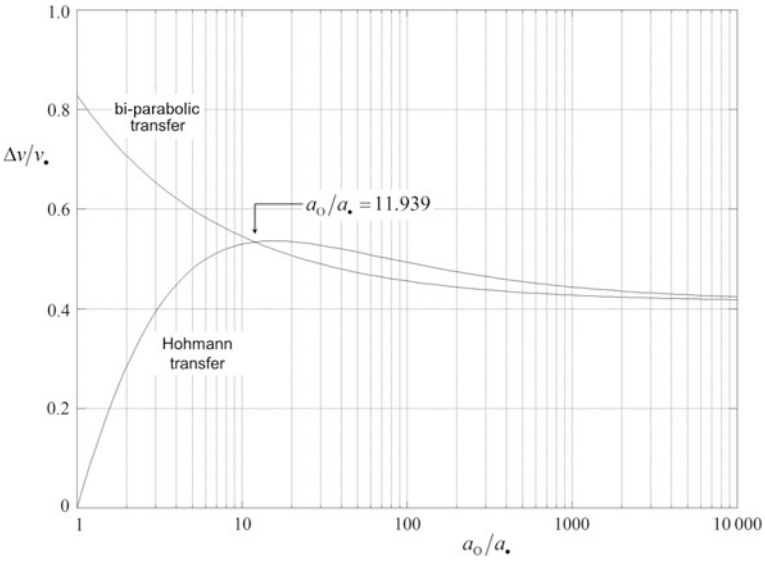

Fig. 8.18 Comparison between an infinite bi-parabolic transfer and a Hohmann transfer

This implies

$$\frac{v_\times}{v_O} < 1 - \frac{1}{\sqrt{2}} - \frac{3}{2\sqrt{2}}\frac{v_O}{v_\bullet}$$

and therefore

$$\frac{a_\times}{a_O} > \frac{8}{\left[2\left(\sqrt{2}-1\right) - 3\sqrt{a_\bullet/a_O}\right]^2} \tag{8.4.7}$$

For example let us assume three ratios $a_O/a_\bullet = 20,\ 100,\ 500$. For this we find $a_\times > (322,\ 28.6,\ 16.60) \cdot a_O = (6441,\ 2860,\ 8299) \cdot a_\bullet$.

Finally, one might question at which $a_O/a_\bullet$ the bi-elliptic transfer is most advantageous to a Hohmann transfer, i.e.: When does $v_\times/v_O$ become maximal, or when does the relation $a_\times/a_\bullet$ become minimal? The answer is easily calculated from Eq. (8.4.7) to be $a_O/a_\bullet|_{opt} = \left[3/\left(\sqrt{2}-1\right)\right]^2 = 52.456$ and $a_\times/a_\bullet|_{\min} = 2445.8$. This optimum case corresponds roughly to a transition from an Earth parking orbit at altitude $h = 250\ km$ to the Moon, $a_{Moon}/a_{park} = 57.3$. Even at this near optimal situation one would need to travel to $a_\times = 2455 \cdot a_{park} = 42.8 \cdot a_{moon}$ to break even with a Hohmann transfer, not to talk about the travel time to get there and back to the Moon. This impractical situation, providing only humble delta-v advantage, is why bi-elliptic transfers are academic cases that are rarely employed.

8.4.3 Super-Synchronous Transfer Orbits

This section is about some special types of transfer orbits to GEO. A classical transfer orbit is the GEO transfer orbit (GTO), which is Hohmann transfer from a low Earth orbit to GEO. In practice, though, there is no LEO. The launch vehicle injects directly from its launch ascent trajectory into an elliptic orbit with apogee at GEO.

There are cases where other transfer orbits, so-called *super-synchronous (GEO) transfer orbit* (SSTO), a.k.a. Super-GTO, or GTO+, are superior to a regular GTO. A SSTO generally is an orbit that rather than a GEO synchronous orbit (GSO), which is any elliptic orbit (incl. GEO) with period of a sideral day (see Sect. 13.2), T_{GSO}, features $T_{SSTO} > T_{GSO}$. According to Eq. (7.4.12) this implies $a_{SSTO} > a_{GSO}$. There exist the following two types of SSTOs.

Bi-Elliptic Transfer

The delta-v benefit of a bi-elliptic transfer increases with the inclination to be changed at the apoapsis. This benefit is decisive for launches from launch sites at high latitude β, which equals the launch orbit inclination i (see Sect. 8.6.1), to GEO. For such a bi-elliptic transfer the upper stage of the rocket injects the satellite into an SSTO at the descending node of the launch trajectory, i.e. when crossing the equator. This injection burn includes the so-called minimum residual shutdown strategy (MRS) where any excess propellant is expended to reduce the inclination

as far as possible, usually by 2–3°. The apogee of the SSTO usually is chosen to be twice to three times the GEO radius (see Fig. 8.19). At SSTO apogee an apogee boost places the spacecraft into a so-called interim transfer orbit (ITO) to GEO and at the same time zeroing the residual inclination. When arriving at GEO, a final burn brings the spacecraft into a so-called circular drift orbit, which is just little smaller than GEO to let the S/C drift from the burn position to its final longitude position. Having arrived there, tiny adjustment burns bring the S/C into its operational orbit state.

The key point with such SSTOs is that, even though the total Δv of all three burns may be larger, the satellite's propellant spending for the SSTO apogee boost and the final burns are lower than for a standard GTO. So, as long as the additional Δv of the rocket upper stage for SSTO is within its propellant budget, any reduction of the satellite's Δv is welcome to invest the saved propellant into later station-keeping and thus extend the satellite's orbital life time. This is why bi-elliptic SSTOs for transfering satellites into GEO are quite frequent for high latitude launch sites such as Cape Canaveral (Atlas) and Baikonur (Proton).

Common to all such SSTOs is the fact that the SSTO injection burn is performed at the descending node of the launch trajectory, which implies $\omega = 180°$ for the SSTO. Hence the tangent plane maneuver (see Sect. 8.1.4) at SSTO apogee into a ITO is a nodal transfer. The RAAN of the ITO is irrelevant because the inclination is usually nullified at SSTO apogee.

Hence both Δv_1 and Δv_2 are nodal transfers as determined by Eq. (8.1.20). The delta-v for the three burns are therefore as follows

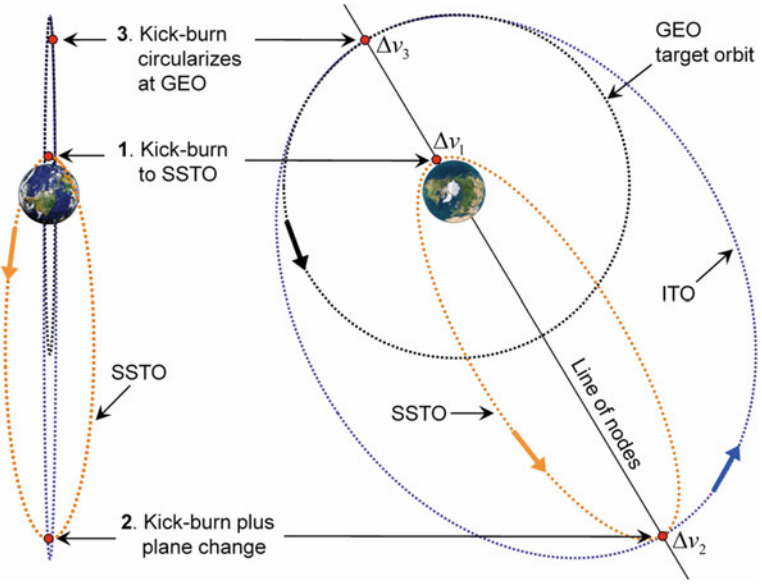

Fig. 8.19 A bi-elliptical super-synchronous transfer with its three kick-burns. Views are in Earth's equatorial plane (left) and normal to it (right)

$$\begin{aligned}\Delta v_1 &= \sqrt{v_{LEO-}^2 + v_{LEO+}^2 - 2v_{LEO-}v_{LEO+}\cos\Delta i_1}\\ \Delta v_2 &= \sqrt{v_{ITO-}^2 + v_{ITO+}^2 - 2v_{ITO-}v_{ITO+}\cos\Delta i_2}\\ \Delta v_3 &= v_{GEO-} - v_{GEO+}\end{aligned} \tag{8.4.8}$$

where the subscripts − and + indicate the values before and after the burn, respectively.

Case Study: The Super-Synchronous Transfer Orbit Mission of *Orion 1*

The Telstar 11 telecommunications satellite, operated by Loral Skynet, provided video for broadcast and business television, high-speed internet access and multimedia services, broadband and data networking to Europe, the United States to the Rocky Mountains and parts of Canada and Mexico.

It was launched as Orion 1 (a.k.a. Orion F1) on November 29, 1994, on an Atlas IIA rocket from Cape Canaveral (latitude 28.5°). The standard Atlas IIA GTO foresees a nodal transfer at the descending node, i.e. a GTO injection burn at 185 km altitude including an inclination change of about 2.8° (depending on the wind conditions during ascent and hence on the decisive propellant excess just before main engines cut off, MECO). A transfer burn at apogee, which is GTOs ascending node and a circularization burn including an inclination change of $\Delta i = 25°$ at the point where GTO touches the GEO, delivers the satellite into a so-called drift orbit. There the satellite drifts with a rate of 0.3°W per day into its final station-keeping box at 37.5°W. This earlier and standard Atlas IIA LEO→GTO→GEO sequence requires a GTO-injection boost of $\Delta v_{rocket} = 2.497\,\mathrm{km/s}$ for the rocket's last stage and a $\Delta v_{sat} = 1.764\,\mathrm{km/s}$ for the spacecraft. The latter would imply a lifetime in GEO to be less than 7 years, much less than required.

It was therefore decided that at the descending node the launcher should inject the spacecraft into a SSTO, in order to significantly reduce the later spacecraft's $\Delta v_{sat} = \Delta v_2 + \Delta v_3$ at the expense of a relatively small Δv_1 increase of the launcher. The SSTO chosen had the properties

$$\begin{aligned} r_{apo} &= 129{,}885\,\mathrm{km}\\ r_{per} &= 6563.1\,\mathrm{km}\\ i &= 25.7°\\ \Omega &= 173.6°\\ \omega &= 179.98° \end{aligned}$$

To bring the spacecraft from SSTO apogee into GEO, one apogee burn would change the inclination $\Delta i = 25^\circ$ and bring the S/C into the interim transfer orbit (ITO) to GEO, while a final burn at ITO perigee would circularize it into GEO. For safety reasons each burn was split into two, which in view of delta-v, however, are equal to the said two burns. According to Eq. (8.4.8) the delta-v for the three burns are as follows

$$\begin{aligned} v_{LEO-} &= 7.793\,\text{km/s}, \\ v_{LEO+} &= 10.753\,\text{km/s} \\ \Delta v_1 &= \sqrt{v_{LEO-}^2 + v_{LEO+}^2 - 2v_{LEO-}v_{LEO+}\cos(28.5^\circ - 25.7^\circ)} \\ &= 2.993\ \text{km/s} \end{aligned}$$

$$v_{ITO-} = 0.5434\ \text{km/s}, \quad v_{ITO+} = 1.227\ \text{km/s}$$

$$\begin{aligned} \Delta v_2 &= \sqrt{v_{ITO-}^2 + v_{ITO+}^2 - 2v_{ITO-}v_{ITO+}\cos(25.7^\circ - 0.6^\circ)} \\ &= 0.770\ \text{km/s} \end{aligned}$$

and

$$\begin{aligned} v_{GEO-} &= 3.778\ \text{km/s}, \quad v_{GEO+} = 3.075\ \text{km/s} \\ \Delta v_3 &= v_{GEO-} - v_{GEO+} = 0.703\ \text{km/s} \end{aligned}$$

So, the Atlas rocket had to provide a $\Delta v_1 = 2.993$ km/s and hence an additional

$$\Delta v_{rocket+} = 2.993 - 2.497\ \text{km/s} = 0.496\ \text{km/s}$$

which was within the fuel budget. On the other hand, the total delta-v for the Orion satellite was $\Delta v_1 + \Delta v_2 = 0.770 + 0.703 = 1.473$ km/s thus providing a benefit of

$$\Delta v_{sat+} = 1.473\,\text{km/s} - 1.764\,\text{km/s} = -291\ \text{m/s}$$

This delta-v benefit extended Orion's lifetime for an additional 5 years, sufficient to meet the mission requirements.

Because any reduction of the satellite's total delta-v, $\Delta v_{sat} = \Delta v_2 + \Delta v_3$, is essential for the satellite's lifetime, Fig. 8.20 plots $\Delta v_2 + \Delta v_3$ for $\Delta i_1 = 0$ and different $\Delta i \equiv \Delta i_2$ as a function of SSTO apogee distance.

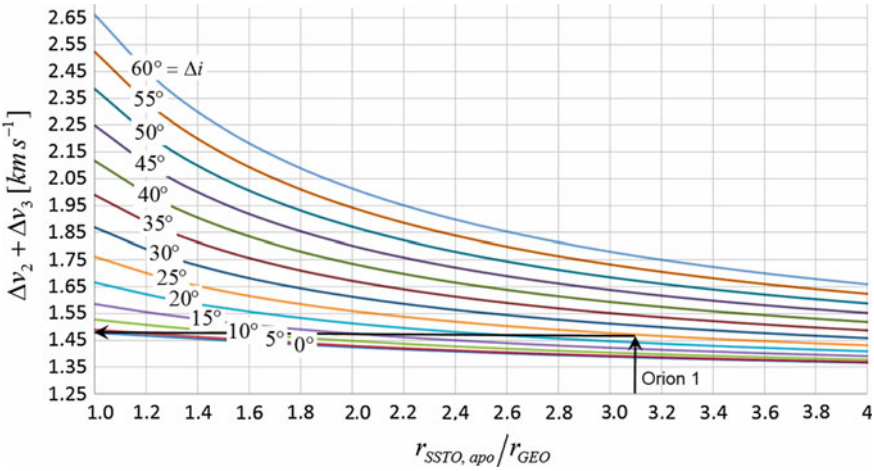

Fig. 8.20 The total delta-v of the satellite for a LEO → SSTO → ITO → GEO transfer as a function of relative SSTO apogee distance and for different inclination changes at the second kick-burn (SSTO apogee) and vanishing inclination change at the first and third kick-burn

Continuous Thrust Transfer

With today's trend to all-electric propulsion platforms (cf. Sect. 5.2.2, Subsection *Comparsion with other Thrusters*) there is the need for an efficient electric propulsion transfer from a SSTO, as provided by the launch vehicle, to GEO.

Early transfers were based on GTOs using a thrust arc strategy around apogee, similar to the chemical apogee-thrusts. Such a transfer requires about 150 days. In 1995, A. Spitzer proposed a thrust arc strategy based on SSTO (so-called *Spitzer's scheme*) with 16% less delta-v and a significantly reduced transfer time of about 110 days. Immediately thereafter it was found by C.R. Koppel that a continuous thrust strategy (CTS, see Sect. 8.4.5), i.e. continuously thrusting over all orbits, was even more practical. Although CTS requires a 17% larger delta-v than *Spitzer's scheme*, it reduces the transfer time to about 90 days, with an equivalent reduction of orbits passing the radiation of the Van Allen belts. This is why CTS for all-electric propulsion S/C today is the means of choice.

For a CTS the launch vehicle injects the S/C into a SSTO with typically 200 km × 60,000 km altitude and with a launch-specific non-zero RAAN and inclination. The electric thrust vector then is inertially oriented (star mode) with some out-of-plane component, such that in course of the transfer the in-plane component gradually removes the eccentricity (see Eq. (8.1.1b)) and the out-of plane component decreases the inclination to zero (see Eq. (8.1.1c), RAAN hence becomes irrelevant). The orbit thus gradually crosses over to the target GEO (see Fig. 8.21).

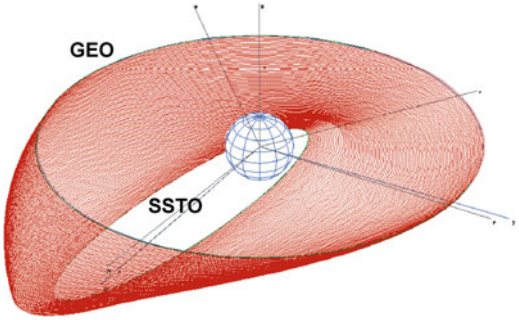

Fig. 8.21 Continuous thrust transfer from a SSTO (185 km × 6000 km, $i = 28°$) to GEO (*Credit* C.R Koppel, 1999)

8.4.4 n-Impulse Transfers

Very generally it can be shown that for a transition between *any* two elliptic orbits the total delta-v budget for a three-impulse transfer (not necessarily bi-elliptic) might be smaller, but does not have to be, than that with the two-impulse Hohmann transfer. The above bi-elliptic transfer for $a_O/a_\bullet > 11.94$ is an example for this. In addition, it can also be shown that the total delta-v budget minimized by Hohmann or a three-impulse transfer cannot be further minimized by maneuvers with more than three impulses. So the Hohmann transfer or the minimum three-impulse transfer represents the absolute minimum for the propulsion demand in a two-body problem. But note that things are different in the three-body problem (see Note in Sect. 8.3.1).

8.4.5 Continuous Thrust Transfer

If we have electrical propulsion engines such as ion thrusters, thrust is low and continuous, so impulse transfers are impossible. An ion engine would rather have to fire permanently in the direction of motion (recall: $\Delta\varepsilon \propto \boldsymbol{v} \cdot \Delta\boldsymbol{v}$) to optimally but slowly spiral the satellite into higher and higher orbits. We now want to calculate the transfer orbit and the delta-v for a continuous tangential thrust maneuver for an initially circular orbit. How does an infinitesimal small tangential thrust $dv := \delta v_{||}$ alter a circular orbit? The answer is given by Eq. (8.1.14):

$$\frac{dr}{r} = 2\sqrt{\frac{r}{\mu}}\, dv$$

To find the total delta-v, we have to integrate the differentially small velocity increase between an initial $r_\bullet$ and final orbit radius r_O

$$\Delta v = \int dv = \frac{\sqrt{\mu}}{2} \int_{r_\bullet}^{r_O} \frac{dr}{r^{3/2}} = -\sqrt{\frac{\mu}{r}}\Big|_{r_\bullet}^{r_O} = v_\bullet - v_O \tag{8.4.9}$$

Of course it does not make a difference for the propulsion demand Δv whether we spiral up from $r_\bullet$ to r_O or down from r_O to $r_\bullet$. If we compare this result with Eq. (8.3.8), we see from Fig. 8.13 that the Hohmann transfer is always more favorable than a continuous thrust transfer. But with ion propulsions and their very tiny thrusts there is no alternative to that.

To calculate the transfer time between an initial circular orbit with orbit radius $r_\bullet$ and the instantaneous circular orbit with radius r, we need the explicit trajectory $r = r(t)$. As the circular condition $v = \sqrt{\mu/r}$ is valid for each point of the orbital curve, it is sufficient to find $v = v(t)$. We find it with the help of the thrust equation $F_* = m \cdot \dot{v} = \dot{m} v_*$. To be able to apply it, we have to consider the mass reduction $\dot{m}$ due to the propellant consumption. We assume that the vehicle with the mass m is accelerated by a constant thrust F with constant mass flow rate $\dot{m}_p = -\dot{m} = const$, so: $m = m_0 + \dot{m}t$. With this relation, we integrate the corresponding equation $dv = \dot{m} v_* / m \cdot dt$

$$\int_{v_\bullet}^{v} dv' = \int_0^t \frac{\dot{m} v_*}{m}\, dt'$$

to get

$$v - v_\bullet = v_* \int_0^t \frac{dt'}{m_0/\dot{m} + t'} = v_* \ln\left(\frac{m_0/\dot{m} + t}{m_0/\dot{m}}\right) = v_* \ln\left(1 - \frac{\dot{m}_p}{m_0} t\right) \qquad (8.4.10)$$

Because of $v = \sqrt{\mu/r}$, this results in the following spiral trajectory (see Fig. 8.22)

$$r(t) = \mu \left[v_\bullet + v_* \ln\left(1 - \frac{\dot{m}_p}{m_0} t\right)\right]^{-2} \quad @\ \dot{m}_p = const \qquad (8.4.11)$$

By solving for t we get the following from Eq. (8.4.10) for the transfer time

$$t_{CT} = \frac{m_0}{\dot{m}_p}\left[1 - \exp\left(\frac{v - v_\bullet}{v_*}\right)\right] = \frac{m_0 v_*}{F_*}\left\{1 - \exp\left[\frac{\sqrt{\mu}}{v_*}\left(\frac{1}{\sqrt{r}} - \frac{1}{\sqrt{r_\bullet}}\right)\right]\right\} \qquad (8.4.12)$$

Example

A satellite is released from the Space Shuttle payload bay at an altitude of 300 km, and it is supposed to spiral with an ion thruster ($F_*/m_0 = 100\,\mu g = 10^{-3} m\ s^{-2}$ and $v_* = 10\,000\ m\,s^{-1}$) to GEO. Because $v_\bullet = 7.72\,km\ s^{-1}$ and $v_{GEO} = v_O = 3.07\,km\ s^{-1}$, the transfer time is calculated to be $t_{CT} = 43$ days.

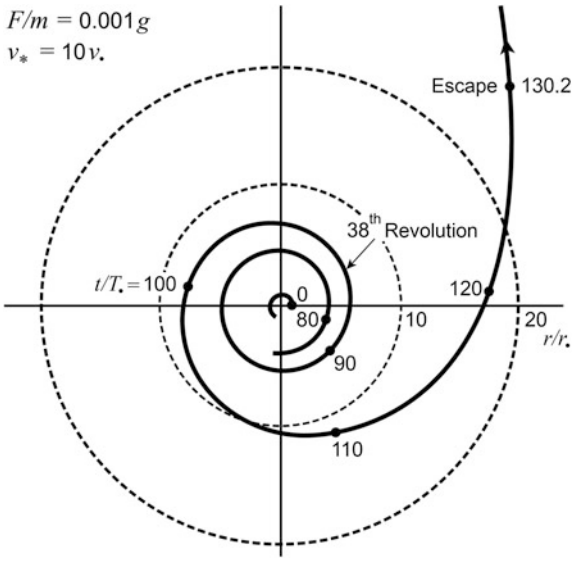

Fig. 8.22 Continuous thrust trajectory as a result of a continuous tangential thrust. Index • refers to the initial orbit. Because the spiral is very narrow at the beginning, only the last two revolutions are shown

8.5 Relative Orbits

Having explored the conditions for a general transfer between orbits, the more delicate problem is to meet a target point in the final orbit, a so-called orbital rendezvous. In this and the next section we will focus on orbital rendezvous in Earth orbits though the described methods apply to any planetary orbit. For interplanetary orbital rendezvous we refer the reader to Sect. 9.3.

In orbital rendezvous, there is generally a passive target object to rendezvous with an interceptor (a.k.a. *chaser*) as the active part that performs the rendezvous maneuvers. Rather than describe the required rendezvous maneuvers in an inertial reference frame such as a geocentric reference frame, it is very convenient to describe them relative to the target. It is convenient because if the interceptor moves in the vicinity of the target we can linearize the equations of motion, which will enable us to solve them analytically. On the other hand, the target in a conical motion about the center of gravity constitutes a non-inertial reference system, a fact that will complicate our equation of motion somewhat. Nevertheless, the description of relative motion about a target object, which is done in the following, is a prerequisite for analyzing rendezvous maneuvers, which is the objective of Sect. 8.6.

8.5.1 General Equation of Motion

Suppose there is a target object in a planetary orbit and a S/C (usually dubbed chaser) wants to navigate in its vicinity and with respect to it. Good examples are the approach maneuvers of a Soyuz vehicle to the ISS or the re-docking of the ascending Lunar Module to the Command/Service Module in low Lunar orbit during the Apollo moon missions. For this mission we need to know the relative motion to the target and how to maneuver to reach the target. This is the subject of the next two sections.

Let us assume the target (for instance, we assume to be the ISS) is in an arbitrary terrestrial conic orbit with position vector $\boldsymbol{R}$ in the geocentric reference frame. For this orbit Newton's gravitational EoM (7.1.19) must hold

$$\ddot{\boldsymbol{R}} = -\frac{\mu}{R^3}\boldsymbol{R} \tag{8.5.1}$$

Of course, Newton's gravitational EoM must equally hold for the chaser's orbit with position vector $\boldsymbol{\rho}$ in the geocentric reference frame, i.e.

$$\ddot{\boldsymbol{\rho}} = -\frac{\mu\boldsymbol{\rho}}{\rho^3}$$

We start deriving the chaser's equation of motion relative to the ISS by defining the relative vector $\boldsymbol{r} = \boldsymbol{\rho} - \boldsymbol{R}$ as shown in Fig. 8.23. The specific reference frame is the ISS-centric coordinate system RSW as described in Sect. 13.1.4, Fig. 13.4, with unit vectors $\boldsymbol{u}_x, \boldsymbol{u}_y, \boldsymbol{u}_z = \boldsymbol{S}, \boldsymbol{W}, \boldsymbol{R}$: The z-axis points along the radial vector while the x-axis points along the moving direction of the target. The y-axis completes the right-handed reference system. Our goal is to find the equation of motion of the relative vector

$$\boldsymbol{r} = \boldsymbol{\rho} - \boldsymbol{R} = x\boldsymbol{u}_x + y\boldsymbol{u}_y + z\boldsymbol{u}_z =: (x, y, z)$$

expressed in the co-moving coordinate system $(\boldsymbol{u}_x, \boldsymbol{u}_y, \boldsymbol{u}_z)$. Since we seek for a differential equation for $\boldsymbol{r}$, we first have to express $\boldsymbol{\rho}$ in terms of $\boldsymbol{R}$ and $\boldsymbol{r}$. Because $r \ll R$ we can expand the term $1/\rho^3$ as follows:

$$\begin{aligned}\frac{1}{\rho^3} &= \frac{1}{\left[x^2 + y^2 + (z+R)^2\right]^{3/2}} = \frac{1}{\left[r^2 + 2zR + R^2\right]^{3/2}} \approx \frac{1}{R^3}\frac{1}{(1+z/R)^3} \\ &\approx \frac{1}{R^3}\left(1 - 3\frac{z}{R}\right)\end{aligned}$$

and hence

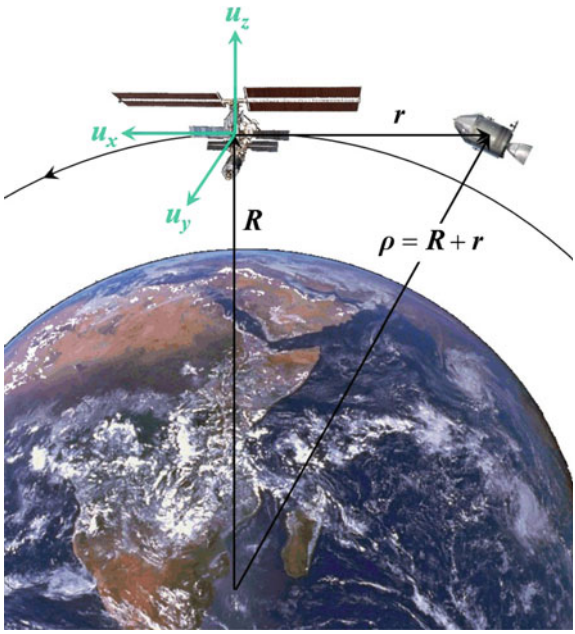

Fig. 8.23 Definition of relative vectors and RSW coordinate system in the target object (ISS), that moves on a circular orbit. The z-axis points along the radial vector while the x-axis points along the moving direction of the target object. The y-axis completes the right-handed reference system

$$\ddot{\boldsymbol{\rho}} = -\frac{\mu\boldsymbol{\rho}}{\rho^3} \approx -\frac{\mu}{R^3}(\boldsymbol{R}+\boldsymbol{r})\left(1-3\frac{z}{R}\right) \approx -\frac{\mu}{R^3}(\boldsymbol{R}+\boldsymbol{r}-3z\boldsymbol{u}_z)$$

Because from the definition of $\boldsymbol{\rho}$ and from Eq. (8.5.1) also $\ddot{\boldsymbol{\rho}} = \ddot{\boldsymbol{R}} + \ddot{\boldsymbol{r}} = -\mu\boldsymbol{R}/R^3 + \ddot{\boldsymbol{r}}$ holds, we get

$$-\frac{\mu}{R^3}\boldsymbol{R} + \ddot{\boldsymbol{r}} \approx -\frac{\mu}{R^3}(\boldsymbol{R}+\boldsymbol{r}-3z\boldsymbol{u}_z)$$

and finally

$$\ddot{\boldsymbol{r}} = -\frac{\mu}{R^3}(\boldsymbol{r}-3z\boldsymbol{u}_z) \quad @\ x,y,z \ll R \tag{8.5.2}$$

We want to solve this vector equation in the non-inertial co-moving target RSW coordinate system $(\boldsymbol{u}_x, \boldsymbol{u}_y, \boldsymbol{u}_z)$. Now, as $\boldsymbol{r} = x\boldsymbol{u}_x(t) + y\boldsymbol{u}_y + z\boldsymbol{u}_z(t)$ is already given in RSW, how is $\ddot{\boldsymbol{r}}$ expressed in it?

The answer is provided by Eq. (7.2.2) for $\boldsymbol{a} \equiv \boldsymbol{r} = x\boldsymbol{u}_x(t) + y\boldsymbol{u}_y + z\boldsymbol{u}_z(t) =: (x,y,z)_{xyz}$ and for the angular velocity of the target $\boldsymbol{\omega} = \omega(0,1,0)_{xyz}$ as

$$\begin{aligned}\ddot{\boldsymbol{r}} &= \ddot{\boldsymbol{r}}_{xyz} + 2\boldsymbol{\omega} \times \dot{\boldsymbol{r}}_{xyz} + \boldsymbol{\omega} \times (\boldsymbol{\omega} \times \boldsymbol{r}) + \dot{\boldsymbol{\omega}} \times \boldsymbol{r} \\ &= \left(\ddot{x} + 2\omega\dot{z} - \omega^2 x + \dot{\omega} z\right)\boldsymbol{u}_x + \ddot{y}\boldsymbol{u}_y + \left(\ddot{z} - 2\omega\dot{x} - \omega^2 z - \dot{\omega} x\right)\boldsymbol{u}_z \\ &= \begin{pmatrix} \ddot{x} + 2\omega\dot{z} - \omega^2 x + \dot{\omega} z \\ \ddot{y} \\ \ddot{z} - 2\omega\dot{x} - \omega^2 z - \dot{\omega} x \end{pmatrix}_{xyz}\end{aligned}$$

where

$$\dot{\boldsymbol{r}}_{xyz} := (\dot{x}, \dot{y}, \dot{z})_{xyz},\ \ddot{\boldsymbol{r}}_{xyz} := (\ddot{x}, \ddot{y}, \ddot{z})_{xyz}$$

If we insert this into Eq. (8.5.2), we finally obtain the equation of motion

$$\ddot{\boldsymbol{r}} = \begin{pmatrix} \ddot{x} + 2\omega\dot{z} - \omega^2 x + \dot{\omega} z \\ \ddot{y} \\ \ddot{z} - 2\omega\dot{x} - \omega^2 z - \dot{\omega} x \end{pmatrix}_{xyz} = -\frac{\mu}{R^3} \begin{pmatrix} x \\ y \\ z - 3z \end{pmatrix}_{xyz}$$

Because this vectorial equation must hold for each orthogonal component separately, we finally find the three differential equations

$$\begin{aligned} &\ddot{x} + 2\omega\dot{z} - \left(\omega^2 - \tfrac{\mu}{R^3}\right)x + \dot{\omega} z = 0 \\ &\ddot{y} \qquad\qquad + \tfrac{\mu}{R^3} y \qquad\quad = 0 \\ &\ddot{z} - 2\omega\dot{x} - \left(\omega^2 + 2\tfrac{\mu}{R^3}\right)z - \dot{\omega} x = 0 \end{aligned} \quad @\, x, y, z \ll R \quad \textbf{equations of motion} \qquad (8.5.3)$$

This are the equations of motion of a chaser, not being subject to external forces, relative to a target with coordinates (x, y, z) in the target's topocentric RSW coordinate system, which quite generally is in a conic orbit about a center of gravity and, due to its conical trajectory, rotates with angular velocity $\omega(t)$. Note that from Eqs. (7.2.7), (7.3.7) and (7.4.13) follows

$$\frac{\mu}{R^3} = \sqrt{n_e}\omega^{3/2}$$

with

$$n_e := \frac{n}{(1 - e^2)^{3/2}} = \sqrt{\frac{\mu}{a^3(1 - e^2)^3}}$$

Observe that only the first and third equations are coupled. If initially $y(0) = 0$ and $\dot{y}(0) = 0$, i.e., if the chaser initially is in the orbital plane, then $\ddot{y} = 0$ and hence $y(t) = 0$, which means that it will always stay in that plane. Otherwise and if $R \approx const$ it will oscillate about this plane with frequency $\sqrt{\mu/R^3}$.

Elliptic Target Orbit

To get more practical and to find a solution to Eq. (8.5.3) we now assume an elliptic orbit with orbital elements a, e about a planet. For this, we get according to Eq. (7.2.7)

$$\omega = \frac{\sqrt{\mu a(1-e^2)}}{R^2}$$

and with Eqs. (7.3.15a) and (7.4.14c)

$$\dot{\omega} = -2\frac{\mu e \sin\theta}{R^3} = -\frac{2\mu a e}{R^4}\sqrt{1-e^2}\sin E$$

with

$$R(t) = a[1 - e\cos E(t)]$$

where the eccentric anomaly $E(t)$ is the solution of Kepler's Eq. (7.4.15)

$$n \cdot t = t\sqrt{\frac{\mu}{a^3}} = E(t) - e\sin E(t)$$

This transcendental equation can be solved by Newton's iteration method (Eq. (7.4.16))

$$E_{i+1} = E_i - \frac{E_i - e\sin E_i - n\cdot t}{1 - e\cos E_i}$$

Of course, similar equations can easily be derived for a hyperbolic trajectory (cf. Sect. 7.4.3).

Given these time dependent quantities, the differential Eq. (8.5.3) for a rendezvous on an elliptic target orbit can be solved numerically for instance by a Runge–Kutta method.

8.5.2 *Circular Orbits*

We now come to the most common situation where the target is in a circular orbit. Circular orbits are so common because for a given minimum altitude they have the lowest orbital energy, entailing the least delta-v to achieve. Therefore, nearly every target in a low Earth orbit will attain a circular or quasi-circular orbit. For instance, the ISS has an eccentricity of typically $e = 0.0001 - 0.001$, that can be shown to be induced by the anisotropies of Earth's gravitational potential (see Sect. 12.3.2).

For a circular orbit we have $\ddot{\boldsymbol{R}} = -\mu\boldsymbol{R}/R^3 = -n^2\boldsymbol{R}$ and $n = \sqrt{\mu/R^3} = 2\pi/T = const$. If be insert this into the general equation of motion Eq. (8.5.3) we

obtain

$$\boxed{\begin{aligned}\ddot{x}+2n\dot{z}&=0\\ \ddot{y}+n^2y&=0\\ \ddot{z}-2n\dot{x}-3n^2z&=0\end{aligned}}\quad @\,x,y,z\ll R\quad \textbf{Hill's equations}\qquad (8.5.4)$$

These are the famous *Hill's equations* (a.k.a. *Clohessy–Wiltshire equations*) governing the motion of a S/C, not being subject to external forces, with coordinates (x, y, z) in the topocentric RSW coordinate system of a target object circling a planet with constant orbital velocity $\omega = n$.

µg-Forces on Space Stations

A modest application of Hill's equation in a circular orbit is the residual forces acting on parts of a satellite or a space station. Such residual forces are important for experiments in space, which contribute some unwanted artificial gravity to the otherwise weightlessness in space. To determine their level, let us assume we have an experimental drawer in a science rack in one of the ISS laboratories located at the distance $\boldsymbol{r} = (x, y, z)$ from the center of mass (CM) of the ISS, which orbits at orbital frequency $n = \sqrt{\mu/R^3}$. Since the drawer is fixed relative to CM, we have $\dot{\boldsymbol{r}} = (\dot{x}, \dot{y}, \dot{z}) = 0$. If the sample in the drawer is further out in the z-direction (see Fig. 8.24) than CM, it experiences an enhanced centrifugal force, but smaller gravitational force. If it is further toward Earth it experiences the opposite effect: a smaller centrifugal force but a larger gravitational force. In total, it thus experiences some residual force, a so-called *tidal force*. We can determine this tidal force if we interpret the terms $\ddot{x}, \ddot{y}, \ddot{z}$ in Eq. (8.5.4) as the residual accelerations making up the tidal force. In doing so we end up with the tidal acceleration in terms of *Earth's mean gravitational acceleration at its surface* (see Sect. 7.1.2), $g_0 := \mu/R_\oplus^2 \approx \mu/R^2 = 9.80\,\mathrm{m\,s^{-2}}$, as

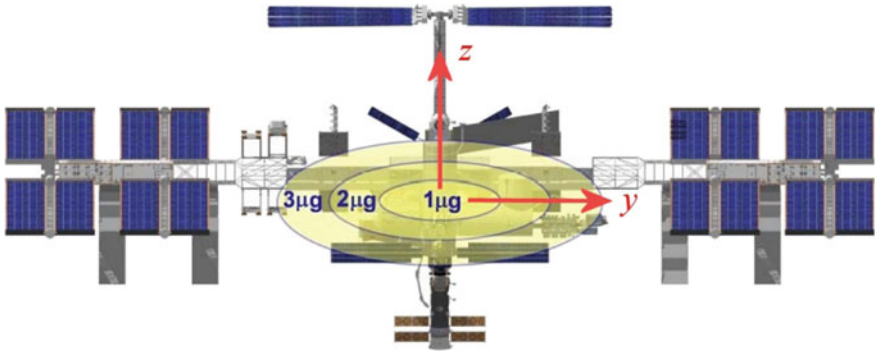

Fig. 8.24 The levels of residual µg-forces on the International Space Station at positions off the center of mass

$$\frac{\ddot{x}}{g_0} = 0, \quad \frac{\ddot{y}}{g_0} = -\frac{y}{R}, \quad \frac{\ddot{z}}{g_0} = 3\frac{z}{R}$$

So, depending on the distances y, z from CM we get different levels of tidal forces. By analyzing Eq. (8.5.3) we realize that in the z-direction there are two gravitational tide contributions and just one centrifugal tide contribution in the overall total of 3. In the y-direction there is just one contribution from the gravitational (lateral) tide. In general the tidal forces are of order $10^{-6}g = 1\mu g$. This is why experiments on space stations are commonly called μg-experiments. For instance, on the ISS, having a typical altitude of 350 km, a level of $1\mu g$ is obtained at a horizontal distance of $y = 10^{-6} \times 6.73 \times 10^6\,\mathrm{m} = 6.73\,\mathrm{m}$ and at a vertical distance of $z = \frac{1}{3} \times 10^{-6} \times 6.73 \times 10^6\,\mathrm{m} = 2.24\,\mathrm{m}$ from CM. Overall, we have μg-ellipses as depicted in Fig. 8.24.

Solution of Hill's Equations

To describe the explicit motion $\boldsymbol{r}(t) = (x(t), y(t), z(t))$ of a chaser, we have to solve Hill's equations. This can be done straightforwardly with only little effort. To do so efficiently, we first replace time by the dimensionless mean anomaly and define both it and its derivatives.

$$\begin{aligned} M &= nt \\ (.)' &:= \frac{d}{dM} = \frac{1}{n}\frac{d}{dt}(.) \\ (.)'' &:= \frac{d^2}{dM^2} = \frac{1}{n^2}\frac{d^2}{dt^2}(.) \end{aligned} \tag{8.5.5}$$

and initial conditions at $t = 0$ as

$$\begin{array}{ll} x(0) = x_0, & x'(0) = x'_0 \\ y(0) = y_0, & y'(0) = y'_0 \\ z(0) = z_0, & z'(0) = z'_0 \end{array} \quad \textbf{initial conditions} \tag{8.5.6}$$

With this Hill's equations read

$$\begin{aligned} x'' + 2z' &= 0 \\ y'' + y &= 0 \\ z'' - 2x' - 3z &= 0 \end{aligned} \tag{8.5.7}$$

First observe that the second Hill equation is decoupled from all others. It has the form of a harmonic oscillator. We therefore find its solution as

$$y = y_0 \cos M + y_0' \sin M$$

We now integrate the first Hill equation directly. By taking the initial conditions into account we get

$$x' = -2z + 2z_0 + x_0'$$

We insert this result into the third Hill equation getting

$$z'' = 2x' + 3z = -\left[z - \left(4z_0 + 2x_0'\right)\right]$$

This, too, is the equation of a harmonic oscillator for the expression $z - \left(4z_0 + 2x_0'\right)$ yielding

$$z - \left(4z_0 + 2x_0'\right) = z_0' \sin M - \left(3z_0 + 2x_0'\right) \cos M$$

under consideration of the initial conditions $z(0) = z_0, z'(0) = z_0'$. We solve for z and find

$$z = 4z_0 + 2x_0' + z_0' \sin M - \left(3z_0 + 2x_0'\right) \cos M$$

Inserting this into the above equation $x' = -2z + 2nz_0 + x_0'$ we get

$$x' = -\left(6z_0 + 3x_0'\right) - 2z_0' \sin M + \left(6z_0 + 4x_0'\right) \cos M$$

This can be integrated directly to deliver with initial condition $x(0) = x_0$

$$x = x_0 - 2z_0' - \left(6z_0 + 3x_0'\right)M + 2z_0' \cos M + \left(6z_0 + 4x_0'\right) \sin M$$

We summarize the results as

$$\begin{pmatrix} x \\ z \\ x' \\ z' \end{pmatrix} = \begin{bmatrix} 1 & 6\sin M - 6M & 4\sin M - 3M & 2\cos M - 2 \\ 0 & -3\cos M + 4 & -2\cos M + 2 & \sin M \\ 0 & 6\cos M - 6 & 4\cos M - 3 & -2\sin M \\ 0 & 3\sin M & 2\sin M & \cos M \end{bmatrix} \begin{pmatrix} x_0 \\ z_0 \\ x_0' \\ z_0' \end{pmatrix} \tag{8.5.8}$$

and in convenient terms

$$\underbrace{\begin{pmatrix} x \\ z \\ \dot{x} \\ \dot{z} \end{pmatrix}}_{\substack{final \\ state\ vector}} = \underbrace{\begin{bmatrix} 1 & 6(\sin nt - nt) & (4\sin nt)/n - 3t & 2(\cos nt - 1)/n \\ 0 & 4 - 3\cos nt & 2(1 - \cos nt)/n & (\sin nt)/n \\ 0 & 6n(\cos nt - 1) & 4\cos nt - 3 & -2\sin nt \\ 0 & 3n\ \sin\ nt & 2\sin nt & \cos nt \end{bmatrix}}_{time-evolution\ \ matrix} \underbrace{\begin{pmatrix} x_0 \\ z_0 \\ \dot{x}_0 \\ \dot{z}_0 \end{pmatrix}}_{\substack{initial \\ state\ vector}} \tag{8.5.9}$$

and

$$\boxed{\begin{pmatrix} y \\ \dot{y} \end{pmatrix} = \begin{bmatrix} \cos nt & (\sin nt)/n \\ -n \sin nt & \cos nt \end{bmatrix} \begin{pmatrix} y_0 \\ \dot{y}_0 \end{pmatrix}} \tag{8.5.10}$$

These are the basic equations for orbital motion in the vicinity of the reference object and with respect to its co-moving topocentric coordinate system RSW.

Application to Orbital Rendezvous

A typical application of Eq. (8.5.9) is the design of an orbital rendezvous. If at time $t_0 = 0$ a S/C is at an initial point $\boldsymbol{r}_0 = (x_0, y_0, z_0)$ the problem to solve is: What should be the initial velocity $\boldsymbol{v}_0 = (\dot{x}_0, \dot{y}_0, \dot{z}_0)$ to meet after time t a given target point $\boldsymbol{r} = (x, y, z) = (0, 0, 0)$? The solution can be derived from the equations for x, y, and z of Eqs. (8.5.9) and (8.5.10) by setting $x = y = z = 0$ and solving for $\dot{x}_0, \dot{y}_0, \dot{z}_0$. If this is done, one straightforwardly obtains

$$\begin{aligned} \frac{\dot{x}_0}{n} &= \frac{(4 \sin nt - 3nt \cos nt)x_0 + 2(\cos nt - 1)z_0}{3nt \sin nt + 8(\cos nt - 1)} \\ \frac{\dot{z}_0}{n} &= \frac{\sin nt \cdot z_0 - [6nt \sin nt + 14(\cos nt - 1)]x_0}{3nt \sin nt + 8(\cos nt - 1)} \\ \frac{\dot{y}_0}{n} &= -\frac{y_0}{\tan nt} \end{aligned} \tag{8.5.11}$$

or in matrix expression

$$\begin{pmatrix} \dot{x}_0 \\ \dot{z}_0 \end{pmatrix} = \frac{n}{3nt \sin nt + 8 \cos nt - 8} \begin{pmatrix} 4 \sin nt - 3nt \cos nt & 2 \cos nt - 2 \\ 14 - 14 \cos nt - 6nt \sin nt & \sin nt \end{pmatrix} \begin{pmatrix} x_0 \\ z_0 \end{pmatrix}$$

$$\dot{y}_0 = -\frac{n}{\tan nt} y_0$$

The required delta-v for these maneuvers then is given by

$$\Delta v = \sqrt{(\dot{x}_0 - \dot{x}_{0-})^2 + (\dot{y}_0 - \dot{y}_{0-})^2 + (\dot{z}_0 - \dot{z}_{0-})^2} \tag{8.5.12}$$

where $\boldsymbol{v}_{0-} = (\dot{x}_{0-}, \dot{y}_{0-}, \dot{z}_{0-})$ is the velocity of the S/C just before the impulse maneuver at (x_0, y_0, z_0).

It is an easy exercise to show that in the limit $t \to 0$ Eq. (8.5.11) pass over into

$$\begin{aligned} \dot{x}_0 &= -\frac{x_0}{t} - n z_0 - \frac{1}{6} n^2 x_0 t + O(n^3 z_0 t^2) \\ \dot{z}_0 &= -\frac{z_0}{t} + n x_0 - \frac{5}{6} n^2 z_0 t + O(n^3 x_0 t^2) \qquad @\, t \to 0 \\ \dot{y}_0 &= -\frac{y_0}{t} + \frac{1}{3} n^2 y_0 t + O(n^4 y_0 t^3) \end{aligned}$$

Therefore, for $(nt)^2 \ll 1$, which implies roughly $t < 0.02 \cdot T$, we can write

$$\begin{aligned} \dot{x}_0 &= -\tfrac{x_0}{t} - n\, z_0 \\ \dot{z}_0 &= -\tfrac{z_0}{t} + n\, x_0 \\ \dot{y}_0 &= -\tfrac{y_0}{t} \end{aligned} \qquad @\ (nt)^2 \ll 1 \tag{8.5.13}$$

These expressions will later be useful to explore maneuvers in the vicinity of the target object.

8.5.3 *Flyaround Trajectories*

In order to fly in a controlled way in the vicinity of a target object we need to know: What does a flyaround trajectory of a S/C look like? We will now explore the two different types of trajectories because they are essential for understanding the general behavior of such a S/C.

The Prolate Cycloid

On November 18, 2008, the astronaut Heidemarie Stefanyshyn-Piper lost her toolbox in space when carrying out repair work outside the International Space Station. She accidentally and gently touched the toolbox (which should have been secured by a line either to her or the ISS, but was not) giving the box a push such that it slowly drifted away from the station (see Fig. 8.25).

This accident is a good example to study the trajectory of slowly moving objects near a reference system, which for our purposes is the ISS at an average altitude of 350 km. So, what was the trajectory of the toolbox? It is important to know in which direction the push was relative to the flight direction of the ISS. Because we do not know, we will assume two different situations. First, Heidemarie pushed the toolbox along the flight direction, with an initial velocity of, say, $\boldsymbol{v}_0 = (\dot{x}_0, \dot{y}_0, \dot{z}_0) = (v_0, 0, 0)$.

Fig. 8.25 The toolbox (top right) of astronaut Stefanyshyn-Piper slowly drifting away from the ISS truss structure (bottom left). *Credit* NASA

We study the trajectory in the RSW coordinate system of Heidemarie, so $\boldsymbol{r}_0 = (x_0, y_0, z_0) = (0, 0, 0)$. Under these initial assumptions, we read from Eq. (8.5.9)

$$\begin{aligned} x(t) &= \frac{v_0}{n}(4\sin nt - 3nt) \approx v_0 t \\ \dot{x}(t) &= v_0(4\cos nt - 3) \\ z(t) &= 2\frac{v_0}{n}(1 - \cos nt) \approx n v_0 t^2 \\ \dot{z}(t) &= 2v_0 \sin nt \end{aligned} \tag{8.5.14}$$

where the approximations are for early times on the trajectory, $nt \ll 1$. If we solve the approximation for x and insert it in the approximation for z, we obtain a parabolic trajectory

$$z = \frac{nx^2}{v_0}$$

To be more concrete, let us assume that Heidemarie pushed the toolbox backward, against flight direction, with an initial velocity of, say, $v_0 = -0.1\,\mathrm{m\,s^{-1}}$. Because v_0 is negative we get a down curved parabola (see Fig. 8.26): The toolbox dives below the orbit of the ISS, which first seems to be quite surprising. Interestingly the toolbox comes to a halt in $-x$-direction when $\cos nt = 3/4$ and thereafter moves back toward the ISS, yet at increasingly lower altitudes. After half an orbit, it reaches the lowest point (perigee), and then it climbs up to reach the initial altitude of 350 km after a full revolution of the ISS, however at a distance of 1.65 km in front of the ISS. The toolbox will repeat this loopy motion indefinitely thereby moving away from the ISS—the toolbox will be lost. Such a winding trajectory is mathematically called a *prolate cycloid*.

What is the reason for such a weird trajectory? When the toolbox is kicked off backward it has a lower velocity as it should have for a circular orbit at this altitude.

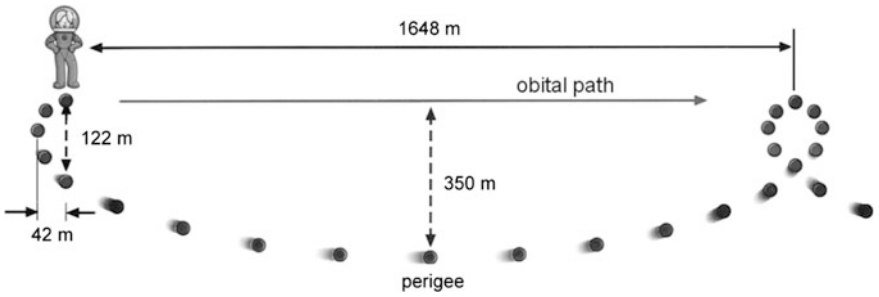

Fig. 8.26 The prolate cycloid trajectory of the toolbox that Heidemarie lost, if its initial motion, $v_0 = -0.1\,\mathrm{m\,s^{-1}}$, was reverse to the flight direction of the ISS. ISS altitude is $h = 350\,\mathrm{km}$

So the centrifugal force $F_c = mv^2/r$ is lower than the gravitational force, which rapidly pulls the box down. But upon dropping it gains speed, which brings it to a lateral halt at 42 m away from the ISS. With increasing speed the centrifugal force increases that after half a revolution at perigee brings the decline to a halt at 350 m below and 824 m ahead of the ISS. Since the speed now is too large for this altitude, the box dives up and decelerates until it "kisses" the orbit to iterate its dive.

The size of the cycloid depends linearly on the initial velocity while its orientation reverses when v_0 is with or against the flight direction of the ISS. Figure 8.27 gives an overview of this behavior for different initial x_0.

The reason for this weird motion can be understood when seen in a geocentric reference system (see Fig. 8.28). An object initially slower than the ISS at point 0 will have less orbital energy and hence move on an elliptic trajectory with smaller major-axis than the ISS. This implies that the object will drop below the ISS and will have a smaller orbital period, so showing up in front of the ISS after one revolution at the initial point 0. An object with a larger initial velocity will move on a larger ellipse with reversed behavior.

This view in an inertial reference frame makes clear that the prolate cycloid is the trajectory of a Hohmann transfer as observed in the target's reference frame. This should have been clear from the very beginning, because the initial kick-burn is tangential to the initial orbit. This is the attribute of a Hohmann transfer.

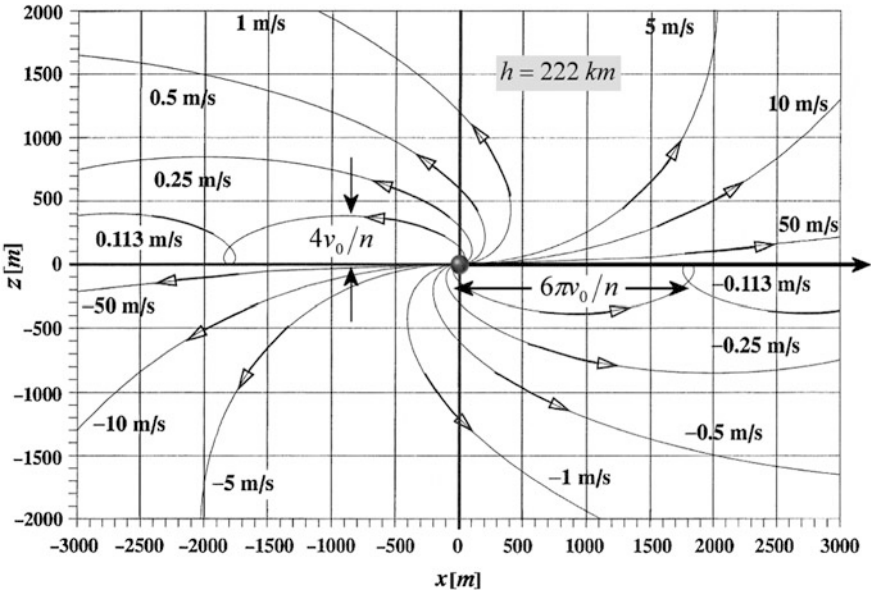

Fig. 8.27 Shown are for different v_0 in x-direction the trajectories (prolate cycloid) of the object moving relative to a reference point [center dot, which itself moves on an orbit at altitude $h =$ 222 km to the right (bold arrow)]. *Credit* Vallado (2007)

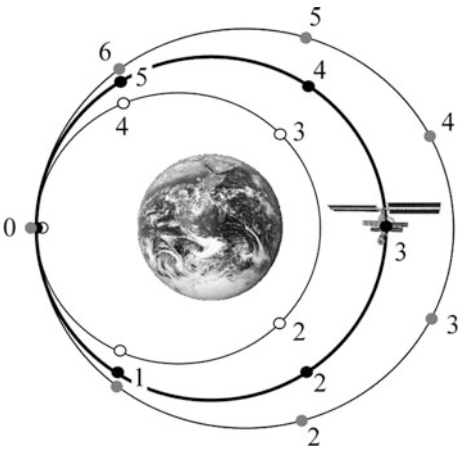

Fig. 8.28 A schematic sketch of the prolate cycloid motion as viewed from the inertial reference frame of Earth. The smaller ellipse is for an object with smaller velocity and the larger ellipse with a larger velocity at point 0. The numbered points give the positions on each orbit after constant time intervals

The Ellipse

We now assume that Heidemarie pushed the toolbox vertically to the flight direction, with initial velocity $\boldsymbol{v}_0 = (\dot{x}_0, \dot{y}_0, \dot{z}_0) = (0, 0, v_0)$. Interestingly, the trajectory of the toolbox would be totally different. From Eq. (8.5.9) we derive the trajectory to be

$$\begin{aligned} x &= 2\frac{v_0}{n}(\cos\, nt - 1) \approx -nv_0t^2 \\ z &= \frac{v_0}{n}\sin\, nt \approx v_0t \end{aligned} \tag{8.5.15}$$

again with approximations for early times on the trajectory, $nt \ll 1$. By removing the time parameter for $nt \ll 1$, we again find a parabola, that, however, opens to the rear side of the ISS.

$$z = \sqrt{-\frac{v_0}{n}x}$$

To derive the full trajectory we recognize that we can solve both equations for $\cos\, nt$ and $\sin\, nt$ and via the trigonometric equation $\sin^2 x + \cos^2 x = 1$, we find

$$\frac{(x + 2v_0/n)^2}{(2v_0/n)^2} + \frac{z^2}{(v_0/n)^2} = 1$$

which is the equation of an ellipse with semi-major axis $a = 2v_0/n$ along the x-axis and semi-minor axis $b = v_0/n$ along the z-axis, and therefore eccentricity $e = \sqrt{1 - b^2/a^2} = \sqrt{3/4} = 0.8660\ldots$. Details of such ellipses with $v_0 = 0.1\,\mathrm{m\,s^{-1}}$ are shown in Fig. 8.29 and for varying initial velocities in Fig. 8.30.

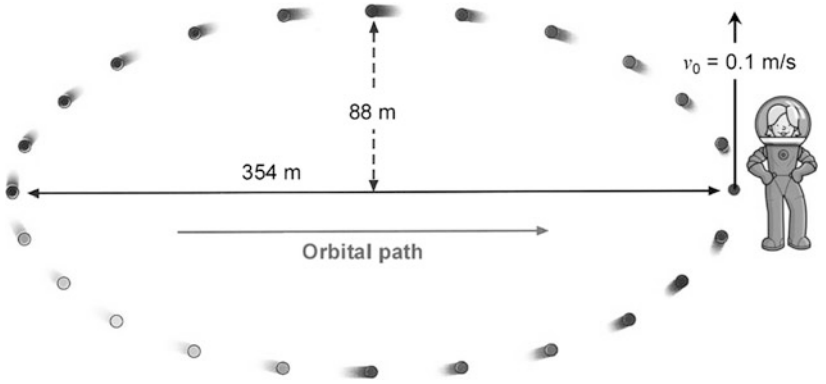

Fig. 8.29 The path of Heidemarie's toolbox if pushed with $v_0 = 0.1$ m s^{-1} along the positive z-direction. The box follows a closed elliptic path and returns to Heidemarie after one orbital revolution of the ISS. ISS altitude is $h = 350$ km

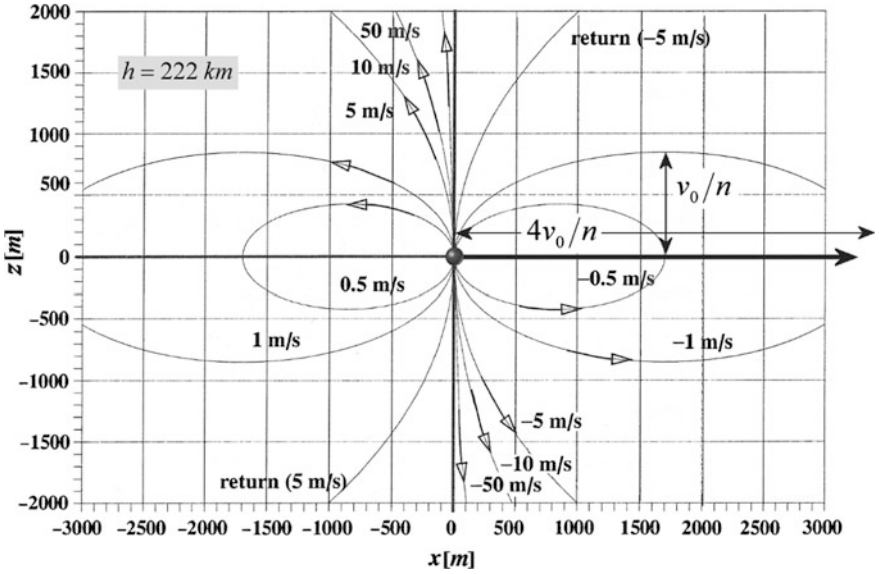

Fig. 8.30 Trajectories (ellipses) of an object moving relative to a reference point [center dot, which itself moves on an orbit at altitude $h = 222$ km to the right (bold arrow)] for different v_0 in z-direction. *Credit* Vallado (2007)

We can summarize the behavior of the toolbox as follows: When initially moving up, the orbital velocity remains constant. However, the angular velocity $\omega = v/r$ and the centrifugal force $F_c = mv^2/r$ decrease. Owing to this, the toolbox falls behind the ISS and also loses vertical speed, because the gravitation pull

becomes bigger than the centrifugal force. After a quarter of an orbital revolution of the ISS, the toolbox drops down and crosses the orbit after half an orbital revolution, but now with downward velocity. The inverse behavior thereafter would bring the toolbox back to Heidemarie.

If a S/C relative to a target object starts its trajectory from the orbital path of the target object and initially moves along the x- or z-direction, the ellipse and the prolate cycloid are the two possible forms of this trajectory. The trajectories become more intricate if $\boldsymbol{v}_0$ is not pointing into the x- or z-direction, or the initial location is displaced from the orbital path, or both. In any of these cases the main features of such convoluted trajectories are the ellipse and the prolate cycloid. The reason is, whatever the initial conditions of the S/C might be, it will move on an ellipse around the Earth. If its semi-major axis a is the same as that of the target object it will just fly around the target object periodically. If its a is different, its orbital period will be different and therefore the periodic motion will be superimposed by a motion that let the S/C and the target object drift relative to each other. These two features are extensively used for applied orbital rendezvous maneuvers to which we will turn now.

8.5.4 Near-Circular Orbits

Differential Equations

We now want to convey these results to near-circular orbits, i.e. orbits with $e \ll 1$. For small eccentricities it is easy to show (exercise, Problem (8.9)) that Eq. (8.5.3) pass over into

$$\begin{aligned} \ddot{x} + 2n\dot{z} &= en(nx\cos nt + 2nz\sin nt - 4\dot{z}\cos nt) \\ \ddot{y} + n^2 y &= -3en^2 y\cos nt \qquad @\ e \ll 1 \quad (8.5.16) \\ \ddot{z} - 2n\dot{x} - 3n^2 z &= 2en(-nx\sin nt + 5nz\cos nt + 2\dot{x}\cos nt) \end{aligned}$$

or in our dimensionless notation (see Sect. 8.5.2)

$$M = nt, \quad (.)' := \frac{d}{dM} = \frac{1}{n}\frac{d}{dt}, \quad (.)'' = \frac{d^2}{dM^2} = \frac{1}{n^2}\frac{d^2}{dt^2}$$

they read

$$\begin{aligned} x'' + 2z' &= e(x\cos M + 2z\sin M - 4z'\cos M) \\ y'' + y &= 3e(-y\cos M) \qquad @\ e \ll 1 \quad (8.5.17) \\ z'' - 2x' - 3z &= 2e(-x\sin M + 5z\cos M + 2x'\cos M) \end{aligned}$$

Here M is measured relative to the periapsis of the elliptical target orbit.

Solution to Differential Equations

It is quite intricate to solve these differential equations. We therefore leave this as an exercise to the reader (see Problem 8.10) and provide here only the exact results:

$$x(M) = \left[\begin{pmatrix} 1 \\ 6\sin M - 6M \\ 4\sin M - 3M \\ 2\cos M - 2 \end{pmatrix}^T + e \begin{pmatrix} -\cos M + 1 \\ \sin M \cos M + 12 \sin M - 6M \cos M - 15M \\ 6\sin M \cos M - 3M \cos M - 3M \\ 3\cos^2 M - 2\cos M - 1 \end{pmatrix}^T \right] \begin{pmatrix} x_0 \\ z_0 \\ x_0' \\ z_0' \end{pmatrix}$$

$$y(M) = \left[\begin{pmatrix} \cos M \\ \sin M \end{pmatrix}^T + e \begin{pmatrix} \cos^2 M + \cos M - 2 \\ \sin M \cos M - \sin M \end{pmatrix}^T \right] \begin{pmatrix} y_0 \\ y_0' \end{pmatrix} \tag{8.5.18}$$

$$z(M) = -\left[\begin{pmatrix} 0 \\ 3\cos M - 4 \\ 2\cos qM - 2 \\ -\sin M \end{pmatrix}^T + e \begin{pmatrix} 0 \\ 6\cos^2 M + 10\cos M + 6M\sin M - 16 \\ 4\cos^2 M + 2\cos M + 3M\sin M - 6 \\ -2\sin M \cos M + 2\sin M \end{pmatrix}^T \right] \begin{pmatrix} x_0 \\ z_0 \\ x_0' \\ z_0' \end{pmatrix}$$

We recall that M is measured relative to the periapsis of the elliptical target orbit. Observe that these solutions satisfy our standard initial conditions

$$\begin{aligned} x(0) &= x_0, \quad x'(0) = x_0' \\ y(0) &= y_0, \quad y'(0) = y_0' \\ z(0) &= z_0, \quad z'(0) = z_0' \end{aligned}$$

Flyaround Trajectories

At the periapsis let us first place a S/C at $(x_0, 0, 0)$ behind the ISS with initial zero relative velocity, $\boldsymbol{v}_0 = (0, 0, 0)$, and see what happens. From Eq. (8.5.18) we obtain

$$\begin{aligned} x(t) &= [1 + e(1 - \cos nt)]x_0 \\ y(t) &= 0 \\ z(t) &= 0 \end{aligned}$$

If the reference orbit were circular we would get a steady distance, $x(t) = x_0 = const$ to the target because the orbit velocity is always constant. For an elliptical target the distance slightly changes over one orbit in the interval $x_0 \le x(t) \le (1 + 2e) \cdot x_0$. Where $x = (1 + 2e) \cdot x_0$ happens at the apoapsis (Fig. 8.31).

The Prolate Cycloid

We now start with an initial longitudinal velocity $\boldsymbol{v}_0 = (\dot{x}_0, \dot{y}_0, \dot{z}_0) = (v_0, 0, 0)$ and again study the trajectory in the RSW coordinate system of the ISS, so $\boldsymbol{r}_0 = (x_0, y_0, z_0) = (0, 0, 0)$. Under these initial assumptions, we read from Eq. (8.5.18) after some minor modification

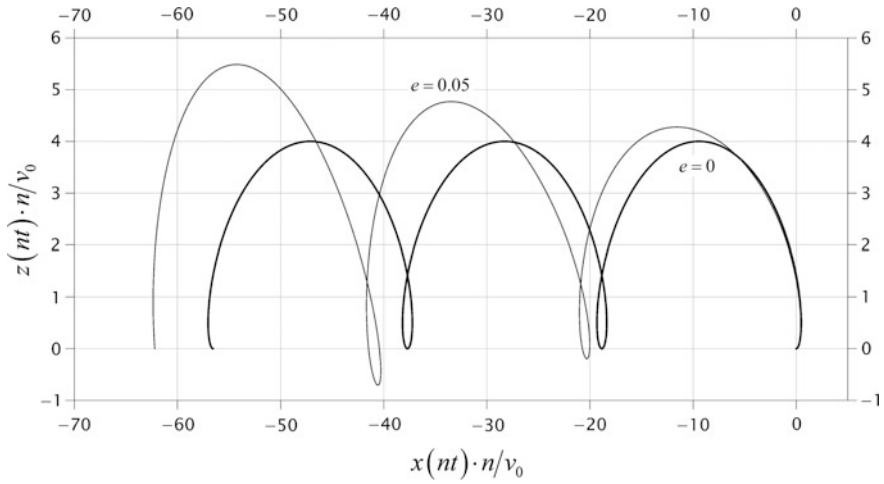

Fig. 8.31 The prolate cycloid as given by Eq. (8.5.19) with $e = 0.05$ and with $e = 0$ for reference

$$\begin{aligned} x(t) &= \frac{v_0}{n}[4\sin nt - 3nt + 3e(2\sin nt\cos nt - nt(1+\cos nt))] \\ \dot{x}(t) &= v_0[4\cos nt - 3 + 3e(2\cos 2nt - \cos nt + nt\sin nt - 1)] \end{aligned} \tag{8.5.19}$$

and

$$\begin{aligned} z(t) &= -\frac{v_0}{n}\left[2\cos nt - 2 + e\left(4\cos^2 nt + 2\cos nt + 3nt\sin nt - 6\right)\right]\dot{z}(t) \\ &= v_0[2\sin nt + e(4\sin 2nt - \sin nt - 3nt\cos nt)] \end{aligned}$$

The Ellipse

As in Sect. 8.5.2 we finally examine the flyaround trajectory with an initial transversal velocity $\boldsymbol{v}_0 = (\dot{x}_0, \dot{y}_0, \dot{z}_0) = (0, 0, v_0)$. In this case we find

$$\begin{aligned} x(t) &= \frac{v_0}{n}\left[2\cos nt - 2 + e\left(3\cos^2 nt - 2\cos nt - 1\right)\right] \\ z(t) &= \frac{v_0}{n}\sin nt[1 + 2e(\cos nt - 1)] \end{aligned} \tag{8.5.20}$$

We eliminate the time dependency by using $\sin^2 nt + \cos^2 nt = 1$ and find the trajectory

$$\left[\frac{x + 2v_0/n[1 - \frac{e}{2}(3\cos^2 nt - 2\cos nt - 1)]}{2v_0/n}\right]^2 + \left[\frac{z - 2ev_0\sin nt(\cos nt - 1)/n}{v_0/n}\right]^2 = 1$$

This is also an ellipse, with an center offset by $2e$ as shown in Fig. 8.32.

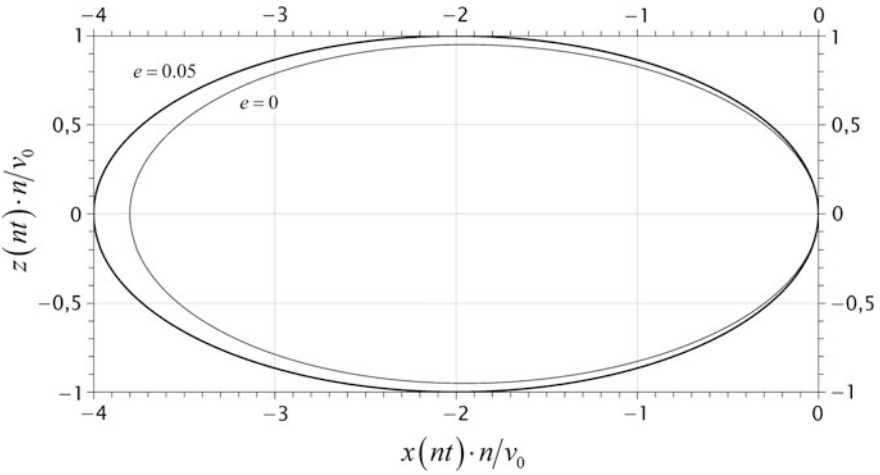

Fig. 8.32 The ellipse as given by Eq. (8.5.20) with $e = 0.05$ and $e = 0$ for reference

8.6 Orbital Rendezvous

Rendezvous and docking (R&D) form some of the most complex maneuvers to be carried out by a spacecraft in spaceflight. To accomplish successful rendezvous and mating of two spacecraft, absolute and relative navigation on orbit, sensing of the target object, precise attitude determination and control, maneuver planning, and the use of highly complex mechanisms must be mastered. The development of these skills was the purpose of the US Gemini program and the early Soviet Soyuz program, and they were further refined in the era of the Space Shuttle and the ISS. In recent years, the desire for autonomous robotic on-orbit servicing systems and plans for more ambitious human and robotic exploration of the solar system create new challenges for technology and mission designers.

The purpose of any R&D mission is to establish physical contact between two or more spacecraft to establish electrical, material, and crew exchange. Therefore R&D is a prerequisite for the construction and maintenance of space stations such as the ISS, as well as any servicing mission to satellites in Earth orbit. Such missions can be manned (e.g., the Hubble servicing missions) or unmanned (e.g., future On-Orbit Servicing). R&D is also a mission-enabling skill in human and robotic exploration of the solar system. Without successful R&D, the Apollo missions would not have been possible.

As the established term *rendezvous and docking* implies, the involved operations are divided into two distinct parts, each with a particular set of goals.

Rendezvous: During the rendezvous part of the mission, the involved spacecraft are guided to meet in the same volume of space, at the same time. In most applications, the target object (also often referred to as *resident space object*) is inert, and the

interceptor (a.k.a. chaser) performs all maneuvers to meet the position and time requirements. However, as an exception to this rule, in the so-called *control box rendezvous*, it is the target spacecraft that executes a number of maneuvers to meet the interceptor after it was launched. This reduces interceptor vehicle propellant consumption, naturally at a cost to the target. It therefore can only be performed with targets having orbit maneuvering capabilities, which usually rules out space stations and a large number of satellites. Nonetheless, this type of rendezvous was performed on some Space Shuttle missions (e.g., STS-49 to service Intelsat VI) and was also planned for the contingency rescue mission STS-400 to Atlantis' Hubble Servicing Mission 4.

Docking: The goal of docking in a mission is to establish physical contact between the involved spacecraft. Although commonly the term *docking* is used, there actually exist two distinct cases: *docking*, and *capture and berthing*. In

(1) *Docking*. The interceptor approaches the target with non-zero relative velocity, brings its docking tool into alignment with the target's counterpart, and establishes a firm structural connection by using its own momentum. Docking therefore relies only on maneuvering capabilities of the two spacecraft and on properly functional docking tools. This approach was used during Gemini and Apollo and still is in use with Soyuz/Progress, the Space Shuttle, and ESA's Automated Transfer Vehicle (ATV) missions to ISS.
(2) *Capture and berthing*. The interceptor is maneuvered into close proximity of the target and an initial mechanical connection between both is established by a robotic manipulator. This manipulator can be either situated on the interceptor (as is the case with the Shuttle Robotic Manipulator System (RMS) used for capturing the Hubble Space Telescope), or on the target vehicle. This is the approach taken with the Space Station Remote Manipulator System (SSRMS) on ISS capturing the Japanese H-II Transfer Vehicle (HTV). After capture, the captured spacecraft is then moved by the manipulator to a berthing position, which is a device similar to a docking port.

The choice of the manipulator's location is, on the one hand, dependent on the sizes and masses of the spacecraft. The attitude of a heavier spacecraft is less influenced by the disturbance torques caused by the movement of the manipulator. On the other hand, a space manipulator is a very complex and hence an expensive mechanism. It will therefore be mounted on the spacecraft with the longer lifetime and/or reentry capability, and not on the disposable spacecraft like HTV.

The combination of both rendezvous and docking is not an end to itself, but serves to fulfill the purpose of a mission. It therefore must always be carefully planned and designed within the larger mission context. This influences not only design decisions such as launch windows, approach trajectories, and the selection of sensors, but also the general approach modes, be it operator-in-the-loop or autonomous robotic. To understand the challenges, choices, and trade-offs involved, the following section provides details about R&D mission design.

Mission Phases

Generally, R&D missions involve both an interceptor spacecraft, which begins the mission on the launch pad, and a target spacecraft, which is usually already in orbit by the time of the interceptor's launch. The following sections will discuss the mission phases of typical R&D missions in Low Earth Orbit (LEO), which are in the following order:

1. Launch
2. Phasing
3. Homing
4. Closing
5. Final Approach
6. Docking/Capture

This sequence of mission steps results in a typical R&D mission profile as shown in Fig. 8.33.

This R&D mission profile typically takes two days to accomplish. This is why it is sometimes called a *2-day rendezvous profile*. It is a standard profile used for R&D missions in particular for ISS R&D by Soyuz, Shuttle or ESA ATV.

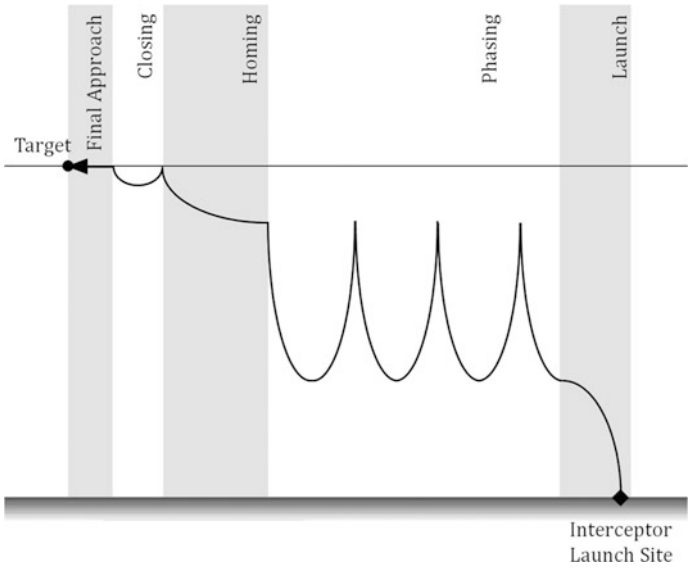

Fig. 8.33 Sketch of a typical R&D mission profile consisting of launch phase, phasing maneuvers, homing, and close-range rendezvous (closing and final approach) including docking

8.6.1 Launch Phase

The launch phase comprises the injection of the interceptor into the orbital plane of the target, as well as achieving stable orbital conditions. To directly meet the plane of the target, the interceptor must be launched inside a narrow launch window. This launch window is derived in the following steps.

First, we derive the launch azimuth φ, which is the angle between the launch trajectory and the geographic North, i.e., the local direction in which to launch. If we denote the target's orbit inclination as i and the launch site latitude as β, we have from Fig. 8.34 and according to Napier's rules for spherical angles $\cos i = \cos\beta \cdot \sin(180^\circ - \varphi) = \cos\beta \cdot \sin\varphi$ from which we obtain the following two solutions:

$$\begin{aligned} \varphi_1 &= \arcsin\frac{\cos i}{\cos\beta} \quad @\ \text{ascending pass} \\ \varphi_2 &= 180^\circ - \arcsin\frac{\cos i}{\cos\beta} \quad @\ \text{descending pass} \end{aligned} \tag{8.6.1}$$

The reason is, a launch site passes twice a day through a given orbital plane: Once on the ascending pass of the target orbit with launch azimuth φ_1, the other on the descending pass with launch azimuth φ_2. So, if for a launch site the launch azimuth is not limited there are two launch opportunities every day.

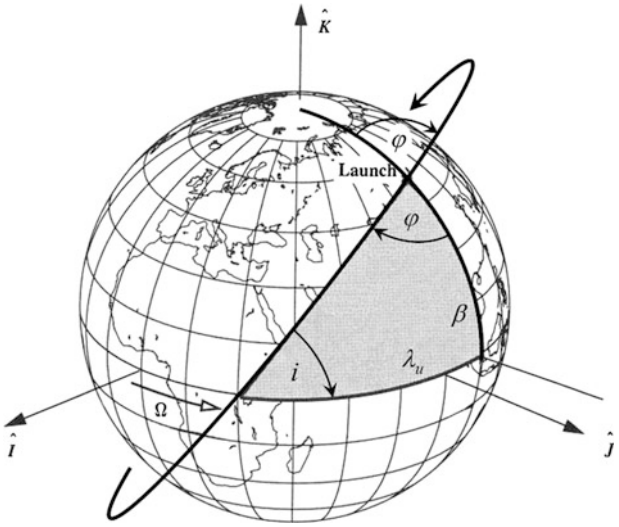

Fig. 8.34 Launch window trigonometry. Illustrated are the target orbit with RAAN Ω and inclination i, launch site latitude β, launch azimuth φ, and the auxiliary angle λ_u. *Credit* Vallado (2007)

From $\cos i = \cos \beta \cdot \sin \varphi$ we can read that because $|\sin \varphi| \leq 1$, we have $\cos i \leq \cos \beta$ implying $i \geq \beta$. So there exists no launch azimuth to achieve an $i < \beta$, or in other words: Orbits with $i < \beta$ cannot be reached directly. This seemingly paradoxical situation is elucidated in Fig. 8.35. For example, launchers from Kennedy Space Center with $\beta = 28.47°$ cannot reach orbits with $i < 28.47°$. Only in the limiting case $\varphi = 90°,\ 270°$, i.e., if the launch azimuth is East or West (into a retrograde orbit), we obtain $i = \beta$. If orbits $i < \beta$ need to be reached, the launcher is first launched with $i = \beta$. When its orbit intersects the desired target orbit having $i < \beta$, a plane change maneuver (a.k.a. dogleg maneuver) is performed that, however, is associated with large propellant consumption and thus reduced payload for a given target orbit.

What is the right time to launch? The Universal Time of launch, T_{UT}, defines the moment in time when the launch site is in the plane of the International Space Station's orbit, the so-called *in-plane time*. At this launch time the interceptor reaches the targeted orbital plane with the least effort (delta-v). It is given by

$$T_{UT} = \frac{\theta_{GMST} - \theta_{GMST0}}{\omega_{\oplus}} \quad \textbf{in-plane time (launch time)} \tag{8.6.2}$$

where $\omega_{\oplus} = 7.2921150 \times 10^{-5}\ \mathrm{s}^{-1}$ is Earth's sidereal rotation rate $\omega_{\oplus}$. The hour angle θ_{GMST}, representing the Greenwich Mean Sidereal Time (GMST) for the launch to occur at, is calculated as

$$\theta_{GMST} = \Omega + \lambda_u - \lambda$$

where the auxiliary angle λ_u (see Fig. 8.34), which is the difference between the launch site longitude λ and the target orbit is Right Ascension of Ascending Node (RAAN) Ω, is calculated from Napier's rules as

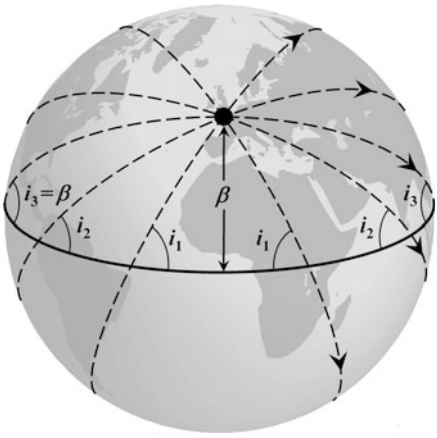

Fig. 8.35 Whatever the launch azimuth is, the accessible orbit inclination i is always larger than the latitude of the launch site β. If the launch azimuth is $\varphi = 90°$ then $i = \beta$ is achieved

$$\lambda_u = \arccos \frac{\cos\ \varphi_{1,2}}{\sin\ i} = \pm\ \arcsin \frac{\sqrt{1 - (\cos\ i/\cos\ \beta)^2}}{\sin\ i}$$

The required hour angle θ_{GMST0} of a particular launch day at hour 00:00 h can be obtained from the Astronomical Almanac of the given year or from

$$\begin{aligned}\theta_{GMST0} =& 100.4606184^\circ + 3600.77005361^\circ\,\mathrm{s}^{-1} \cdot T_{UT1} \\ &+ 0.00038793^\circ\,\mathrm{s}^{-2} \cdot T_{UT1}^2 - 2.6 \times 10^{-8}\ ^\circ\,\mathrm{s}^{-3} \cdot T_{UT1}^3\end{aligned}$$

The term T_{UT1} denotes the number of *Julian centuries* of the launch day at 00:00:00 h elapsed since the *standard epoch* J2000, which is given as

$$T_{UT1} = \frac{JD - 2\ 451\ 545.0}{36\ 525}$$

where in turn the Julian date JD of the given launch day at 00:00:00 h, which should be provided in terms of years $\langle yyyy \rangle$, months $\langle mm \rangle$, and days $\langle dd \rangle$, is computed by

$$\begin{aligned}JD = 367 \cdot \langle yyyy \rangle - INT\left\{1.75 \cdot \left[\langle yyyy \rangle + INT\left(\frac{\langle mm \rangle + 9}{12}\right)\right]\right\} \\ + INT\left(\frac{275}{9}\langle mm \rangle\right) + \langle dd \rangle + 1\ 721\ 013.5\end{aligned}$$

where the function $INT(x)$ truncates the real number x to the next lower integer number.

Launch Windows

Any deviation from the in-plane launch time would implicate a dogleg maneuver and hence an additional propulsion demand for a plane-change maneuver (see Eq. (8.1.22) and Fig. 8.4 for details). On the other hand, since this precision is impractical to achieve both for organizational and technical reasons, one allows a small amount of time for the launch of the interceptor on both sides of the ideal launch time T_{UT}. This is the so-called **planar launch window**. The width of the planar launch window depends on the launch azimuth. If the launch azimuth is $\varphi \approx 90^\circ$, i.e., if the inclination matches the launch site latitude, the launch window is typically up to 1 h because no later plane adjustment would be necessary. With decreasing launch azimuth any deviation of the launch time from the in-plane time will cause increasing plane differences and hence an increasing propulsion demand to correct them. For Shuttle launches to the ISS ($i = 51.6^\circ$) the planar launch window decreases to only 10 min. Targets above 57° inclinations have planar launch windows of less than 5 min. In missions to ISS, in practice the Shuttle launch time is appointed to the opening of the launch window, i.e., 5 min before the in-plane time. In case of a launch delay due to a possible countdown problem there

remain 10 min to fix the problem. If no problem occurs, the Shuttle is put on hold for 5 min and is launched on in-plane time.

Apart from orbital mechanics there are other restrictions defining other kinds of launch windows on different time scales. An important consideration is the *sun angle*, which is the angle between the direction to the Sun and the targeted orbital plane. The sun angle is important for visibility conditions during final approach (cf. Fig. 8.45 where the Shuttle needs to see the ISS during daytime conditions, in particular during final approach) and for solar power generation of the docked spacecraft. For the Space Shuttle another concern is the ability to monitor its ascent and to visually check the external tank for damages during launch and ascent.

When launching toward ISS, traffic conditions also impact launch window planning, since multiple spacecraft such as Soyuz, Progress, ATV, HTV, or Shuttle want to approach the station, during beneficial lighting conditions. All these factors must be considered in mission planning, which leads to the small number of launch windows available to ISS or Hubble per year. This is the reason why the failure to launch a mission during the originally intended window can cause launch delays of months, instead of hours or days as dictated by orbital mechanics. Also the so-called *phase window* (see next section) restricts the launch opportunities.

For a given launch site the range of permitted launch azimuths is usually restricted due to safety concerns of flying a launch vehicle over densely populated areas. For instance, the launch azimuth restrictions at Kennedy Space Center are $35^\circ \leq \varphi \leq 120^\circ$, where the lower bound is due to the US West Coast and the upper bound to the Caribbean islands. This restricts the Shuttle to have only one launch opportunity per day to the ISS.

8.6.2 Phasing

After successful completion of the launch phase, the interceptor spacecraft achieves a stable orbit within the same plane as the target. The two orbits are thus coplanar and typically near circular. (Alternatively, the interceptor is in a plane from which the target plane can be reached within the capabilities of the orbital maneuvering system of the interceptor.)

However, the target might be anywhere on its orbit. Therefore, the first part of the target rendezvous, the so-called *far range rendezvous*, requires first a reduction in the distance to the target, until it can be acquired by the sensors of the interceptor, and then a transfer to a stable holding point on the trailing side of the target.

This first part of far range rendezvous phase is called *phasing* because it is to reduce the so-called *(orbital) phase angle* ϑ , which is the difference in true anomaly as measured in the flight direction from the target to the interceptor. Phasing is typically conducted in absolute navigation, i.e., with reference to an inertial reference frame, and guided by ground control. As an example, Space Shuttle phasing maneuvers are planned by mission control using orbit determination data obtained by ground radar and *Tracking and Data Relay Satellite System*

(TDRSS) Doppler measurements. By processing both the target and interceptor tracking data, the orbital phase angle is determined.

Usually, the interceptor needs to chase the target, so only negative initial phase angles are permitted. This is why the interceptor is often called *chaser*. In addition, only certain initial phase angles are permitted. Owing to performance limitations and constrained crew activities this so-called **phase window** (window accounting for phase angle makeup capability) varies for the Shuttle between $40° \leq -\vartheta_i \leq 360°$. The relationship of the phase window to the planar launch window changes each day and depends on the target's orbital period and inclination.

Owing to a given initial phase angle to be made up, the interceptor will have finalized its launch trajectory on a generally slightly elliptic or circular orbit with its semi-major axis a_I smaller than the a_T of the target orbit. Whether the initial apogee coincides with the target orbit depends on the particular rendezvous strategy, but usually the interceptor orbit nowhere crosses the target orbit. Because $a_I < a_T$ the orbital frequency (mean motion) is larger than that of the target, which implies that the orbital phase angle is reduced continuously—the goal of phasing.

How much is the phase angle reduced in course of one orbital revolution? Assuming small differences in the semi-major axes, which is a quite good approximation for LEO and since $n = \sqrt{\mu/a^3} = 2\pi/T$ of the target the phase reduction after one orbital revolution is

$$\Delta\vartheta = -\Delta n \cdot T = -\left(\frac{dn}{da} \cdot \Delta a\right) \cdot T = \frac{3}{2}\frac{n}{a} \cdot \Delta a \cdot T$$

Therefore

$$\Delta\vartheta = 3\pi\frac{\Delta a}{a} \text{ per orbit} \tag{8.6.3}$$

So, the phase angle from the interceptor (behind the target) to the target decreases if $a_I < a_T$, i.e., if $\Delta a = a_I - a_T < 0$. This phase angle reduction relates to a closing distance of

$$\Delta x = \Delta\vartheta \cdot a = -3\pi \cdot \Delta a \quad \text{per orbit}$$

To give an example, the ISS orbits Earth at an altitude of about $h = 350$ km. Owing to drag becoming too excessive, the lowest chaser altitude is limited to about $h = 250$ km. This implies $\Delta a \geq -100$ km.

So, for instance the Soyuz is able to approach the ISS typically with $\Delta\vartheta_{\max} = 7°$ per orbit equaling $\Delta x_{\max} = 820$ km per orbit. To limit the physical and fatigue stress to astronauts in the small S/C one typically sets a limit of two days to get to ISS docking. Accounting also for the first checkout orbit, the homing, closing, and final approach phases, the number of Soyuz phasing orbits are typically limited to 21 orbits equaling a maximum initial phase angle of $\Delta\vartheta_i \leq 150°$. This of course has a

grave impact on the possible launch windows. To ease this problem and to even further reduce the stress to astronauts the trajectory department of RSC Energia in March 2013 implemented a new rendezvous profile for Soyuz TMA-08M and for later Soyuz missions, where the phasing orbits were reduced to 5 orbits or less (typically 4), which has become known as the *fast rendezvous profile* a.k.a. *four-orbit rendezvous profile*. This fast profile was tested first on the unmanned ISS supply mission Progress M-16M in August 2012, while it was first applied to the manned mission Soyuz TMA-08M in March 2013 and to all manned Soyuz mission since then. This new 4-orbit rendezvous profile implies and initial phase angle of $\Delta\vartheta_i 15^\circ - 20^\circ$, which is achieved by adjusting the ISS orbit raising maneuvers months before launch day such that the ISS falls within this initial phase angle range.

8.6.3 Homing Phase

The interceptor is now on a phasing orbit about 50 km away from the target drifting slowly toward the target. The objective of the upcoming homing transfer, the second part of the far range rendezvous, is to transfer the interceptor to a stable holding and aiming point in the vicinity of the target (see Figs. 8.33 and 8.36). A prerequisite of the transfer is that the target must be acquired by the relative navigation sensors of the interceptor. For the Space Shuttle, mission control hands over rendezvous guidance to the orbiter's crew at 74 km from the target. At this point a target like the ISS can be tracked using star trackers or radar.

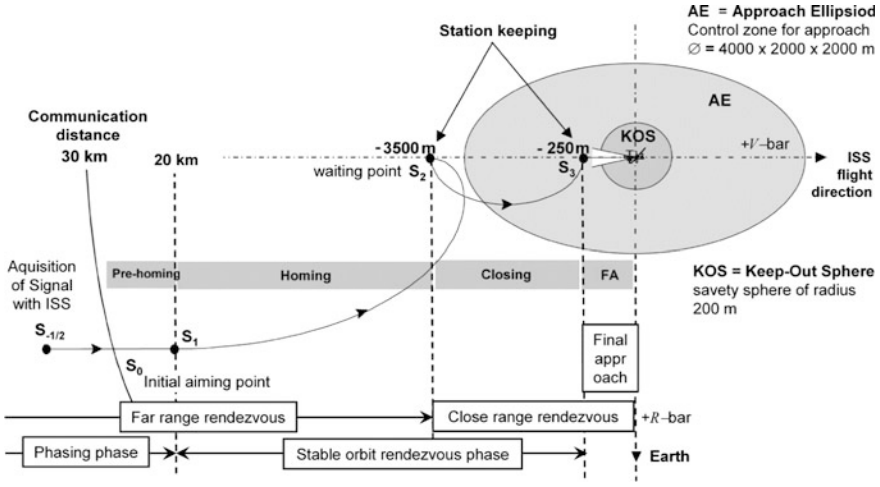

Fig. 8.36 Homing, closing, and final approach profile and phases for ISS rendezvous. ISS safe-approach procedures require station-keeping points S on the V-bar, an approach corridor, and a keep-out sphere around ISS that approaching spacecraft must use. *Credit* Wartenberg and Amadieu/ESA

With the homing maneuver also the relative approach velocity must be reduced to a safe level. In addition, the dispersions in position, orientation, and angular rate must be reduced to meet the conditions required for the upcoming close range rendezvous. This includes the synchronization of the motion timeline of the two spacecraft.

LVLH Reference Frame

For the discussion of the now following rendezvous approaches, the *Local Vertical Local Horizontal* (LVLH) reference frame is defined (see Fig. 8.37). The origin of LVLH is located at the center of mass of the target. Its +x-axis, also called the +V-bar, points along the target's velocity vector. The −z-axis, referred to as +R-bar, points antiparallel to the target's radial vector. The −y-axis, also called +H-bar, completes the right-handed system and thus points along orbit normal. In the following a "+V-bar approach" means that the interceptor approaches the target on the target's +V-bar (into −V-bar direction). Accordingly, a "−R-bar approach" is on the target's −R-bar (into +R-bar direction), etc.

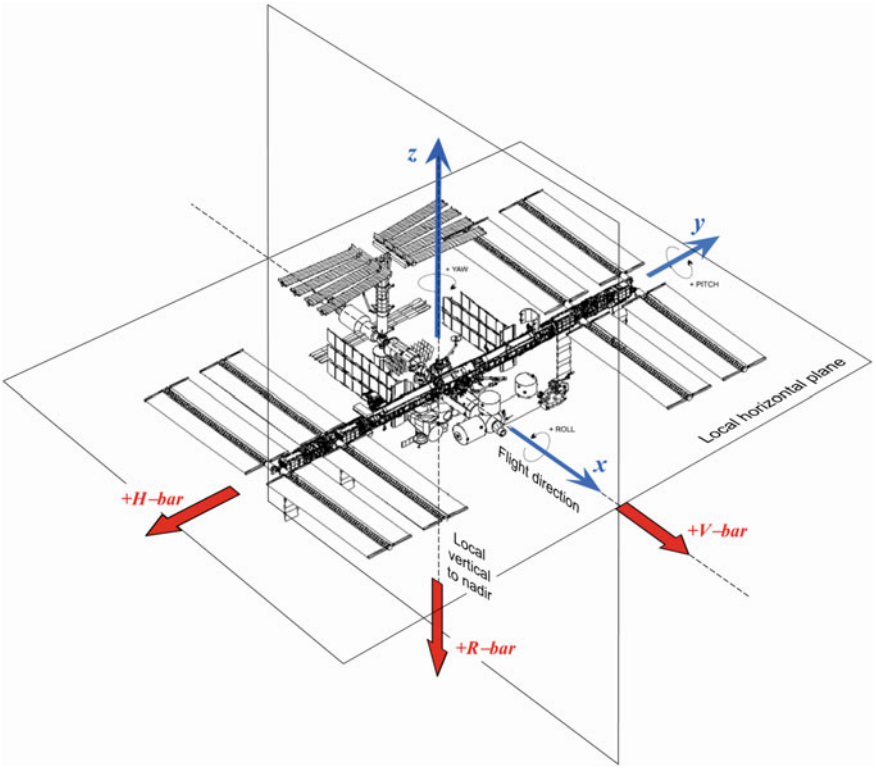

Fig. 8.37 Local vertical local horizontal (LVLH) reference frame: +V-bar (+x-axis) is in the direction of the spacecraft's velocity vector, +R-bar (+z-axis) is in the direction of the negative radius vector, and +H-bar (−y-axis) completes the right-handed system

Homing Transfer

The homing transfer, which commences at point S1 in Fig. 8.36, is a classical Hohmann transfer as described in Sect. 8.3. The principle situation is shown in Fig. 8.38, where the orbits, however, are not to scale because at the end of the phasing phase, the two orbits with $a \approx 6750\,\text{km}$ in LEO have a radial distance of typically only about 10 km. Owing to this, the phase angle at the beginning of the Hohmann maneuver is practically zero while its complement to 180°, the so-called *lead angle*, is $\alpha_L = 180° - \vartheta \approx 180°$.

Let ϑ_i be the initial phase angle and let ϑ_f be the final phase angle at S2 behind the target. The key question is: At a given a, Δa, and ϑ_f, what is the right ϑ_i and the right tangential kick-burn Δv to get to S2? To find an answer we apply from Sect. 8.3.2 the essential results of a Hohmann transfer to adjacent circular orbits as for rendezvous orbits

$$a_H = \frac{1}{2}(a_I + a) = a\left(1 + \frac{\Delta a}{2a}\right)$$

$$t_H = \pi\sqrt{\frac{a_H^3}{\mu}}$$

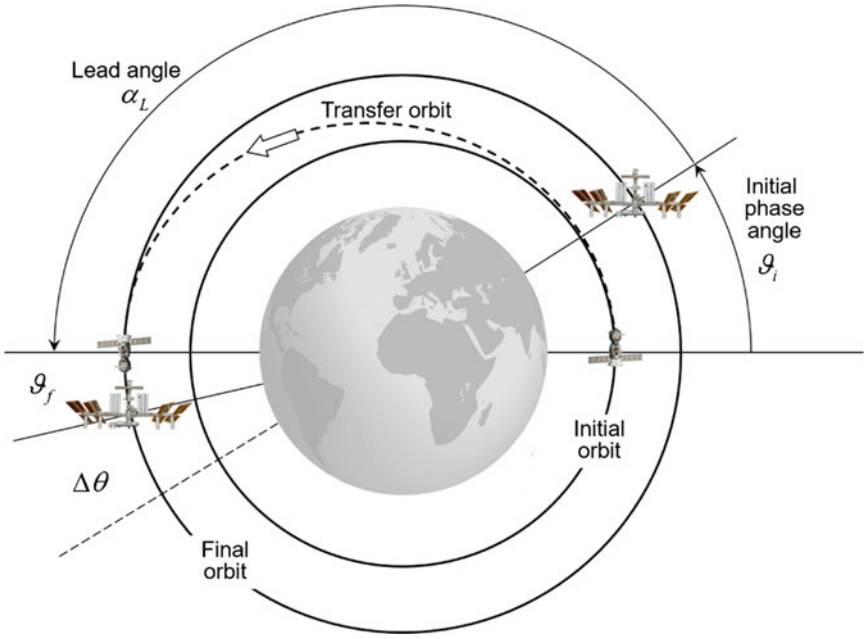

Fig. 8.38 General homing transfer of an interceptor (Soyuz) to meet a target point behind a target (ISS) in a circular coplanar orbit. Initially the required phase angle is ϑ and the interceptor begins the phasing maneuver by applying a thrust. After a half revolution on the transfer orbit, the interceptor reaches the target point, where a thrust maneuver brings the interceptor to a steady relative position behind the target and thus finalizes the Hohmann transfer

Now, while the interceptor transits over an orbit angle of 180° on the Hohmann transfer orbit, the target with $n = \sqrt{\mu/a^3}$ covers the orbit angle (see Fig. 8.38)

$$180^\circ - \Delta\theta = n \cdot t_H = 180^\circ \cdot \left(\frac{a_H}{a}\right)^{3/2} = 180^\circ \cdot \left(1 + \frac{\Delta a}{2a}\right)^{3/2} \approx 180^\circ \cdot \left(1 + \frac{3}{4}\frac{\Delta a}{a}\right)$$

Because in LEO $\Delta a/a \approx 10^{-3}$, we could safely neglect terms of higher order. Therefore, we have for the initial phase angle (see Fig. 8.38)

$$\vartheta_i = \vartheta_f + \Delta\theta = \vartheta_f - 180^\circ \cdot \frac{3}{4}\frac{\Delta a}{a}$$

or

$$\vartheta_i = \vartheta_f - 135^\circ \frac{\Delta a}{a} \tag{8.6.4}$$

For the required delta-v, we find with a circular orbital velocity $v = \sqrt{\mu/a}$

$$\Delta v = v_I - v_T = v_T \left(\sqrt{\frac{a}{a + \Delta a}} - 1\right) = v_T \left(\sqrt{1 - \frac{\Delta a}{a}} - 1\right)$$

and hence

$$\Delta v = -\frac{1}{2}\frac{\Delta a}{a}\sqrt{\frac{\mu}{a}} \tag{8.6.5}$$

Example

The Shuttle shall perform a homing maneuver from $\Delta a = -10\,\text{km}$ to a waiting point $S2 = 3\,\text{km}$ behind the ISS at $h = 350\,\text{km}$.

We have $\vartheta_f = (180^\circ/\pi) \cdot (10/6728) = 0.085^\circ$ and $v_T = 7.697\ \text{km s}^{-1}$. With this we get $\vartheta_i = \vartheta_f + 0.201^\circ = 0.286^\circ$. This means the Shuttle has to perform a burn with $\Delta v = 5.72\ \text{m s}^{-1}$ into flight direction at a position 33.6 km behind the ISS. Because the Shuttle initially is 10 km below the ISS, the viewing distance to the ISS at burn is $\sqrt{10^2 + 33.6^2} = 35.0\,\text{km}$

NASA's Space Rendezvous History

At NASA there exist two general approaches for homing and closing maneuvers: The historical *coelliptic rendezvous* and today's *stable orbit rendezvous* (SOR).

Coelliptic Rendezvous

Coelliptic orbits are coplanar elliptic (including circular) orbits with a common occupied focus (see Fig. 8.39). The arguments of perigee ω are equal, meaning that the lines of apsides of the orbits are congruent. In addition to this, the differences in perigee and apogee radii are equal. In a spacecraft-fixed reference frame, coelliptic orbits appear as two parallel lines. These particular orbits allow for easy, intuitive,

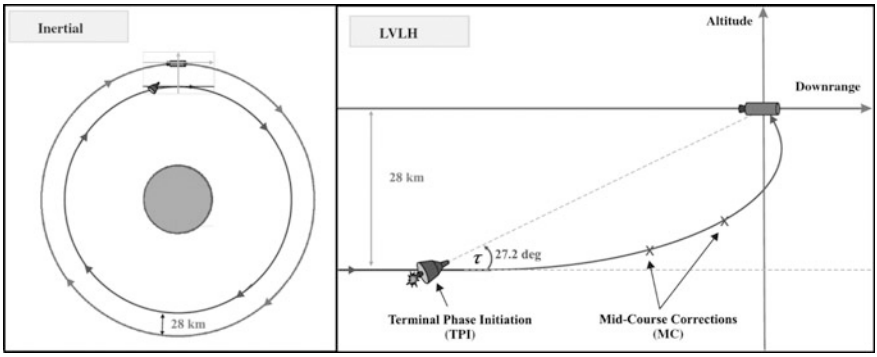

Fig. 8.39 Gemini coelliptic rendezvous in inertial and spacecraft reference frames; τ denotes the trigger angle between the direction to the target and the local horizontal plane at which the transfer maneuver is triggered. *Credit* Woffinden and Geller (2007)

and robust maneuver planning by means of so-called *trigger angle targeting*. This technique was developed during the Gemini program. It allows astronaut pilots to reliably achieve rendezvous by pointing the interceptor spacecraft at the target at a certain trigger angle τ (see Fig. 8.39) relative to the direction of flight and then engaging the orbital maneuvering thrusters, the so-called *Terminal Phase Initiation* (TPI). The trigger angle can be measured with simple cueing devices similar to a sextant. During the transfer, the target will move along its orbit within the so-called *transfer angle* α (the orbit angle covered during transfer). If rendezvous is achieved within a single revolution of the target, thus with $\alpha < 360°$, it is called a *direct rendezvous*. Any case with multiple target revolutions is referred to as *indirect rendezvous*. The point aimed at by the interceptor, in front of or behind the target, is referred to as the *downrange targeting location*.

It can be shown (see Woffinden (2007)), and this is a key property of coelliptic rendezvous, that for direct rendezvous, the elevation trigger angle τ is independent of the angular velocity ω and the relative altitude of the coelliptic trajectory. Hence, the same trigger angle applies for all orbits, regardless of the coelliptic height differential. For indirect rendezvous, the trigger angles show dependency on the ratio between the downrange targeting location and the relative altitude of the coelliptic trajectory. In recent numerical simulations it was determined that the optimal trigger angle for a minimum-Δv intercept maneuver is 27.0°, with a transfer angle of 163.1°. Interestingly, this is not equal to a Hohmann transfer with a trigger angle of 0° and a transfer angle of 180°. In reality, this optimal angle will not be perfectly achievable. A range between 26.8° and 27.3° was therefore identified as providing optimal combinations of required Δv, Line-of-Sight (LOS) approach rates, and positioning accuracy.

Interestingly, without running numerical computer simulations, NASA selected a trigger angle of 27° with a transfer angle of 130° for Gemini/Apollo rendezvous operations. For these manned rendezvous missions trigger angle targeting was particularly attractive. It allowed the use of the astronauts' eyes and simple elevation cueing for maneuver triggering in case of the failure of the

rendezvous radar system. After applying the initial Δv along LOS, the pilot performed one or two mid-course correction maneuvers, before finally approaching the target for docking. During final approach, the pilot benefited from a low inertial LOS approach rate during final breaking and approach, as well as from good visibility of the target against the star background. This was important since LOS closing rates are difficult to judge visually without ambient references.

Coelliptic rendezvous remained NASA's rendezvous approach of choice throughout Gemini and Apollo. Its major strength was the backup capability to perform the TPI burn manually. It was then modified into a *dual coelliptic rendezvous* profile for the Skylab missions. In this profile, the interceptor flew a coelliptic transfer onto a holding orbit below the target. From there another coelliptic maneuver finalized rendezvous. The modifications were applied to improve the final approach lighting conditions for manual piloting, as well as the quality of long-range optical tracking using reflected sunlight. This dual coelliptic profile was then also the baseline for Shuttle R&D missions. Given the characteristics of typical Shuttle rendezvous targets, there existed concerns regarding the usability and quality of optical tracking of small target objects using reflected sunlight in the presence of Earth's illuminated surface and bright celestial objects. Another issue was the depletion of the Shuttle's *Reaction Control System* (RCS) propellant due to high relative approach velocities. This initially led to the adoption of a so-called *tuned coelliptic rendezvous* (TCR) profile.

Stable Orbit Rendezvous (SOR)

For current space station operations all these coelliptic rendezvous approaches were replaced by the so-called *stable orbit rendezvous*. Such a SOR was first flown on Gemini XI and was later suggested to address the concerns over target tracking and propellant consumption for Space Shuttle R&D. The reason is that it supports inertial approaches with lower relative velocity than the inertial approaches from the Apollo legacy coelliptic profile. In addition, a stable orbit profile desensitizes the mission timeline from trajectory considerations, as the interceptor could theoretically remain at the waiting point for indefinite periods of time. Stable orbit station-keeping at multiple kilometers of distance to the target (15 km for Space Shuttle ISS approaches) was also preferable to the close-range (at distances of tens of meters) station-keeping associated with coelliptic approaches. In such close proximity, continuous crew monitoring and frequent correction maneuver are needed, resulting in high propellant expenditure. Therefore, the advantages of SOR profiles over coelliptic approaches are lower propellant consumption and stable station-keeping points on V-bar, leading to less demand on crew position monitoring and correction. Hence, the SOR has become the standard for ISS operations for Space Shuttle, Soyuz and ATV, as well as for other rendezvous operations, such as with the Hubble Space Telescope.

For more details on coelliptic and Space Shuttle R&D missions refer, e.g., to Goodman (2006).

8.6.4 Closing Phase

Once on the target orbit at S2 (see Fig. 8.36) jets are fired to bring the interceptor to a hold at a safe distance about 3 km behind the target. The target now is within range of the interceptor sensors and thus relative navigation can commence. This station-keeping point S2 is essential to assess the situation and plan the upcoming closing maneuver.

The closing maneuver depends on the type of final approach: For a final ±R-bar approach the interceptor needs to get to the ±R-bar below/above the target. For a final +V-bar approach the interceptor needs to proceed further on the −V-bar closer to the target to the station-keeping point S3, and for a +V-bar approach the interceptor has to fly around the target to approach it from the leading end. Anyway, with the closing maneuver we ingress the *Approach Ellipsoid* of the ISS. All operations inside the Approach Ellipsoid are "combined operations" involving the mission control authorities in Houston and Moscow. From here on safety as not to collide with the ISS has the highest priority.

−V-Bar Approach

Let us assume that the docking port is on the trailing end of the target and therefore an approach further on the −V-bar is favorable. What are the options to carry it out? In Sect. 8.5.3 we have seen that we may approach the target on the V-bar either via a prolate cycloid (which is a Hohmann trajectory; see end of section "Ellipse" in Sect. 8.5.3) or via an ellipse. The decision is based on safety versus efficiency: If in course of the prolate cycloid we would lose control over the interceptor we would drift away infinitely and if it is a "flat" cycloid we might even hit the target. However, if safety is not paramount then one could traverse the distance from S2 to S3 by one or several cycles keeping the momentum along the V-bar and hence save fuel. At each reversal point one could even stop the approach, assess the situation, and fine-tune the further approach. This option is chosen by NASA for the Shuttle closing phase (see Fig. 8.45). If safety is top priority then the ellipse trajectory is the choice, because if control over the interceptor would be lost, it would automatically return to S2. However, this method requires to fire the jet at every intersection with the V-bar, thus coming to a halt and thereafter repeat the whole cycle procedure. "Safety-first" requirement of course comes at the expense of a higher propulsion demand.

So, for +V-bar approach of a "safety-first" rendezvous with the ISS as shown in Figs. 8.36 and 8.40 the ellipse maneuver is used. As shown in Sect. 8.5.3, in particular Figs. 8.29 and 8.30, a vertical (radial) burn v_0 will bring us on an ellipse to the next waiting point S3 that lies by $\Delta x = \mathrm{S2} - \mathrm{S3} = 4v_0/n < 0$, with $\mathrm{S2} < 0,\ \mathrm{S3} < 0$, closer to the target. When arriving at S3 a reverse burn must be fired to bring the interceptor to a halt. For the required delta-v for such a step of width Δx we find from Fig. 8.30

$$\Delta v = \pm 2 \times \frac{\Delta x}{4}\sqrt{\frac{\mu}{a^3}} \quad @\ \text{elliptic trajectory} \tag{8.6.6}$$

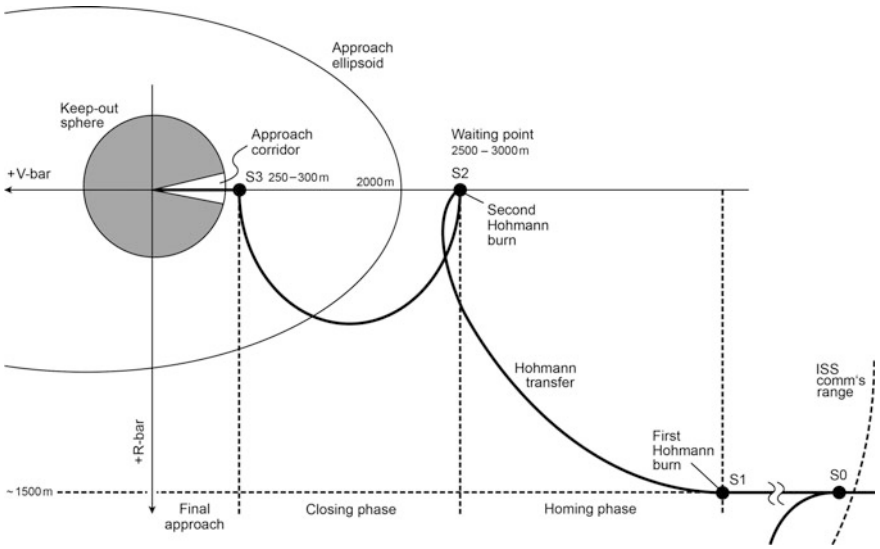

Fig. 8.40 ISS stable orbit approach on −V-bar as typically adopted by an ATV rendezvous. First, a Hohmann transfer brings the interceptor to the waiting point S2. Then, it approaches the ISS on an elliptic trajectory to waiting point S3. *Credit* Fehse (2003) and U. Walter

where the factor 2 indicates that we need two burns for the entire approach maneuver and the ± sign that the elliptic trajectory might be on either side of the V-bar. This maneuver can be performed at any step size and as often as wanted to get to S3. Observe that it does not make any difference for the total delta-v if a given distance is covered with more or less steps because $\Delta v \propto \Delta x$. How many increments are to be chosen is just a matter of safety and time (every step lasts one orbital period). So, if Δx is the total distance between S2 and S3, Eq. (8.6.6) provides the delta-v for the entire closing transfer independent of the number of steps. To approach the ISS, every incremental distance of 1 km requires $\Delta v = 2 \cdot 0.286\,\mathrm{m\,s^{-1}}$.

If the cycloidal approach would be chosen, we have from Fig. 8.27 $\Delta x = 6\pi v_0/n$ and hence

$$\Delta v = \pm 2 \times \frac{\Delta x}{6\pi \cdot k}\sqrt{\frac{\mu}{a^3}} \quad @\ \text{cycloidal trajectory} \tag{8.6.7}$$

where Δx is the total distance between S2 and S3 and k is the number of cycloidal revolutions to traverse this distance. Here again the factor 2 indicates that we need a initiation burn at S2 plus a stop burn of equal absolute value at S3. We therefore see

that the cycloidal approach is by a factor $6\pi \cdot k/4 = 4.7 \cdot k$ more efficient that the elliptic approach—at the expense of safety. We recall that every cycloidal or elliptic cycle takes a full orbital period.

Approach to +V-Bar

If one wants to approach on the –V-bar from S2 to the waiting point S3 on the +V-bar, i.e., to the other side of the target, one has to apply the same maneuvers (elliptic or cycloidal trajectories) as above, the only difference being that for $\Delta x = \mathrm{S2} - \mathrm{S3} < 0$ holds $\mathrm{S2} < 0,\ \mathrm{S3} > 0$.

Approach to ±R-Bar

If the final approach is on +R-bar or −R-bar the closing phase must bring the interceptor in a loop from −V-bar to ±R-bar (see Fig. 8.41) at below/above the target. Here again both the cycloidal and elliptic trajectory would do, but here both approaches are equally safe. This is because if control is lost for a cycloidal trajectory it would just pass by the target at the aimed distance and after that drift away from the target. In the elliptic trajectory case the interceptor would just orbit the target on an ellipse. Because we have seen that the cycloidal trajectory is much more efficient it is the preferred approach method.

The cycloidal loop is performed in two (or one) steps. First, a tangential burn Δv brings the interceptor on a prolate cycloid (Hohmann trajectory) to the transition point S3_ where a burn Δv is fired against the direction of movement. This brings the interceptor into a circular Earth orbit below/above the ISS. On this orbit it slowly drifts to the point S3 below the ISS from where the final approach commences. Note that neither S3_ nor S3 are stable points with respect to the ISS. If the first burn is accurate enough it can be set such that S3_ coincides with S3.

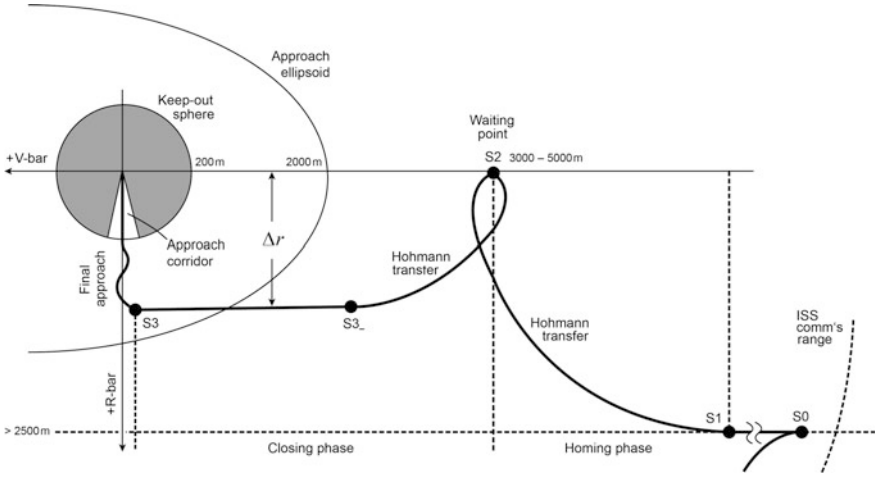

Fig. 8.41 From −V-bar to +R-bar approach to ISS. A Hohmann transfer brings the interceptor first to the intermediate point S3_ where it crosses over into a circular orbit on which it drifts to the final point S3. *Credit* Fehse (2003) and U. Walter

What needs to be determined is: Given the initial point S2 and a radial distance Δr (counted positively outward along the z-axis) the interceptor shall dive below ($\Delta r < 0$) or above ($\Delta r > 0$) the ISS, what is the delta-v to perform the entire maneuver? From Fig. 8.27 we derive that the diving distance is $\Delta r \equiv \Delta z = 4v_0/n$. We therefore find for the initial delta-v

$$\Delta v_i = \frac{\Delta r}{4}\sqrt{\frac{\mu}{a^3}} \quad \text{@ initial burn} \tag{8.6.8}$$

Upon diving down/up, the interceptor speeds up and according to Eq. (8.5.14) achieves at the lowest/highest point of the trajectory, which is S3$_-$, the relative velocity $\dot{x} = v_0(4\cos\pi - 3) = -7v_0$. This corresponds in an Earth centered system to

$$v_- = \sqrt{\frac{\mu}{a}} - 7v_0$$

At $r = a + \Delta r$, the anticipated circular orbit has an orbital velocity of

$$v_+ = \sqrt{\frac{\mu}{a+\Delta r}} = \sqrt{\frac{\mu}{a}}\left(1 - \frac{1}{2}\frac{\Delta r}{a}\right) = \sqrt{\frac{\mu}{a}} - 2v_0$$

where the latter follows by applying Eq. (8.6.8). For the delta-v of the braking burn at S3$_-$, we therefore obtain

$$\Delta v_f = v_- - v_+ = -5v_0 \tag{8.6.9}$$

So the total delta-v is

$$\Delta v = |\Delta v_i| + |\Delta v_f| = 6 \times \frac{\Delta r}{4}\sqrt{\frac{\mu}{a^3}}$$

Thus, while for the −V-bar approach our effort to get to S3 is maximally $\Delta v = 2|v_0|$ (elliptic trajectory), it is much bigger, namely $\Delta v = 6|v_0|$, in the case of an approach to ±R-bar.

8.6.5 *Final Approach*

The interceptor is now on the waiting point S3 just outside of the Keep-Out Sphere, about 200 m away from the ISS (see Fig. 8.42). This is where the *final approach* (a.k.a. *proximity operations or terminal phase*) begins. Other than during the stable orbit rendezvous where the interceptor approached the target via stable orbits (i.e., cycloidal trajectories that can be stopped at the reversal points or elliptic trajectories that even back off from the target if rendezvous control is lost and therefore are "safe" orbits), the trajectories now are more or less straight to directly intercept the

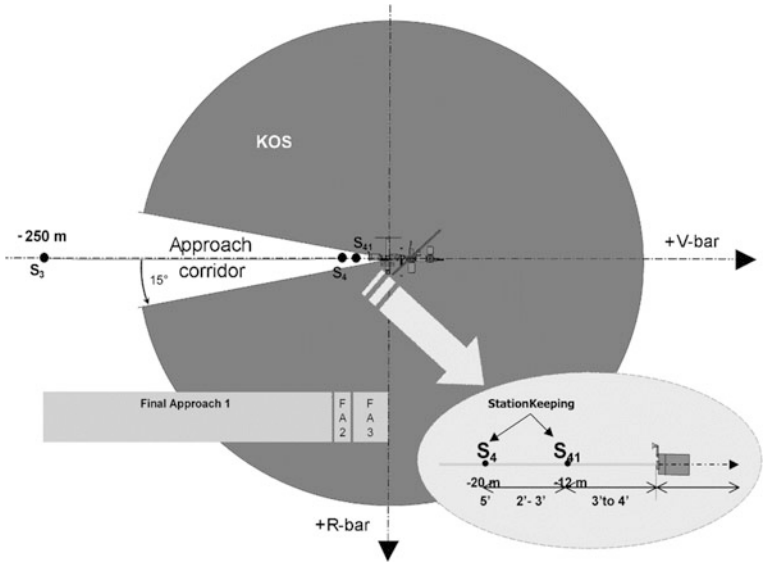

Fig. 8.42 ISS approach corridor for V-bar approach. *Credit* Wartenberg and Amadieu/ESA

target and therefore are on "collision course" with it. The final approach ends at a distance of a few meters upfront the ISS, either when docking is imminent or when the target is within capture distance of the manipulator. During this phase the spacecraft usually maneuvers autonomously, i.e., without intervention by ground control. The spacecraft control loop must therefore be closed locally, either by the crew or by the automatic controllers. Final approach can thus be considered the most critical part of the R&D mission. During this phase, minor errors can cause accidents.

±V-Bar approach

First, we consider the approach on +V-bar or on −V-bar (see definition of "±V-bar approach" in the section *LVLH Reference Frame* above) from waiting point S3 through the conical approach corridor with half angle 15° to the next waiting point S4 (the initial waiting point for docking approach). To penetrate the cone one could continue to apply the ellipse maneuvers. However, every incremental step takes one orbital period of 91.5 min in case of the ISS, which is far too much.

One therefore switches to another approach mode called *forced translation.* Figure 8.43 shows its principle. Let us assume a burn is performed aiming directly at the target. According to Fig. 8.27, the higher speed would force the interceptor to drift upward (centrifugal force is bigger than the gravitational force at this circular altitude), violate the approach cone, and never encounter S4 (see Fig. 8.43). However, we can counteract the updrift by providing in addition to the forward translation an initial small downward force. If this is done properly, it forces the

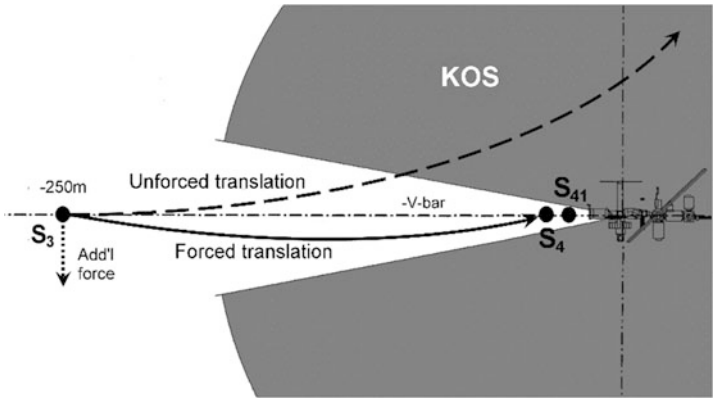

Fig. 8.43 A straight trajectory would turn up and leave the approach corridor. A downward forced translation enforces the trajectory to stay in the corridor and hit the waiting point

initial trajectory slope down just that the trajectory at its end hits S4. The forward translation with this extra little downward force is called *forced translation*.

It needs to be determined how big the additional delta-v, equivalent to the downward force, is. We therefore revisit Sect. 8.5.2 where we have shown that for translation times $(nt)^2 \ll 1$ Eq. (8.5.13) holds. These equations give the answer to the question what the initial velocity $\boldsymbol{v}_0 = (\dot{x}_0, \dot{y}_0, \dot{z}_0)$ at the initial point (x_0, y_0, z_0) should be in order to meet after time t a given target point at the origin $(0, 0, 0)$. In our case the vector from the target point to the initial distance of the interceptor is $(x_0, y_0, z_0) = (\pm\Delta x, 0, 0)$ for a $\pm$V-bar approach. Therefore, for a projected time (τ) to arrival Eq. (8.5.13) reduces to

$$\boldsymbol{v}_0 = \left(v_{0x},\ v_{0y},\ v_{0z}\right) = \left(\mp\frac{\Delta x}{\tau},\ 0,\ \pm n \cdot \Delta x\right) \quad @\ \pm\text{V-bar approach} \qquad (8.6.10)$$

$$\Delta\boldsymbol{v} = \boldsymbol{v}_0 - \boldsymbol{v}_i$$

where $n = \sqrt{\mu/a^3}$, $\Delta\boldsymbol{v}$ is the initiation burn vector, and $\boldsymbol{v}_i$ is the interceptor's velocity incident of the starting point S3 (if the starting point was a waiting point, $\boldsymbol{v}_i = 0$). Of course, for braking the forced translation at S4 the same amount of Δv is required, however, for v_{0x} into the opposite direction. The initial speed in x-direction, v_{0x}, is easy to grasp: The required speed is distance divided by flight time. The delta-v in negative z-direction (radial thrust downward) is just the forced part. Assuming that the delta-v in each direction is generated by separate thrusters (as usually the case), the absolute value of the total approach delta-v is

$$\Delta v = 2\left(\frac{\Delta x}{\tau} + n \cdot \Delta x\right) = 2 \cdot \Delta x \cdot \left(\frac{1}{\tau} + n\right)$$

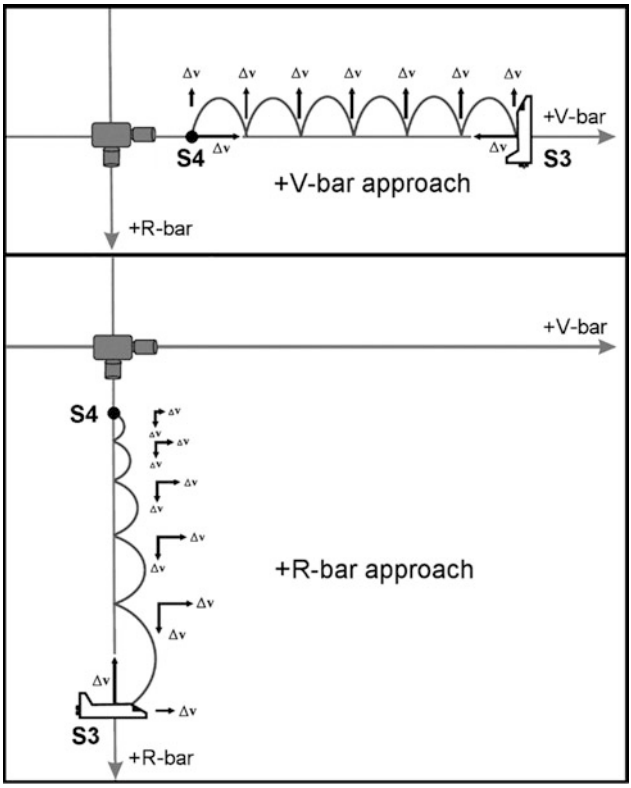

Fig. 8.44 Final approach hopping profiles of a Shuttle final approach along the +V-bar (above) and the +R-bar (below, including deceleration burns). *Credit* Woffinden and Geller (2007)

It would not be wise to cover the final approach distance in one move. Initial point and/or firing errors would jeopardize encountering exactly the target point. One rather splits the distance into two or more parts and whenever the trajectory meets the V-bar a new forced delta-v of $\pm 2 \times n \cdot \Delta x$ is applied starting the forced translation anew. This leads to a hopping approach as depicted in Fig. 8.44 (top) for a Shuttle +V-bar approach. This is why it is called *hopping trajectory*. Because the total delta-v has the linear dependency $\Delta v \propto \Delta x$, it does not make any difference in terms of delta-v effort to split the final approach distance into k shorter hops of length ε, $\Delta x = k \cdot \varepsilon$, but still cover the total distance in the same time t, or not. However, owing to boost errors, it is preferable to make more shorter hops.

±R-Bar Approach

Forced translation can also be applied on the +R-bar or −R-bar, which for instance is performed by a Soyuz or Progress docking to the radial port (Pirs docking compartment) of the ISS. This approach was originally designed for docking the Shuttle with *MIR*. It was also used on Hubble servicing mission STS-82. To

determine the initiating delta-v for the forced translation from S3 to S4 we have from Eq. (8.5.13) with the initial distance vector $(0, 0, \mp\Delta z)$ for ±R-bar approach and for a projected time (τ) to arrival

$$\boldsymbol{v}_0 = \left(v_{0x},\ v_{0y},\ v_{0z}\right) = \left(\pm n \cdot \Delta z,\ 0,\ \pm\frac{\Delta z}{\tau}\right) \quad @\ \pm\text{R-bar approach} \tag{8.6.11}$$

$$\Delta\boldsymbol{v} = \boldsymbol{v}_0 - \boldsymbol{v}_i$$

where $n = \sqrt{\mu/a^3}$, $\Delta\boldsymbol{v}$ the initiation burn vector, and $\boldsymbol{v}_i$ is the interceptor's velocity incident to the starting point S3. The total approach delta-v is by the same token as above

$$\Delta v = 2 \cdot \Delta z\left(\frac{1}{\tau} + n\right)$$

And also in this case owing to the linear dependency $\Delta v \propto \Delta z$ it does not make any difference in terms of delta-v effort to split the distance into more shorter hops. Thus, we might have also hopping trajectories as shown in Fig. 8.44 (bottom).

Proximity Operations

From an orbital mechanics point of view the last few meters starting out from S4, the docking approach in the proximity of the target, is the most easy part of the rendezvous. This is because for very short distances $x,\ z,\ \tau \to 0$ and hence

$$\begin{aligned} v_{0x} &= -\frac{x_0}{\tau} - nz_0 & v_{0x} &= -\frac{x_0}{\tau} \\ v_{0z} &= -\frac{z_0}{\tau} + nx_0 \ \rightarrow & v_{0z} &= -\frac{z_0}{\tau} \\ v_{0y} &= -\frac{y_0}{\tau} & v_{0y} &= -\frac{y_0}{\tau} \end{aligned} \tag{8.6.12}$$

$$\Delta\boldsymbol{v} = \left(v_{0x},\ v_{0y},\ v_{0z}\right) - \boldsymbol{v}_i$$

where $\boldsymbol{v}_i$ is the interceptor's velocity incident to the starting point S4. Therefore, if on this docking approach the commander or pilot navigates the interceptor, steering becomes intuitively easy because the required momentary speed is just distance per time. However, in order not to crash into the docking port the approach speed has to be continuously reduced (see Fig. 8.44, bottom).

Docking/Capture Phase

At the end of the final approach phase, the interceptor is in position in front of the target's docking port or capture interface and all thrusting has ceased. The interceptor's relative velocity is either zero for capture & berthing, or slightly above zero for docking. On one hand, this approach rate must be great enough to prevent the vehicles from bouncing off each other without capture being achieved. On the other

hand, it must be low enough to prevent structural damage or loss of control and/or the ability to attenuate the momentum. The exact position, velocity, orientation, and angular rate tolerances depend on the specific docking or capture tools being used.

The docking/capture phase is the conclusion of a R&D mission. It encompasses the following activities:

- docking/capture of the target by the interceptor (or vice versa)
- establishment of a rigid structural connection
- connection of fluid, gas, electrical, propellant and communication lines
- establishment of a pressurized passageway, if crew transfer is part of the mission goals.

Docking means that the active spacecraft positions itself and establishes the physical connection using its own momentum. In capture and berthing, either the target or interceptor is captured, positioned and connected by a robotic manipulator to a berthing mechanism. Berthing thus allows contact to be made at a near-zero cloture rate, which means a higher level of control for the operator and avoids the process of one vehicle basically flying into the other. It is therefore the generally preferable approach but comes at the cost of requiring a complex, heavy and expensive *Remote Manipulator System* (RMS).

8.6.6 Shuttle-ISS Rendezvous

The Shuttle's close range rendezvous with the ISS is somewhat different, though, because the docking port is on the leading side (+V-bar) of the ISS. Therefore, beginning at S2 the Shuttle flies in two cycloidal steps and within two orbits a homing approach from S2 to S3 such that it goes up just below the ISS (see Fig. 8.45). Note that the launch window was chosen such that daytime (i.e., sunlight) condition is at those parts of the trajectory, including the final approach and docking (see Figs. 8.46 and 8.47), where the ISS needs to be seen from the Shuttle and vice versa. Just before arriving at S3 the commander of the Shuttle takes over manual control for the remainder of the approach and docking. He will stop the Shuttle at S3 some 180 m below the ISS and will maneuver the Shuttle through a 9 min, 360° backflip (a.k.a. *Rendezvous Pitch Maneuver*, RPM) that allows the station crew to take pictures of the Shuttle's heat shield to see whether it was damaged during launch. The Commander then will move the Shuttle at a so-called TORVA maneuver from the +R-bar to the +V-bar in a position about 120 m directly in front of the station in preparation for the final approach to the pressurized mating adapter PMA-2 located at the leading end of the US utility hub *Harmony*.

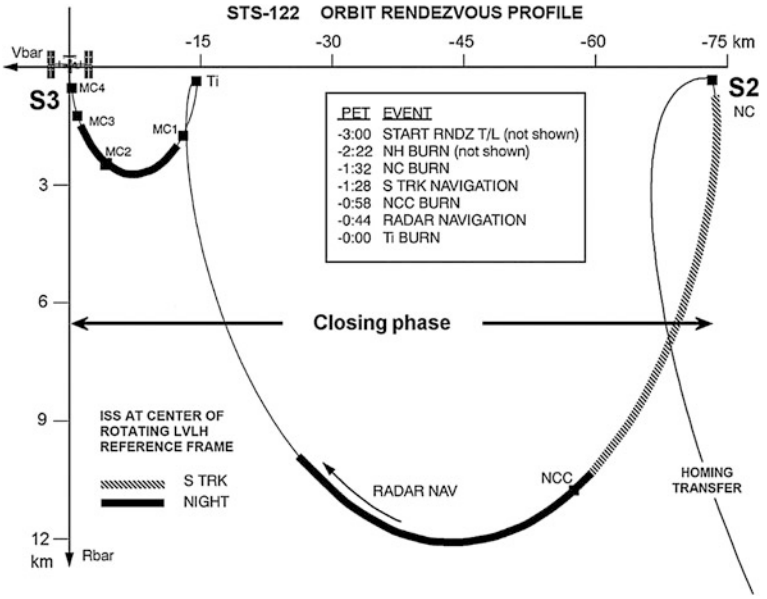

Fig. 8.45 The cycloidal trajectory in the closing phase of a Shuttle STS-122 rendezvous with the ISS. *Credit* NASA

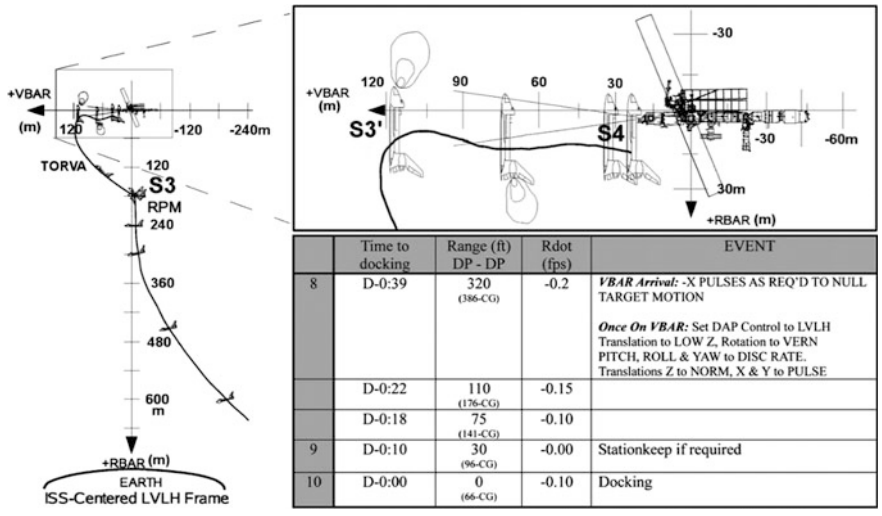

	Time to docking	Range (ft) DP - DP	Rdot (fps)	EVENT
8	D-0:39	320 (386-CG)	-0.2	***VBAR Arrival:*** -X PULSES AS REQ'D TO NULL TARGET MOTION ***Once On VBAR:*** Set DAP Control to LVLH Translation to LOW Z, Rotation to VERN PITCH, ROLL & YAW to DISC RATE. Translations Z to NORM, X & Y to PULSE
	D-0:22	110 (176-CG)	-0.15	
	D-0:18	75 (141-CG)	-0.10	
9	D-0:10	30 (96-CG)	-0.00	Stationkeep if required
10	D-0:00	0 (66-CG)	-0.10	Docking

Fig. 8.46 Final approach trajectory of the Shuttle STS-122 approaching the ISS. *Credit* NASA

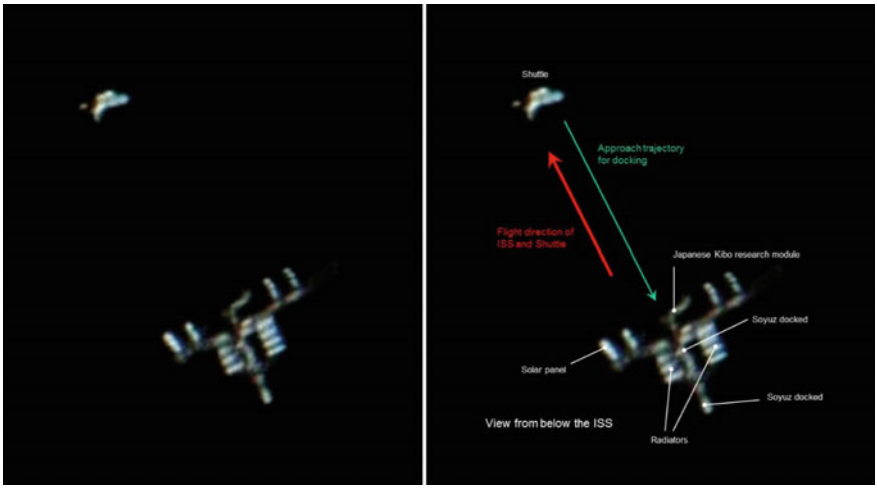

Fig. 8.47 Final approach trajectory of Shuttle STS-133 approaching ISS (left raw, right annotat ed picture). Picture taken with ISO 800, 1/800 s, through a 8.5″ Newtonian on February 26, 2011, 18:35:54 h GMT, over UK. *Credit* Rob Bullen

Acronyms for NASA Rendezvous Maneuvers

NC	(Phasing correction burn) Performed to hit a range relative to the target at future times
NH	(Height adjust burn) Performed to hit a delta-height relative to the target at future times
NPC	(Plane change burn) Performed to remove planar errors relative to the target at future times
NCC	(Corrective combination burn) First on-board targeted burn in the rendezvous sequence to reduce phasing and height errors relative to the target at Ti
Ti	(Terminal intercept burn) Second on-board targeted burn in the rendezvous sequence to place the orbiter on a trajectory to intercept the target in one orbit
MC-1,2,3,4	(Midcourse correction burns) On-board targeted burns to correct the post Ti trajectory in preparation of the final approach phase
RPM	(Rendezvous Pitch Maneuver) A 360° backflip that allows the station crew to take pictures from the Zvezda Service Module of the Shuttle's heat shield
TORVA	(Twice Orbital Rate R-bar to V-bar Approach) This manually performed maneuver brings the orbiter from the +R-bar to the +V-bar

8.6.7 Plume Impingement

The term *plume impingement* covers all effects exerted on the target object if it is impacted by the exhaust gases of the interceptor's reaction control system (RCS, the maneuvering control system of an interceptor) thrusters. One of these effects is the plume pressure force acting on the target and causing position and attitude disturbances. Another is the heat load placed on the target's structure by the hot gases. This can lead to overheating of parts of the surface and the underlying structure. The third effect is the contamination of the target's surfaces by combustion products and unburned propellant components. This can cause contamination of not only sensitive elements on the target's surfaces, particularly optical elements such as camera lenses, solar arrays or docking sensors, but also of sealing elements of the docking mechanism. This risk of contamination must be considered in particular during orbit servicing missions such as Hubble servicing, where these considerations impacted the design of final approach trajectories.

Therefore, plume impingement is one of mission planners' major concerns during proximity operations, apart from collision avoidance and maneuver precision. It can only be avoided if thruster activity near the target is minimized. This in turn means that the interceptor's relative velocity must diminish below a threshold value as it approaches the target. During Gemini and Apollo, plume impingement never became a significant issue due to the thrust magnitude, the position and canting of the RCS nozzles, as well as the roughly equal sizes of interceptor and target and the absence of large appendages such as solar arrays. This changed during the Skylab missions. During Skylab 2, the Apollo *Command and Service Module* (CSM) was maneuvered within close proximity so that a crewman standing in the hatch could reach the stuck solar array with a deployment tool. The CSM thrusting to null the closing velocity triggered Skylab AOCS to fire its jets in order to maintain its attitude. This resulted in an opening rate between the two vehicles. On the later Apollo-Soyuz Test Mission, four of the CSM's thrusters were inhibited 2 s prior to docking contact in order to prevent plume loading of the Soyuz solar arrays.

Space Shuttle

These lessons were carried into the Space Shuttle design process. The massive orbiter is designed to assemble and maintain large space stations and service comparatively small and light satellites. These are equipped with large solar arrays and antennas or sensitive optics. Plume impingement therefore is a prime concern. The size of the Shuttle was predetermined by the payload it was designed to carry and the location of RCS thrusters by its shape, which in turn was determined by the requirements of re-entry and atmospheric flight. Plume impingement concerns could therefore be addressed only by careful design of R&D approaches.

The underlying assumptions were as follows: The target spacecraft could not be designed with features preventing contamination (e.g., movable sensor covers as

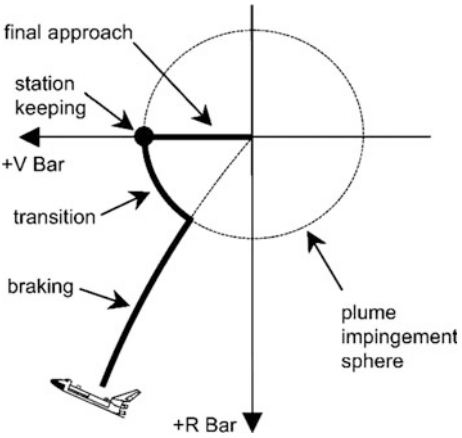

Fig. 8.48 Approach profile to avoid plume impingement on target. When the approaching interceptor reaches the border of a plume impingement sphere, it performs a transition maneuver to a station-keeping point on the V-bar following the borders of the plume impingement sphere. After the station-keeping point is reached, the interceptor flies a forced translation final approach. *Credit* Goodmann (2006)

found on Hubble), and the control of the target attitude could not prevent contamination. Therefore, on each mission a target-dependent minimum range existed, at which the thrusters could still be fired in the direction of the target without contamination concern. At the minimum range, the orbiter was to transition from a direct approach trajectory to a station-keeping point on the V-bar (see Fig. 8.48). From this point on the final approach would be flown in forced translation. A number of such approaches were planned for the Shuttle's *Long Duration Exposure Facility* (LDEF) mission. Simulations showed that an Apollo-type inertial approach and braking technique would cause LDEF to tumble. In addition, plume impingement induced dynamics at grapple ranges that could make both LDEF deployment and retrieval difficult.

Another countermeasure for plume impingement issues specific to the Space Shuttle was the development of the *Low-Z* approach. In this approach, all forward firing RCS jets are inhibited, with all thrust thus acting primarily along the spacecraft's longitudinal x-axis (see Fig. 8.49). All braking thrust in the z-direction therefore results from the canting of the longitudinal thrusters. This provides minimal RCS braking capability while minimizing RCS plume impingement. It is also expensive in terms of propellant use. Notwithstanding its limitations, *Low-Z* mode has been employed on satellite servicing missions, including Hubble servicing, and the missions to MIR and ISS.

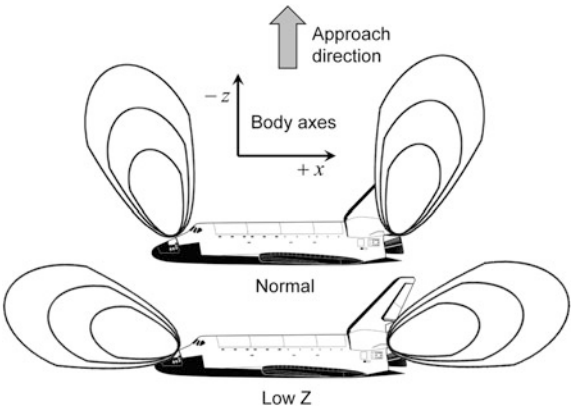

Fig. 8.49 Space shuttle low-Z RCS mode. The orbiter's thrusters are fired only in the Shuttle's longitudinal axis (x-axis). This significantly reduces plume impingement. On the other hand, owing to the canting of the thrusters, this provides minimal braking capability in the forward z-direction

8.7 Problems

Problem 8.1 *Efficiency of Combined Orbital Maneuvers*
Prove the statement in Sect. 8.1.3 that in terms of delta-v an orbit transition with $\boldsymbol{v}_1 || \boldsymbol{v}_2$ combined with a change in orbit orientation $v_1 = v_2,\ \phi \neq 0$ is always more efficient than performing the two changes sequentially at the same point in space.

Problem 8.2 *Adjacent Circular Orbit Approximation*
Prove Eq. (8.3.9)

$$\frac{\sqrt{a_\bullet} + \sqrt{a_O}}{\sqrt{a_H}} - 1 \approx 1 - \frac{1}{16}\left(\frac{a_O - a_\bullet}{a_\bullet}\right)^2 \quad @\ a_O \to a_\bullet$$

Problem 8.3 *Transfer between Aligned Ellipses*
Consider a Hohmann transfer between two coplanar and coaxial ellipses. Show that the propulsion demand for the transition between the periapsis of the inner ellipse and the apoapsis of the outer ellipse is

$$\Delta v = \sqrt{\mu}\left(\frac{1}{\sqrt{r_{\bullet,per}}} - \frac{1}{\sqrt{r_{O,apo}}}\right)\left(\frac{\sqrt{r_{O,apo}} + \sqrt{r_{\bullet,per}}}{\sqrt{a_T}} - \frac{\sqrt{r_{O,apo}}\sqrt{1+e_\bullet} - \sqrt{r_{\bullet,per}}\sqrt{1-e_O}}{\sqrt{r_{O,apo}} - \sqrt{r_{\bullet,per}}}\right)$$
$$\leq \sqrt{\mu}\left(\frac{1}{\sqrt{r_{\bullet,per}}} - \frac{1}{\sqrt{r_{O,apo}}}\right)$$

Remark *For circular orbits this expression passes over to Eq. (8.3.8).*

Problem 8.4 *Hohmann Transfer Maxima*
(a) Prove that the maximum of the circularization impulse $\Delta v_{HO\to O}$ (see Fig. 8.12) is the root of the equation $x^3 - 5x^2 - 5x - 1 = 0$. Find the root $x = r_O/r_\bullet = 5.879362\ldots$ by Newton's method.
(b) By the same token, prove that the propulsion demand of a Hohmann transfer achieves a maximum at $x = a_O/a_\bullet = 15.58172\ldots$, which is the root of $x^3 - 15x^2 - 9x - 1 = 0$.

Problem 8.5 *Hohmann Versus Bi-Elliptic Transfer*
Prove that for $x = r_O/r_\bullet > 11.9387654724\ldots$ the bi-elliptic transfer has a lower propulsion demand than the Hohmann transfer. Show that $x = r_O/r_\bullet$ is the root of the equation $x - 1 = \sqrt{1+x}(\sqrt{x} - \sqrt{2} + 1)$.

Problem 8.6 *Variations of Orbital Elements by Kick-Burns*
(a) Prove Eq. (8.1.1) as described in the text.
(b) Prove Table 8.1 by applying Eq. (8.1.1) at the given positions.

Problem 8.7 *Orbit Phasing*
Suppose two satellites are flying in a close formation on the same orbit at relative distance s and orbital period T. Show that, if s needs to be corrected, a kick-burn $\delta v_{||}$ at the periapsis will cause a position shift of

$$\delta s_{per} = 3T\frac{1+e}{1-e}\delta v_{||}$$

at the periapsis after one orbit, while a kick-burn $\delta v_{||}$ at the apoapsis will cause a position shift of

$$\delta s_{apo} = 3T\frac{1-e}{1+e}\delta v_{||}$$

at the apoapsis after one orbit.

Problem 8.8 *Maximum Transfer Time for Minimum Energy Transfer*
Given the minimum energy transfer orbit between two points P_1 and P_2 having $4a_{\min} = r_1 + r_2 + c$. Show that for any slightly larger transfer orbit with $a = a_{\min} + \Delta a$ the transfer time is

$$\Delta t \approx \Delta t_{\max} - 4a_{\min}\sqrt{\frac{\Delta a}{\mu}} \quad @\ \beta < \pi$$

$$\Delta t \approx \Delta t_{\max} - a_{\min}\sqrt{\frac{\Delta a}{\mu}} \quad @\ \beta \approx \pi$$

and therefore the minimum energy transfer orbit indeed has a maximum transfer time. We will explore the characteristic square root behavior $\delta(\Delta t) \propto -\sqrt{\Delta a}$ near

the maximum transfer time for a Hohmann transfer a bit further in Sect. 9.3.2 before Eq. (9.3.15).

Problem 8.9 *Lambert's Problem for $a \to \infty$*

Prove that from Lambert's Eq. (8.2.13) for $a \to \infty$ follows

$$a = \frac{3}{40} \cdot \frac{\Delta_+^{5/2} - \Delta_-^{5/2}}{6\Delta t\sqrt{\mu} - \left(\Delta_+^{3/2} - \Delta_-^{3/2}\right)}$$

with $\Delta_\pm = r_1 + r_2 \pm \sqrt{r_1^2 + r_2^2 - 2r_1 r_2 \cos\Delta\theta}$. Since $\sqrt{\Delta_\pm} = 2s\sqrt{c}$ this delivers Eq. (8.2.15).

Problem 8.10 *Solution of the Differential Equations for Elliptic Orbits*
It is the objective of this exercise to solve the differential Eq. (8.5.17). According to the theory of differential equations the general solution is the sum of the solution of the homogeneous differential equations given by Eq. (8.5.8) and a special solution to the inhomogeneous differential equations. We therefore just have to seek for this special solution.

(a) Before doing so we make use of the fact that the right hand side of the differential solution is small, namely of order e. We therefore can insert the homogeneous solutions on the right hand side. Show that the differential equations then read

$$x'' + 2z' = e \begin{pmatrix} \cos M \\ -6M\,\cos M + 8\sin M - 6\sin 2M \\ -3M\,\cos M + 4\sin M - 4\sin 2M \\ -2\cos M - 2\cos 2M \end{pmatrix}^T \begin{pmatrix} x_0 \\ z_0 \\ x_0' \\ z_0' \end{pmatrix}$$

$$y'' + y = -3e \begin{pmatrix} \cos^2 M \\ \sin M\,\cos M \end{pmatrix}^T \begin{pmatrix} y_0 \\ y_0' \end{pmatrix}$$

$$z'' - 3z - 2x' = 2e \begin{pmatrix} -\sin M \\ 6M\,\sin M + 8\cos M + \frac{3}{2}\cos 2M - \frac{9}{2} \\ 3M\,\sin M + 4\cos M + \cos 2M - 3 \\ +2\sin M - \frac{1}{2}\sin 2M \end{pmatrix}^T \begin{pmatrix} x_0 \\ z_0 \\ x_0' \\ z_0' \end{pmatrix}$$

(b) Define the second equation as

$$y'' + y = f(M)$$

The homogeneous differential equation is known to have the fundamental system of solutions $y_{1,2}(M) = (\sin M,\ \cos M)$. Now, according to the theory of differential equations a special solution is given as

$$y^*(M) = -\sin M \int_{M_0}^{M} \frac{f(\mu)\cos\,\mu}{W(\mu)} \cdot d\mu + \cos M \int_{M_0}^{M} \frac{f(\mu)\sin\,\mu}{W(\mu)} \cdot d\mu$$

where $W(M)$ is the Wronskian of the fundamental system of solutions. Show that this delivers

$$y^*(M) = -e \begin{pmatrix} \cos^2 M + \cos M - 2 \\ \sin M \cos M - \sin M \end{pmatrix}^T \begin{pmatrix} y_0 \\ y_0' \end{pmatrix}$$

(c) By the same token as in Sect. 8.5.2 derive the differential equation $z'' + z = g(M)$. Show that

$$u'' + u = e \begin{pmatrix} 0 \\ -12\cos M + 9\cos 2M \\ -6\cos M + 6\cos 2M \\ -3\sin 2M \end{pmatrix}^T \begin{pmatrix} x_0 \\ z_0 \\ x_0' \\ z_0' \end{pmatrix} =: g(M)$$

with $u = z - (4 + 13e)z_0 - (2 + 4e)x_0'$. Then apply the above integral expression for the special solution $z^*(M)$. Finally integrate the differential equation $x' + 2z = h(M)$ directly to derive $x(M)$.